

Beate Gabriele Steller, BSc

Diorganotin dihydrides as Building Blocks for functionalised Oligomers and σ -conjugated Materials

MASTER'S THESIS

to achieve the university degree of

Master of Science

Master's degree programme: Chemistry

submitted to

Graz University of Technology

Supervisor

Assoc. Prof. Dipl.-Ing. Dr. techn. Roland Fischer

Institute of Inorganic Chemistry

Faculty of Technical Chemistry, Process Engineering and Biotechnology

AFFIDAVIT

I declare that I have authored this thesis independently, that I have not used other than the declared sources/resources, and that I have explicitly indicated all material which has been quoted either literally or by content from the sources used. The text document uploaded to TUGRAZonline is identical to the present master's thesis.

21.02.2017

Date

S.ella

Signature

Danksagung

Zur Entstehung dieser Arbeit haben viele Menschen beigetragen, die ich an dieser Stelle erwähnen möchte.

Zuallererst möchte ich mich bei meinem Betreuer Roland Fischer bedanken. Nicht nur für die Möglichkeit an diesem großartigen Thema zu arbeiten und Teil eines Projektes zu sein, das dir besonders am Herzen liegt, sondern auch für die vielen Gespräche über Chemie, die mich immer wieder über dein unglaubliches Verständnis von Chemie staunen haben lassen, und das Leben. Danke für dein Vertrauen in mich und meine Fähigkeiten!

Großer Dank gilt auch Frank Uhlig, Michaela Flock und der gesamten Arbeitsgruppe für die gute Zusammenarbeit und den gegenseitigen Wissensaustausch im letzten Jahr und auch schon in den Jahren davor, die ich auf diesem Institut verbringen durfte. Namentlich zu erwähnen sind hier auch Astrid, Babsi und Moni, ohne die wahrscheinlich schon alles im Chaos versunken wäre. Meiner Bürokollegin Melanie möchte ich für ihr immer offenes Ohr und die Gespräche über Basteln, Reisen und vieles mehr danken. Auch die restlichen Kollegen am Institut für Anorganische Chemie sollen hier nicht unerwähnt bleiben.

In den letzten fünf Jahren war die Unterstützung meiner Studienkollegen und Freunde besonders wichtig für mich. An dieser Stelle möchte ich vor allem Anna und Andi hervorheben. Danke für eure ununterbrochene moralische Unterstützung, die Momente in denen wir gemeinsam verzweifelt waren und die vielen Male in denen wir einfach nur herzlich gelacht haben. Ich kann gar nicht in Worte fassen, wie glücklich ich bin euch beide meine Freunde nennen zu dürfen! Den „Mitreitern von Anfang an“, Irene, Anna, Chrissi, Valerian, Maxi, Philipp, Tanja, Max, Schuh und Michi, möchte ich für jedes Laborabschlussfest, jedes Post-Prüfungsbier und jede Feier danken, die ihr unvergesslich gemacht habt. Nicht zu vergessen sind hier auch die selbsternannten „Dampfbacken“, die mich herzlich in ihre Runde aufgenommen haben.

Vermutlich am meisten habe ich meiner Familie zu verdanken, die mir in den letzten Jahren die größtmögliche Unterstützung zukommen lassen hat. Nicht nur habt ihr mir mein Studium finanziell erst ermöglicht, sondern ihr habt mich auch immer dabei bestärkt, meinen Weg zu gehen. Euer Rückhalt hat mich immer wieder motiviert und angespornt.

Unendlich viele Dinge habe ich meiner besseren Hälfte René zu verdanken. Du glaubst an mich, selbst wenn ich es nicht mehr tue. Dabei schaffst du es immer wieder die richtigen Worte zu finden, mich aufzuheitern und zum Lachen zu bringen. Mit deiner unentwegt positiven Art zeigst du mir immer wieder, was im Leben wirklich wichtig ist.

1 Abstract

The present work demonstrates the versatility of easily accessible diorganotin dihydrides as building blocks for the synthesis of functional tin oligomers as well as molecular clusters. Conversion of diphenyltin dihydride with alkaline metals and derivatives gives access to a great structural variety of metalated tin oligomers. Anionic functionality of these catena-, cyclic and bicyclic oligostannyl mono- and dianions allows further functionalisation or linking to give extended, well-defined σ -conjugated materials. Furthermore, reactivity of selected diaryltin dihydrides with varying steric bulk of the *ortho* or respectively *para* substituent towards low valent tin as well as germanium amides is investigated. It is shown, that this approach is a convenient route for the synthesis of various appealing functional tin compounds as wells as molecular clusters featuring non-classical bonding. Isolated molecular compounds are investigated by state-of-the-art methods including X-ray crystallography, heteronuclear NMR, IR- as well as UV/Vis spectroscopy.

2 Kurzfassung

In der vorliegenden Arbeit wird die Vielseitigkeit von Diarylzinndihydriden als Baustein für die Synthese von funktionellen Zinnoligomeren und molekularen Clustern gezeigt. Durch die Umsetzung von Diphenylzinndihydrid mit Alkalimetallen und Alkalimetallverbindungen wurde ein Zugang zur Synthese von metallierten Zinnoligomeren in einer großen strukturellen Vielfalt entwickelt. Die anionische Funktionalität dieser mono- und dianionischen Ketten, Ringe und bityklischen Systeme erlaubt die weitere Derivatisierung oder Verknüpfung um ausgedehnte, wohldefinierte σ -konjugierte Materialien zu erhalten. Außerdem wurde die Reaktivität von ausgewählten Diarylzinndihydriden mit verschiedenen großen Substituenten in *ortho*- bzw. in *para*-Position mit niedervalenten Zinn- und Germaniumamiden untersucht. Es wird gezeigt, dass diese Methode nicht nur eine bequeme Route zur Synthese verschiedener ansprechender, funktioneller Zinnverbindungen ist, sondern auch Zugang zu molekularen Clustern mit nicht-klassischem Bindungsverhältnis gibt. Die isolierten molekularen Verbindungen wurden mittels moderner Analysemethoden darunter Einkristallstrukturanalyse, Multi-Kern-NMR, IR und UV/Vis Spektroskopie untersucht.

Für meine Eltern, meine Schwester Christin und René

“Wissenschaft ist organisiertes Wissen. Weisheit ist organisiertes Leben.”

“Science is organised knowledge. Wisdom is organised life.”

Immanuel Kant

CONTENTS

Danksagung	I
1 Abstract.....	II
2 Kurzfassung.....	III
3 Introduction	1
4 Literature	3
4.1 The Tin-Hydrogen bond.....	3
4.1.1 Reactivity	4
4.2 Geminal, Vicinal and α , ω - Dianions of Tin.....	6
4.2.1 σ -delocalisation	8
4.3 Molecular Cages and Clusters of Tin	9
4.3.1 Categories.....	9
4.3.2 Synthesis Strategies.....	10
4.3.3 Ligand-stabilised Cages and Clusters.....	10
4.3.4 Metalloid Tin Clusters.....	13
5 Results and Discussion.....	18
5.1 Diaryltin dichlorides and dihydrides.....	18
5.1.1 Synthesis.....	18
5.1.2 X-Ray Crystallography.....	21
5.2 Anionic Compounds	25
5.2.1 Anionic Chains and Rings.....	25
5.2.2 Anionic Cages	37
5.3 Clusters and molecules with non-classical bond situation.....	48
5.3.1 Synthesis.....	48
5.3.2 X-Ray Crystallography.....	55
6 Conclusion and Outlook.....	64

7	Experimental Section	66
7.1	Materials and Methods	66
7.1.1	NMR Spectroscopy	66
7.1.2	ATR-FTIR	66
7.1.3	UV/VIS.....	67
7.1.4	Mass Spectrometry.....	67
7.1.5	Crystal Structure Determination	67
7.2	Synthesis.....	68
7.2.1	Synthesis of Aryl bromides	68
7.2.2	Synthesis of Ar_2SnCl_2	69
7.2.3	Synthesis of Ar_2SnH_2	72
7.2.4	Synthesis of Sn(II) and Ge(II) amides.....	74
7.2.5	Synthesis of R_3SiCl	75
7.2.6	Synthesis of Anionic Chains and Rings	76
7.2.7	Synthesis of Anionic Cages	77
7.2.8	Synthesis of Clusters and molecules with non-classical bonding situation	79
8	References	83
9	Appendix.....	90
9.1	Abbreviations	90
9.2	Crystal Structure Analysis Data	93

3 Introduction

Due to their unique properties and their wide application field, σ -conjugated tin polymers as well as tin clusters and cages have received wide interest in the past and in recent times.^[1–3] Both are described as promising materials for non-linear optics as well as electronic devices.^[4–7] The present work focuses on alternative synthesis methods for these classes of compounds applying diaryltin dihydrides as easily accessible building blocks.

Common approaches for the synthesis of tin polymers including WURTZ coupling of diorganotin dichlorides and dehydrogenative coupling of diorganotin dihydrides using amine bases result usually in a mixture of products and an undefined blend of catena- and cyclic oligostannanes. Additionally, these approaches suit only for the synthesis of homopolymers. In course of this research, costly transition metal complexes have proven their advantages in the synthesis of defined oligo- and polystannanes.^[8] In this work, a route towards the synthesis of defined functional subunits of polystannanes is presented *via* the reaction of diphenyltin dihydride with alkaline metals and alkaline metal compounds. Anionic functionality of these compounds provides the opportunity for further derivatisation and linking to give extended, well-defined σ -conjugated materials and block copolymers with chosen degree of polymerisation. In the synthesis of this surprisingly rich variety of anionic cyclic and acyclic oligostannides also phenyl group migration is observed.

In respect to corresponding gallium and aluminium compounds, number and structural diversity of tin cluster and cages are much smaller. Therefore, oligocyclic tin compounds can be considered as a fairly uninvestigated class of compounds.^[3] Among other strategies, these were accessed *via* the thermolysis of oligo-tin fragments,^[9,10] dehydrogenation of organotin(IV) trihydrides,^[11] disproportionation of tin(I) halides^[12] or the derivatisation of ZINTL ions.^[13] Observed phenyl group migration in conversions of diphenyltin dihydride with alkaline metals and alkaline metal derivatives inspired conversions of diaryltin dihydrides with low valent E(II) amides as an approach for the syntheses of molecular cages and clusters, which is presented in this work. Deployment of a low valent amide species enables introduction of naked tin centres into the resulting products already from the precursors and may also simultaneously force aryl group migration while forming Sn-Sn bonds. Therefore, more sterically demanding substituents than a phenyl group were introduced on the diaryltin dihydride for increased stabilisation of eventually formed metastable cages and clusters. Respective aryl substituents are depicted in Figure 3.1.

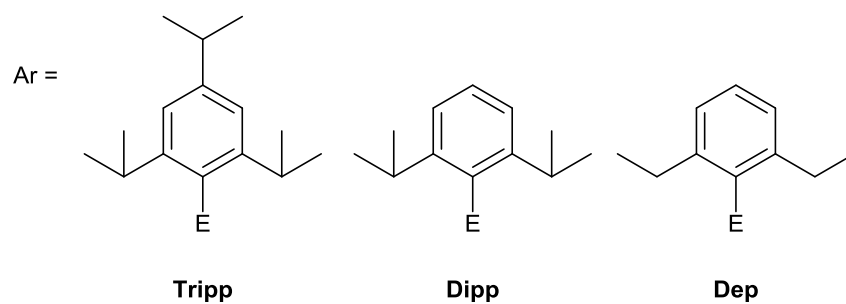


Figure 3.1 Illustration of chosen aryl groups with different sterically demanding *ortho* and *para* substituents.

While application of more stabilised E(II) amides in these reactions like LAPPERT's stannylene and germylene leads solely to Sn–Sn bond formation resulting in appealing compounds, still featuring hydride functionalities, using the more basic and more labile $\text{Sn}(\text{NEt}_2)_2$ resulted in the formation of a pentastanna[1.1.1]propellane and a metalloid tin cluster $\text{Sn}_{10}\text{Ar}_8$.

4 Literature

4.1 The Tin-Hydrogen bond

Compared to its lighter homologues, tin forms a rather instable bond to hydrogen. (See Figure 4.1) Instability and low bond dissociation energy of the tin-hydrogen bond enclose a wide range of possible reaction mechanisms, including heterolytical as well as homolytical bond cleavage. In case of heterolytical bond cleavage, calculated electronegativity difference would imply the release of hydride and the formation of a tin cation as a general reaction trend. Although examples involving R_3Sn^+ species are known, proton abstraction to yield R_3Sn^- fragments is well documented. (Section 4.1.1 Reactivity)

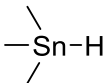
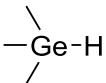
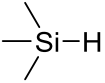
				
BDE (E-H)	253	289	323	[kJ/mol]
Δ EN (E-H)	0.48	0.18	0.46	(ALLRED and ROCHOW)

Figure 4.1 Overview of BDE's (Bond dissociation Energies) and Δ EN (Electronegativity difference) of Group 14 element-hydrogen bonds.^[14]

Stability of R_nSnH_{4-n} increases with increasing number of R substituents, whereas tin hydrides featuring alkyl substituents with equal sterical demand exhibit higher stability than corresponding aryl tin compounds. Under ambient conditions tin hydrides react rapidly with oxygen to the corresponding hydroxides or oxides.^[15] The Sn–H bond length varies, depending on the kind and numbers of substituents R, and its assessment is challenging.^[16] In IR spectroscopy symmetrical stretching ν_s of the Sn–H bond is observable as a strong, mostly isolated band in the range of 1800-1850 cm^{-1} . Corresponding deformation vibration δ falls into the range of 500-600 cm^{-1} .^[17]

Tin hydrides are mainly accessed *via* reduction of the corresponding tin halide, oxide or alkoxide using a metal hydride. Although reduction with $LiAlH_4$ is the most common route, also metal hydrides like R_2AlH , $NaBH_4$, $NaBH_3CN$, B_2H_6 , LiH , $(MeSiHO)_n$, Et_3SiH and R_3SnH are applicable in this reaction.^[18,19] Alternatively thermal decomposition of organotin formate,^[20] hydrolysis of a stannylmetallic compound^[21] or alkylation of a lithium tin hydride^[22] were used to obtain tin hydrides. The latter pathway enables a convenient route for the synthesis of organotin hydrides carrying mixed organic groups.

Organotinhydrides find a wide application in organic synthesis including hydrostannylation,^[23] reductions^[24] and many more. However, these reactions should not be discussed at this point.

4.1.1 Reactivity

The tin-hydrogen bond possesses a rather versatile reactivity. In Figure 4.2 an overview of the different reaction pathways is displayed. Reaction of an organotin hydride with an electrophile leads to the formation of a tin cation **(a)**. Opposed to this, conversion with a nucleophile yields a tin anion **(b)**. Homolytical bond cleavage occurs in the reaction with radicals **(c)**. In reaction with transition metal complexes, the transition metal is able to insert into the Sn-H bond intermediately **(d)**. This insertion intermediate is reported for transition metal catalysed Sn-E bond formation ($E = C^{[25]}, Sn^{[8]}$) using organotin hydrides.

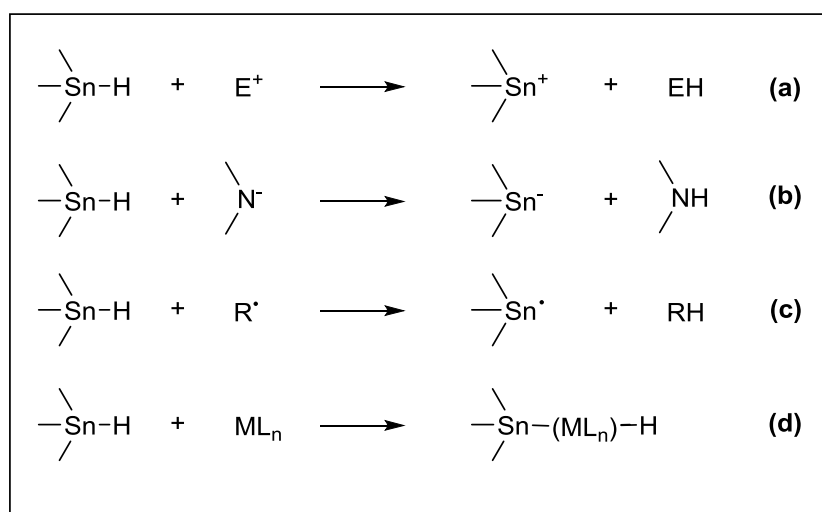
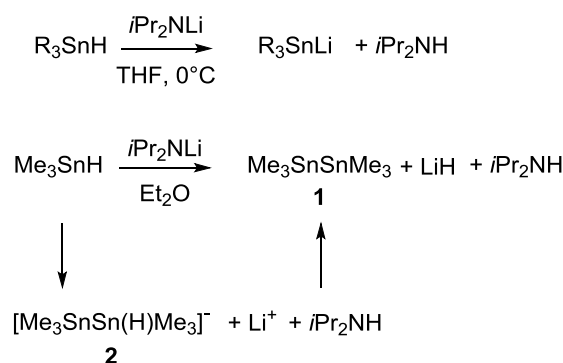


Figure 4.2 Overview of various reaction pathways of organotin hydrides.^[15]

The followed mechanism depends not only on the nature of the reactant, but also on the structure of the tin hydride itself. Additionally, choice of solvent as well as the presence of Lewis base or acid plays an important role in reactivity. Apparently, the presence of a radical initiator or inhibitor can trigger or respectively suppress a homolytical bond cleavage.

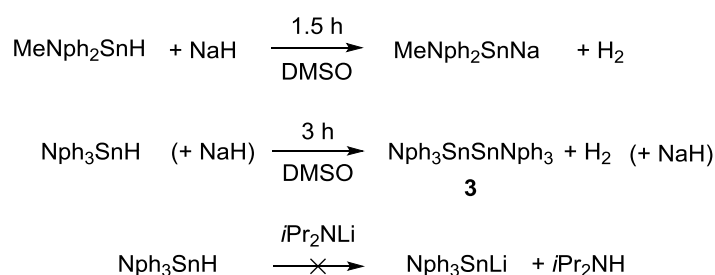
4.1.1.1 Metalation

When organotin hydrides react with strong organometallic bases, preferably mechanism **(b)** takes place and a metalated tin species is usually formed in terms of this reaction. (Figure 4.2) However, final outcome depends strongly on reaction conditions, choice of solvent and organic substituents of the tin hydride. As shown in Scheme 4.1, a trialkyltin hydride in THF at 0°C and lithium diisopropylamide give the corresponding organotin lithium species. In contrast, same reactants in Et₂O give the Sn-Sn bond coupling product hexaalkyldistannane **1** via the hydrostannyllithium intermediate **2**.^[26]



Scheme 4.1 Reactions of R_3SnH ($\text{R} = \text{Me}$ or Bu) with lithium diisopropylamide in different solvents. The choice of solvent and reaction conditions strongly influences the reaction product.^[26]

PODESTA and coworkers demonstrated the effect of the sterically demanding substituents on the reactivity of tin hydride as depicted in Scheme 4.2. Despite the less sterically hindered methyl dineophyltin hydride, conversion of trineophyltin hydride (neophyl = $\text{Nph} = -\text{CH}_2\text{CMe}_2\text{Ph}$) with NaH led, similar to the example above, only to the Sn-Sn coupling product **3**. In contrast to the tin hydride, in the case of trineophylgermanium hydride corresponding metalated species was accessed in a similar approach. Attempts to isolate a trineophylstannide through the reaction with lithium diisopropylamide failed, but were successful from the corresponding tin halide.^[27]



Scheme 4.2 Reactions of mixed hydride MeNph_2SnH and Nph_3SnH ($\text{Nph} = \text{Neophyl} = -\text{CH}_2\text{CMe}_2\text{Ph}$) with NaH in DMSO or respectively with lithium diisopropylamide. The steric demand of the the substituents affects the outcome of this reactions.^[27]

Although, side reactions like tin-tin bond formation occur in metalation of organotin hydrides, it still appears to be a convenient route towards monoanionic tin compounds. However, for isolation of tin-centred dianions other strategies must be applied, as it will be discussed in the next section.

4.2 Geminal, Vicinal and α, ω - Dianions of Tin

In contrast to widely reported class of tin-centred monoanions, only a few examples of dianionic tin species, geminal, vicinal as well as α, ω -dianionic, are described in literature. (Figure 4.3)

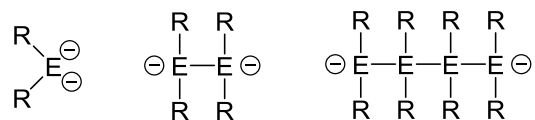
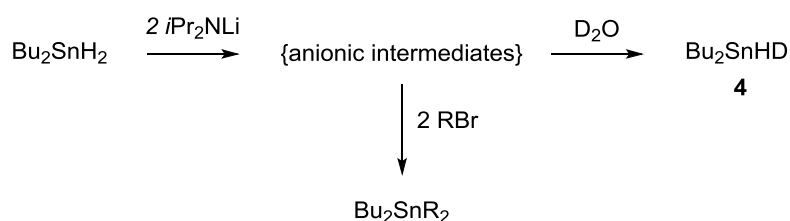


Figure 4.3 Geminal (left), vicinal (middle) and α, ω E-centred Dianions (E = Group 14 Element).

As in the reaction of organotin monohydrides and strong bases tin monoanions are formed, conversion of an organotin dihydride with similar compounds seem as an apparent route to the corresponding geminal dianionic species. However, when using the corresponding amount of strong base and subsequent deuteriolysis, which was already used to chemically confirm aryldialkylgermanes,^[28] only **4** was isolated. In contrast, conversion with organic electrophiles led to the corresponding mixed tetraorganostannane. This reaction product would be expected from a R_2Sn^{2-} species in solution.^[22] (Scheme 4.3) Due to this reaction behaviour, R_2Sn^{2-} , derived from the reaction of R_2SnX_2 (X = Cl, Br) and sodium in liquid ammonia, was earlier believed to be a crucial intermediate in organic synthesis^[29] and was postulated also as a stable product in the metalation of SnH_4 .^[30] Nonetheless, neither R_2Sn^{2-} was isolated from these reactions nor a spectroscopic proof for the existence of this dianionic species was mentioned in literature.

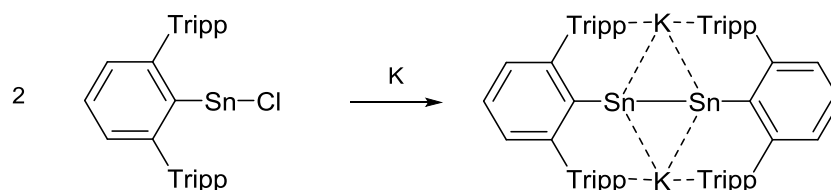


Scheme 4.3 Reaction of dibutyltin dihydride with lithium diisopropylamide and subsequent deuteriolysis respectively conversion with organic electrophiles (R = allyl, benzyl).

TRUMMER and CASERI were the first to investigate reactions of Bu_2SnCl_2 and Ph_2SnY_2 (Y = Cl, H, D) with sodium in liquid ammonia spectroscopically. Their study revealed that instead of the proposed intermediate, the vicinal dianionic species $[R_2Sn-SnR_2]^{2-}$ and monoanionic R_2SnH^- are present in these solutions.^{a,[31]} Accordingly, the only structurally authenticated geminal tin-centred dianion is the highly aromatic stannole dianion isolated by SAITO *et al.*^[32] Similar to CASERI among reductive

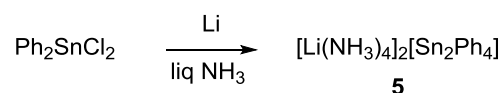
^a After adding bromoethane to investigated solutions, again expected mixed tetraorganostannanes were isolated from these reactions.

conditions, already earlier vicinal dianions were isolated. Likewise also a Sn-Sn bond formation occurs as in the examples shown below.^[33,34] (Scheme 4.4 and Scheme 4.5)



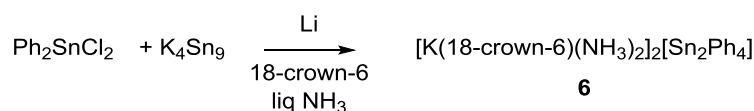
Scheme 4.4 Reaction of the divalent tin species (2, 6-Tripp₂C₆H₃)SnCl (Tripp = 2,4,6-triisopropylphenyl) with an excess of Potassium gives access to the vicinal distanny dianion.^[33]

On a similar preparation method as for compound **5**, access to [Li(NH₃)₄]₂[Sn₂Ph₄] is granted starting from tetraphenyltin.^[35]



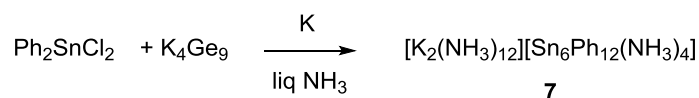
Scheme 4.5 Conversion of Diphenyltin dichloride with elemental lithium in liquid ammonia yielded compound **5**.^[34]

Nine years later KORBER and coworkers reported the synthesis of the same kind of dianionic tin compound. Conversion of Ph₂SnCl₂ with the binary ZINTL-phase K₄Sn₉ in the presence of lithium in liquid ammonia led to compound **6** illustrated in Scheme 4.6. Tin backbones in both structures **5** and **6** exhibit similar geometrical properties and a noticeable bond elongation compared to Ph₆Sn₂.^[36]



Scheme 4.6 Conversion of diphenyltin dichloride with the binary ZINTL phase K₄Sn₉ and an excess of lithium in liquid ammonia resulted in compound **6**. Its anion Sn₂Ph₄²⁻ shows structural similarities to the corresponding tin backbone of **5**.^[36]

The repetition of above depicted reaction with K₄Ge₉ and potassium resulted in the isolation of **7**, which contains a *catena*-[Sn₆Ph₁₂]²⁻ anion in moderate yield. (Scheme 4.7) This substructure is one of sparse examples for α, ω-dianionic tin chains.^[36,37]



Scheme 4.7 From the reaction of diphenyltin dichloride, K₄Ge₉ and potassium compound **7** was isolated. Role of the ZINTL phase in this reaction is not clearly solved.^[36]

Intensive colouring of cited vicinal and α, ω-dianionic tin compounds originates from σ-bond conjugation in covalently linked tin backbones.

4.2.1 σ -delocalisation

Already in the 1970s GILMAN *et al.* reported strong absorption in the UV spectral region of permethylated silane oligomers.^[38,39] This uncommon property compared to corresponding carbon chain was later explained by the widely accepted concept of σ -delocalisation. Due to delocalisation of electrons between Si sp^3 Orbitals in the group 14 element chain, strong $\sigma \rightarrow \sigma^*$ transitions are possible, which decrease in energy with catenation.^[40-42] It was later shown that heavier atoms like germanium in the backbone lead to lower band gaps.^[43,44] Moreover, polystannanes exhibit even more pronounced red-shifted $\sigma \rightarrow \sigma^*$ transitions (390-340 nm) compared to analogous polysilanes and polygermanes. However, choice of substituents affects accomplishable band gaps, too. Not only that they influence the conformational arrangement of the metal backbone – theoretical calculations suggested a planar zigzag conformation for ideal σ -conjugation – but also covalently bonded aryl substituents can cause additional σ - π delocalisation.^[45] (Figure 4.4) Due to their attractive properties σ -conjugated compounds are considered as promising materials in applications like microlithography, semi-conductors and non-linear optical devices.^[4,5] In the past, polystannanes were mainly accessed *via* WURTZ-coupling, condensation reactions, electro-chemical synthesis and dehydrogenative coupling of diorganotin dihydrides using amine bases, heat or transition metal complexes. An overview of these methods of synthesis is given in the review from BRAUNSTEIN and MORISE.^[8]

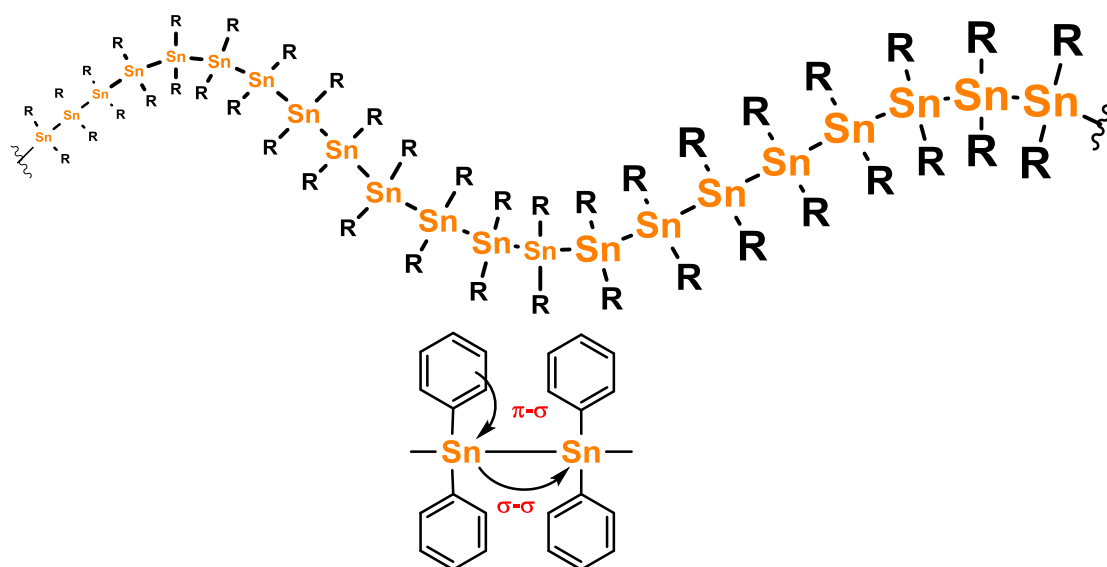


Figure 4.4 Polystannane chain. Illustration of σ - σ -bond conjugation and additional σ - π -conjugation.

4.3 Molecular Cages and Clusters of Tin

Similar to group 14 element polymers, nanometer sized cages and clusters are promising materials for novel technologies, which enclose completely new opportunities in terms of e.g. non-linear optics and electronic devices.^[6,7] It was lately shown that this class of compounds exhibit not only structural similarity to atoms at elemental surfaces, but also related reactivity was observed too.^[46,47] On this account, their synthesis and properties are topics of constant interest.

Next to many others organotin hydrides were found to be promising reagents for the synthesis of ligand stabilized cages as well as metalloid clusters and therefore also prove their versatility.^[11,48] In the following chapter, methods of synthesis, structural investigations and reactivity of molecular tin cages and clusters will be discussed.

4.3.1 Categories

Polyhedral compounds can be mainly classified into three categories. First, anionic ZINTL ions $[\text{Sn}_n]^{x-}$ (for $n = 5$, $x = 2$ and for $n = 9$, $x = 3$ or 4) are derived from binary alloys of tin with an alkaline metal in absence of any ligands.^[49] In contrast, ligand-stabilised cages and clusters possess the same number of organic ligands as metal atoms and are described with the general formula Sn_nR_n . A special class of these compounds is shaped by metalloid clusters Sn_nR_m ($n > m$), in which ligand-bound tin atoms occur next to "naked" tin atoms, which are only bound to other tin atoms.^[12] Examples of each class are illustrated in Figure 4.5.

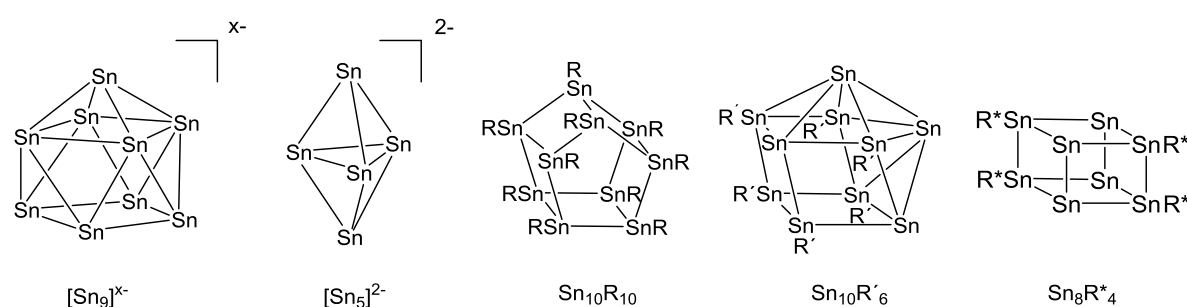


Figure 4.5 Illustration of some examples of each cage or respectively cluster category. On the left two tin ZINTL ions are depicted ($x = 3$ or 4). Two metalloid tin clusters are displayed on the right side ($\text{R}' = \text{Si}(\text{SiMe}_3)_3$, $\text{R}^* = 2,6\text{-Me}_2\text{C}_6\text{H}_3$). In the middle a ligand-stabilised cage is illustrated ($\text{R} = 2, 6\text{-Diethylphenyl}$).

4.3.2 Synthesis Strategies

Most of commonly known strategies for the synthesis of tin clusters can be accounted with one of the following methods. Thermolysis or reduction of oligo-tin fragments was applied already early and has also recently proven to be an encouraging route towards polyhedral compounds.^[9,10,50,51] Solely metalloid tin clusters were accessed by controlled disproportionation of tin(I) halides in the presence of stabilizing ligands. Latter synthesis strategy, which requires high preparative effort and specialized equipment, was mainly established by SCHNEPF in case of group 14 metal clusters.^[12] Derivatisation of Zintl ions also gives access to cluster compounds of tin.^[52] Additionally, reduction of tin halides or amides represents a popular method giving access to a wide range of structures. Last-named strategy was applied in different combinations of tin chlorides, from low valent tin species to spacer-bridged bis(organotin dichloride), and reducing agents, from classical reducing agents like KC_8 to more unusual reagents like Mg(I) and Ga(I) compounds.^[53–56] Similar compounds can be accessed through thermolysis of low valent tin hydrides.^[57,58] Lately, WESEMANN showed that dehydrogenative coupling of organotin trihydrides featuring organic substituents with moderate to high steric bulk can lead to polyhedral compounds, including also metalloid clusters.^[11,48]

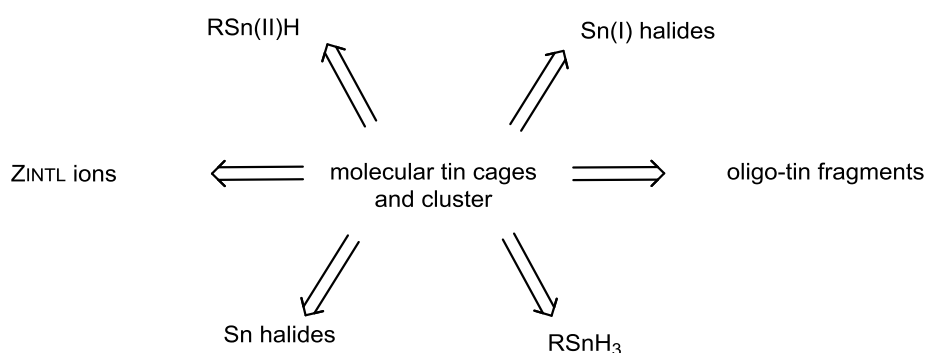


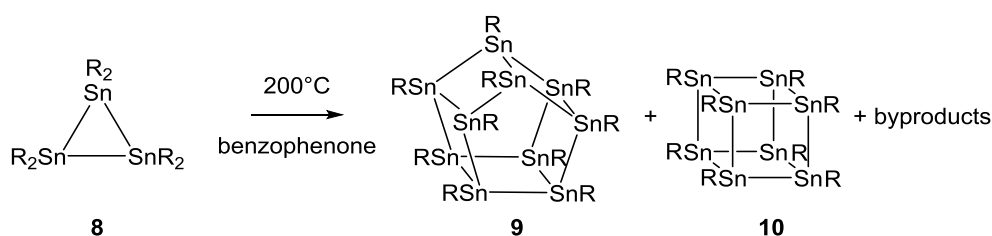
Figure 4.6 „Retrosynthetic“ overview of synthesis methods for molecular tin cage and cluster compounds.

4.3.3 Ligand-stabilised Cages and Clusters

This class of compounds can be described with the general formula Sn_nR_n . However, there are examples in literature, which correspond to this simplified description, but because of “naked” tin atoms in their structural arrangement, they are rather associated with metalloid clusters.^[11] Compounds isolated by SITA and later WIBERG can be considered as paramount examples for this group of compounds.

In 1991, after initial proceedings one and two years earlier, KINOSHITA and SITA reported that thermolysis of hexakis(2,6-diethylphenyl)cyclotristannane (**8**) in the same amount by weight of

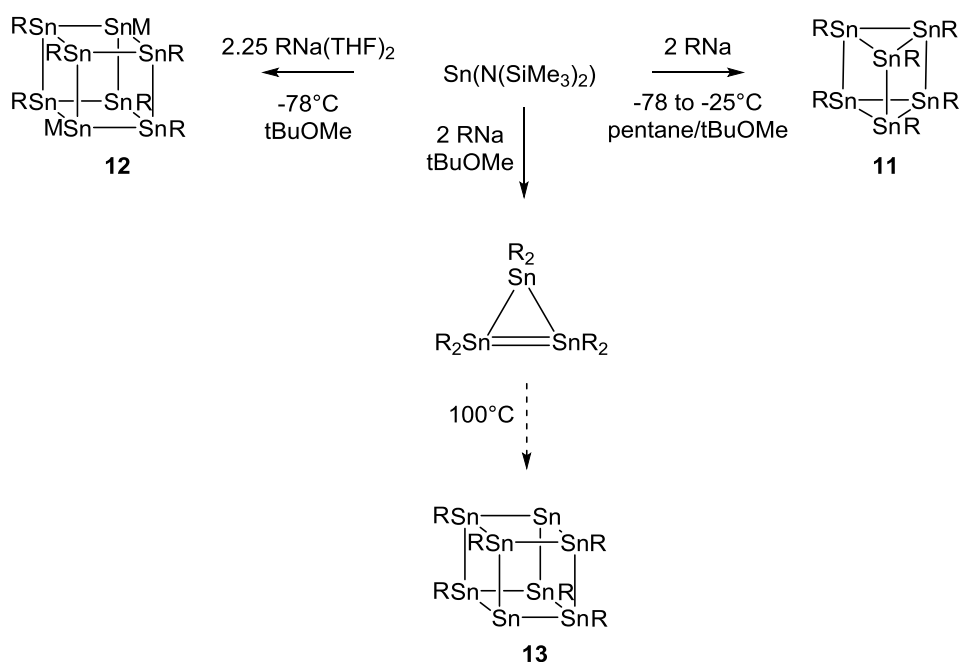
benzophenone at 200°C results in a mixture of polycyclic compounds and other tin-containing structures. The novel prismanes decakis(2,6-diethylphenyl)decastanna[5]prismane (**9**) and octakis(2,6-diethylphenyl)octastanna[4]prismane (**10**) were isolated in a combined yield of 12% from this mixture through purification by chromatography on silica. (Scheme 4.8) Alongside unreacted starting material (12%) and other tin-containing structures, hexakis(2,6-diethylphenyl)distannane and hexakis(2,6-diethylphenyl)pentastanna[1.1.1]propellane were identified as additional products of this reaction. In contrast, changing the solvent to naphthalene, only 49% conversion was observed and previously mentioned stanna[n]prismanes **9** and **10** were isolated in yields below 2-3%. It was suggested, that crucial intermediates leading to (RSn)_n prismanes are stabilised more efficient by benzophenone than naphthalene. Thermal interconversion between the two prismanes was attempted unsuccessfully.^[9,59,60]



Scheme 4.8 Thermolysis of **8** led to **9** and **10** in 12% combined yield (R = 2, 6-diethylphenyl). Cages were isolated in a 2.3:1 ratio. Hexakis(2,6-diethylphenyl)distannane and hexakis(2,6-diethylphenyl)pentastanna[1.1.1]propellane were identified as main byproducts. Additionally, unconverted starting material was isolated.^[9]

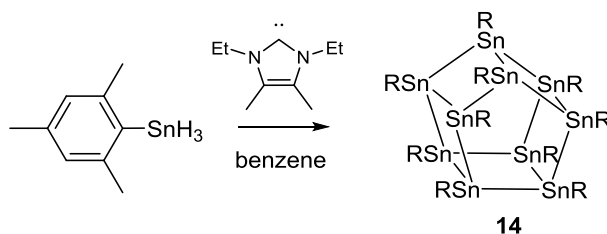
Nine years later, WIBERG *et al.* were able to isolate structural related compounds on a different approach. In the reaction of LAPPERT'S stannylene with two equivalents of sodium supersilylide led to hexakis(tri-tert-butylsilyl)hexastanna[4]prismane (**11**). Using the THF adduct of sodium supersilylide instead, the polyhedral octastannandiide **12** was isolated. In the same work, the formation of compound **13** was proposed in the thermolysis of tetrasupersilyl-tristannacyclopropene. However, appearance of **13**, which would be classified into subsequent described metalloid clusters, could not be proven by NMR^b or structural analysis by X-Ray crystallography sufficiently. Since anionic cages like **12** exhibit "naked" tin centres, which only participate in metal-metal bonds and feature no carbon substituent, these compounds show a close affiliation to metalloid tin clusters as **13**.

^b It was suggested that because of insolubility or paramagnetic properties of compound **13** no sufficient NMR data can be recorded. Recorded EPR spectra remain still unexplained.



Scheme 4.9 Ligand-stabilised tin cages isolated by WIBERG *et al.* Variation of the reaction conditions leads to different products. R-R was isolated as byproduct in every case. (R = Si^tBu₃, M = Na(THF)₂).^[61]

More recently, WESEMANN and coworkers were able to isolate **14**, which is structurally related to compound **9**.^[48] (Scheme 4.10) Compared to the other categories of molecular cages and clusters, ZINTL ions and metalloid clusters, tin cores in ligand-stabilised cages can be considered as electron precise and can be described solely by two-electrons, two-centre bonds.^[2]



Scheme 4.10 Reductive elimination of hydrogen from mesityltin trihydride forming a ligand-stabilised cage (R = 2, 4, 6-Trimethylphenyl).^[48]

4.3.4 Metalloid Tin Clusters

In contrast to previously discussed examples of ligand-stabilised cages, nature of bonding in most metalloid clusters cannot be described by classic valence bond theory. A “two-electrons-two-centre” notation of element-element bonds often seems insufficient for this kind of compounds to describe their behaviour and structure.^[62] Nevertheless, WADE’s rule is widely able to describe bonding situations and structure in non-multishell clusters.^{c, [63]} The formula Sn_nR_m ($n > m$) is a widely accepted guideline to categorise metalloid clusters. A more accurate phrasing was verbalised by SCHNÖCKEL and coworkers: “Metalloid (metal-like) clusters should be epitomised by the property that the number of metal-metal contacts exceeds the number of metal-ligand contacts and by the presence of metal atoms, which participate exclusively in metal-metal interactions.”^[64]

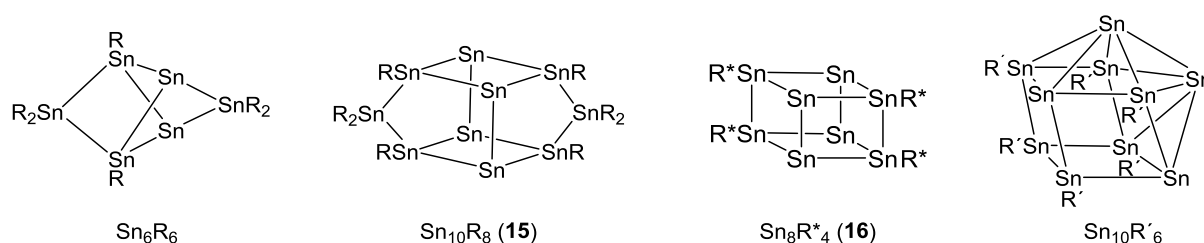


Figure 4.7 Examples for metalloid tin clusters ($\text{R} = 2,4,6\text{-Triisopropylphenyl}$, $\text{R}^* = 2,6\text{-Me}_2\text{C}_6\text{H}_3$, $\text{R}' = \text{Si}(\text{SiMe}_3)_3$). Cluster **15** and **16** show a similar structural pattern in their centre.

4.3.4.1 Thermodynamic and Structural Considerations

Metalloid tin clusters can be considered as a bridge between molecules and solid state. Their structural motifs often resemble parts of solid structure of the metal. Consequently metalloid tin clusters may be regarded as metastable intermediates on the way to bulk phase. (Figure 4.8)

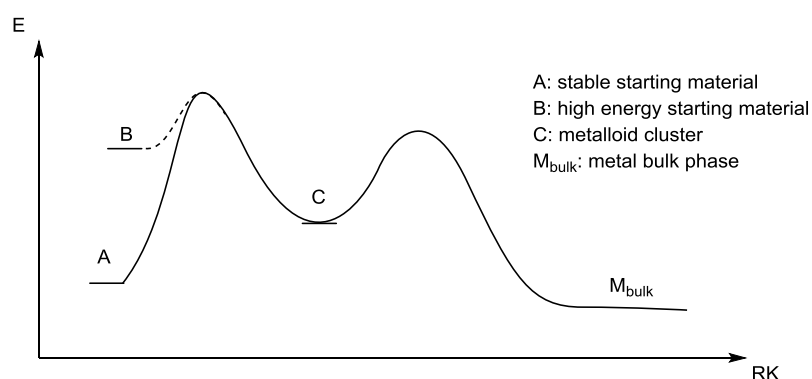
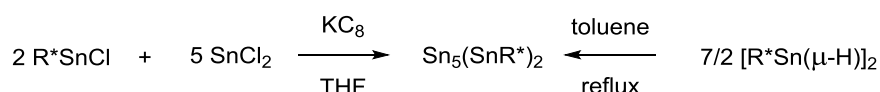


Figure 4.8 Schematic development of the energy during the synthesis of a metal from oxidised starting material.^[3]

^c Multishell clusters are a rare class of compounds in case of tin as opposed to aluminium and gallium. $\text{Sn}_3\{\text{Sn}(\text{NRR}')\}_6$ ($\text{R} = \text{SiMe}_3$, $\text{R}' = 2,6\text{-diisopropylphenyl}$) is the only example for a tin multishell cluster.^[53]

Due to their metastability, clusters are likely to form the bulk metal. Therefore, ligands with a certain sterical demand e.g. terphenyl ligands have to be introduced for stabilising these compounds kinetically and prevent formation of the bulk metal.^[3] As depicted in Scheme 4.11, the reduction of R^*SnCl and $SnCl_2$ with potassium graphite as well as the thermolysis of $[R^*Sn(\mu-H)]_2$ resulted in the same metalloid cluster.^[57] This observation suggests that ligands with similar sterical demand stabilise similar tin cluster cores.



Scheme 4.11 Synthesis of $[Sn_7(R^*)_2]$ ($R^* = 2,6$ -bis(2,6-diisopropylphenyl)phenyl) using two different routes. The reduction of R^*SnCl in presence of $SnCl_2$ with potassium graphite (KC_8) led to the same metalloid tin cluster as thermolysis of the low valent tin hydride dimer $[R^*Sn(\mu-H)]_2$.^[57]

Also FISCHER and coworkers gained compound **17** with the same tin cluster framework *via* the reduction of $SnCl_2$ with $Ga(ddp)$ ($ddp = HC(CMeNC_6H_3-2,6-iPr_2)_2$). As depicted in Figure 4.9 the ligands in the latter two examples show similarities in bulkiness. This leads to the assumption, that similar sterically demanding ligands form same or related stable tin scaffolds, which can be accessed in more than one way.

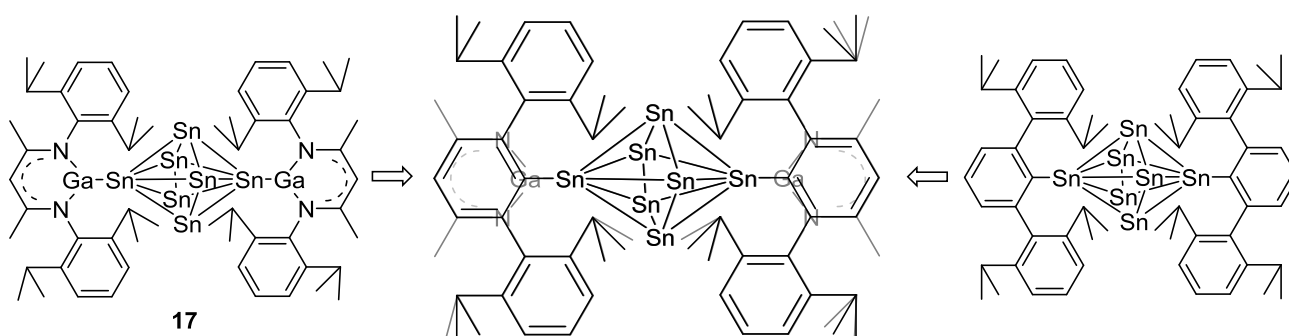
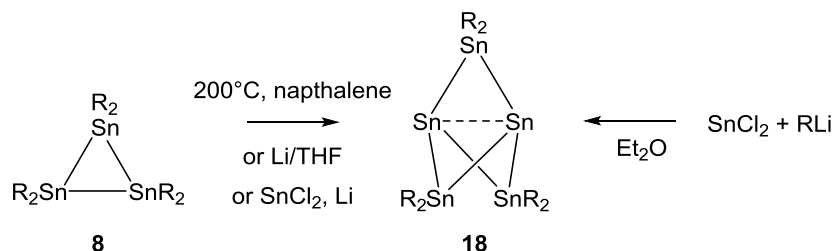


Figure 4.9 Similar sterically demanding ligands can lead to similar compounds. Overlay of the two structurally related clusters featuring similar substituents shows the same structural demand of their ligands.^[55,57]

4.3.4.2 Pentastanna[1.1.1]propellane

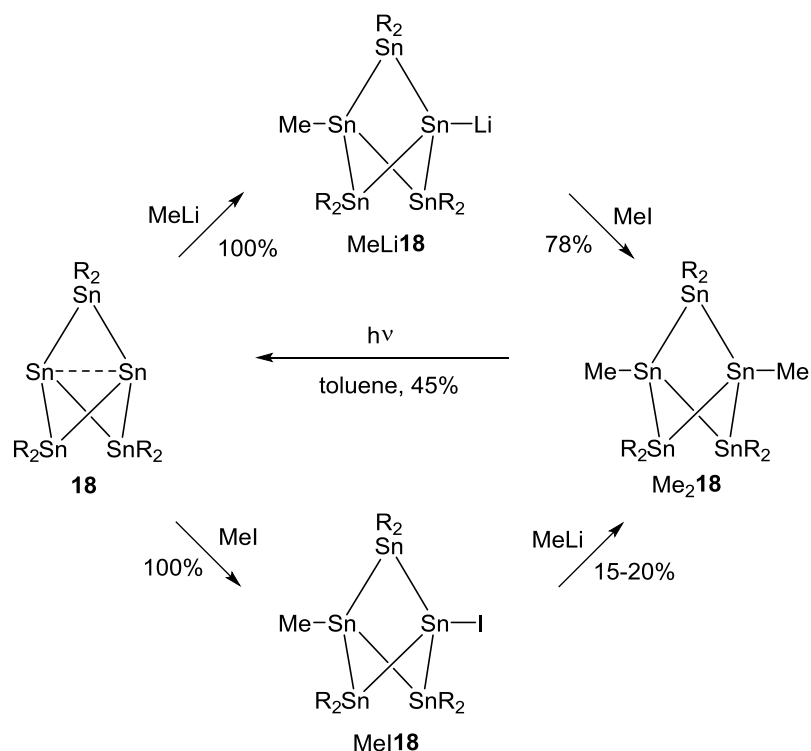
According to general formula Sn_nR_m ($n > m$), heavy [1.1.1] propellanes Sn_5R_6 cannot be numbered among metalloid clusters. Nevertheless, they can be described as metalloid in SCHNÖCKEL'S definition. First isolation of the pentastanna[1.1.1]propellane **18** was accomplished by SITA and coworkers *via* the thermolysis of **8** in xylene at $200^\circ C$.^[59] Later **18** was also gained in the reduction of the same starting material **8** with lithium in THF in higher yields.^[10] Also BREHER and DROST reported synthesis routes to also different substituted pentastanna[1.1.1]propellanes inspired by these early approaches.^[65,66] Applied synthesis methods are summarised in Scheme 4.12. Related silicon and germanium propellanes could also be accessed under reducing conditions using appropriate

germanium and silicon precursors.^[67,68] Due to their structural properties and their “non-classical” bonding situation, heavy [1.1.1]propellanes received wide attention already before their first isolation.^[69–71]



Scheme 4.12 Synthesis of Pentastanna[1.1.1]propellane in different approaches. (Synthesis left: R = 2,6-diethylphenyl; right: R = 2,6-(*i*PrO)₂phenyl). The reduction of **8** with Li in THF also led to octakis(2,6-diethylphenyl)tetracyclo[4.1.0.0^{1,5}.0^{2,6}]heptastannane, a structural related derivative of **18** in 1% yield.^[10,59]

Theoretical as well as synthetic chemists try to clarify the nature of bonding between the two bridgehead atoms Sn^b more specifically. The structure of pentastanna[1.1.1]propellane can be described either with a bond formation between the bridgehead atoms (closed shell), or as a biradical. In the latter case each bridgehead atom keeps an electron itself, while sharing the other three valence electrons with neighbouring {R₂Sn} entities. Indeed, the Sn^b...Sn^b bond obtained in early X-Ray investigations is longer than conventional Sn-Sn bonds, but the singlet ground state and consequently the EPR silence are evidences for the interaction of the two opposing bridgehead atoms. Although heavy [1.1.1]propellanes have been extensively examined by theoretical calculations, e.g. TD-DFT (Time Dependent Density Functional Theory) for singlet triplet gap values and CASSCF (Complete active space self-consistent field) method for natural orbital occupation numbers, the bonding nature cannot be clearly defined, because either few experimental correlations were found or no clear thresholds of these parameters are set to define a biradical or closed shell species. Nevertheless, examination of reactivity can help to understand the nature of bonding between the bridgehead atoms too. For a closed shell species, nucleophilic attack is possible because of an accessible LUMO. In contrast, a radical type of reactivity would be expected for a biradical compound.^[50] First examination of reactivity was done by SITA and KINOSHITA, who were able to access Me₂**18** on two different approaches. (Scheme 4.13) Reaction of **18** and MeLi or respectively MeI led to quantitative conversion. Subsequent conversion of MeLi**18** with MeI resulted in lower yields than the reaction of MeI**18** with MeLi. Through photolysis of Me₂**18** starting material **18** was restored in 45% yield. Recovery of **18** was suggested to proceed *via* a homolytic cleavage of the Sn-C_{Me} bonds.^[72] Posterior reports showed that the pentastanna[1.1.1]propellane **18** and other tin-containing propellanes do not react with simple substrates like H₂O, PhOH, Me₃SnH and H₂anthracene in contrast to related Si and Ge compounds.^[50,67,68,73]

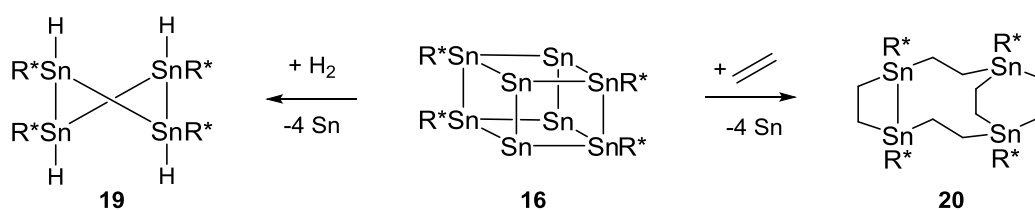


Scheme 4.13 Reactivity examination of **18** done by SITA and KINOSHITA (R = 2,6-Diethylphenyl).^[72]

Yet, **18** could be capped at the bridgehead atoms by the addition of $[\text{MCp}(\text{CO})_2]_2$ (M = Fe, Ru), which may occur *via* a homolytic cleavage of the M-M bond. As opposed to SITA's Me₂**18**, significant lengthening of the Sn^b...Sn^b distance is observed in the transition metal adducts $[\{\text{MCp}(\text{CO})_2\}_2\{\mu\text{-Sn}_5\text{Dep}_6\}]$ (M=Fe, Ru). Coupling in ¹¹⁹Sn NMR between the two bridgehead atoms was still observed, either because of "through space interaction" or through the bridging {R₂Sn} entities.^[65] In conclusion, no definite classification of [1.1.1]propellanes is possible, neither by theoretical calculations nor in terms of reactivity. Nonetheless, coupling of these electrons is required at least to some extent, which contributes to their stability and consequently makes them isolable. Therefore compounds of this class are stated as biradicaloids to distinguish them from true biradicals.^[74]

4.3.4.3 Activation of Small Molecules

Since the reaction of H₂ with the alkyne analogue Ar'GeGeAr' (Ar' = C₆H₃-2,6-(C₆H₃-2,6-iPr₂)₂) yielding a mixture of hydrogenated species,^[75] main group metal compounds are attracting greater interest regarding activation of small molecules.^[76-79] Eventually, also catalytic behaviour was observed.^[80] Just recently, POWER and coworkers showed the capability of metalloid tin clusters to activate small molecules. Under fairly mild conditions the cluster reacted with ethylene and hydrogen with the associated loss of all "naked" tin atoms. (Scheme 4.14) Reaction of the latter small molecule required moderate heating. Thereby formed tetrameric tin hydride **19** was also accessed *via* the reduction of $[\text{Ar}^*\text{Sn}(\mu\text{-Cl})]_2$ using DIBAL-H.^[81]



Scheme 4.14 Activation of ethylene and H₂ using the metalloid tin cluster [Sn₈Ar*₄] (Ar* = 2,6-Mes₂C₆H₃). The metalloid cluster was able to incorporate 5 ethylene molecules.^[81]

Frontier molecular orbitals exhibiting both donating and accepting properties, which are crucial for this kind of reaction,^[74] of model compound Sn₈Ph₄ were evidenced by theoretical calculations. Additionally, computations showed that incorporation of a sixth ethylene into **20** would be thermodynamically favoured, but was potentially blocked kinetically.^[81]

5 Results and Discussion

5.1 Diaryltin dichlorides and dihydrides

5.1.1 Synthesis

In terms of this thesis, five diaryltin dichlorides Ar_2SnCl_2 and respective hydrides Ar_2SnH_2 with varying steric bulk of the *ortho* or respectively *para* substituent were successfully synthesised and characterised by NMR spectroscopy and X-Ray crystallography. Selected aryl substituents are depicted in Figure 5.1.

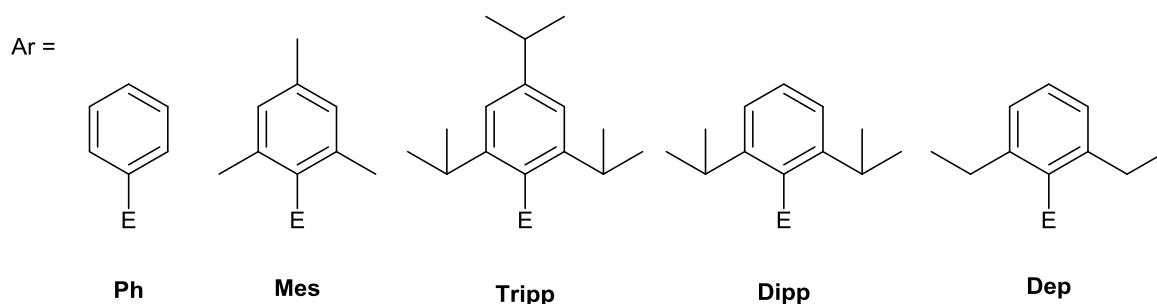
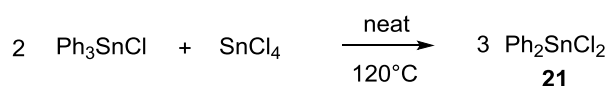


Figure 5.1 Illustration of selected aryl substituents with different sterically demanding *ortho* and *para* substituents for Ar_2SnCl_2 and Ar_2SnH_2 . Phenyl (Ph), 2,4,6-Trimethylphenyl (Mes), 2,4,6-Triisopropylphenyl (Tripp), 2,6-Diisopropylphenyl (Dipp) and 2,6-Diethylphenyl (Dep).

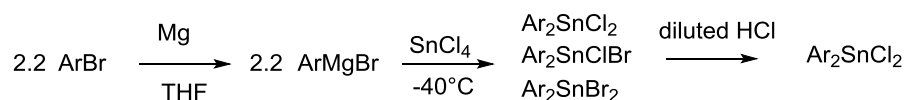
Diaryltin halides are commonly accessed *via* the initial synthesis of the corresponding tetra- or triaryltin halide and subsequent Kozeshkov redistribution reaction with the appropriate amount of SnX_4 (X = halide). Since access to solely the chosen tin halide derivative is granted and no halide mixtures are gained, this strategy is a convenient method for the synthesis of diaryltin dihydrides and was already applied for the synthesis of **21** and other diaryltin dichlorides.^[82] Likewise, we adopted this approach for the synthesis of **21**. (Scheme 5.1) Consumption of Ph_3SnCl and formation of mono as well as diphenyltin dichloride was monitored by ^{119}Sn NMR. If necessary, either Ph_3SnCl or SnCl_4 was added to the reaction.



Scheme 5.1 Synthesis of Ph_2SnCl_2 (**21**) using the Kozeshkov equilibrium.

Nevertheless, this approach was found to be insufficient for all other aryl substituents in terms of this work, as either the intermediate monoaryltin trichloride sublimed out of the reaction or only slow conversion was observed. Therefore, a GRIGNARD based route, already reported by MOLLOY and coworkers, was chosen.^[83] Using a ratio of $\text{ArBr} : \text{Mg} : \text{SnCl}_4 = 2.2 : 2.4 : 1.0$ (Ar = Mes, Tripp, Dipp,

Dep) in the preparation and subsequent slow addition of the GRIGNARD reagent to SnCl₄ at -40°C, led to the expected halide mixture Ar₂SnCl₂, Ar₂SnClBr and Ar₂SnBr₂ in the crude product. (Scheme 5.2) The ratio in abundance between those three species is not consistent and appears to be heavily dependent on solubility of resulting magnesium halides, dilution, temperature and drip rate of the GRIGNARD reagent solution.



Scheme 5.2 Synthesis of Ar₂SnCl₂ applying the direct GRIGNARD approach. (Ar = Mes (**22**), Tripp (**23**), Dipp (**24**), Dep (**25**)).

The crude product of all converted GRIGNARD reactions were investigated NMR spectroscopically after aqueous work up on NMR scale. Due to their complexity, resonances in ¹H and ¹³C spectra cannot be associated to compounds in the product mixture with certainty. In ¹¹⁹Sn NMR three signals can be observed. The most lowfield shifted signal is assigned to be Ar₂SnCl₂ for all aryl substituents because of strong correlations with literature values. Substitution of a chlorine by bromine leads to the successively upfield shifted resonances of Ar₂SnClBr and Ar₂SnBr₂. An overview of these resonances is given in Table 5.1. Distances between these signals range from 45-55 ppm. Same observations were already made by Molloy and coworkers.^[83]

Table 5.1 ¹¹⁹Sn NMR Shifts [ppm] of Ar₂SnCl₂, Ar₂SnClBr and Ar₂SnBr₂ in the crude product in CDCl₃.

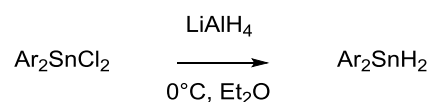
Ar =	Ar ₂ SnCl ₂	Ar ₂ SnClBr	Ar ₂ SnBr ₂
Mes ^d	-51.08	-96.17	-146.22
Tripp	-65.52	-115.64	-170.87
Dipp	-70.06	-120.35	-175.75
Dep	-65.38	-112.81	-164.90

For further treatment, the dry crude product was redissolved in a solvent mixture of DCM/THF (4:1) and was washed extensively with 1.0 M aqueous HCl. Due to this manipulation, a chlorine-bromine exchange occurs and solely diaryltin chlorides were isolated (overall yields 30-90%) and no bromine substituted compounds were detected by ¹¹⁹Sn NMR anymore. Using a small amount of THF to dissolve the crude product turns out to be crucial in case of Ar = Tripp, Dipp or Dep, as no halide exchange occurs when using only DCM as solvent. In case of Ar = Mes, the treatment leads also to the final dichloride by dissolving the crude product only in DCM. However, it appears to be not as

^d Values are in correspondence to literature.^[83]

quick. After this procedure, the organic layer was also washed with saturated brine solution, dried over Na_2SO_4 , filtered and the solvent was removed under reduced pressure. The so-gained crude product was then purified by recrystallization from DCM/*n*-heptane. In contrast to MOLLOY, who found solely the formation of a coupled ditin compound in the reaction of the more sterically demanding carbanion 2, 4, 6-triisopropylphenyl lithium with SnCl_4 , we did not observe the formation of a coupling product under the applied reaction conditions.^[83]

All diaryltin dihydrides were accessed *via* the widely applied reduction with LiAlH_4 in Et_2O of corresponding chlorides gained from above described procedure.^[82] (Scheme 5.3) Especially in the case of $\text{Ar} = \text{Ph}$, it turned out that the amount of reducing agent is crucial. A high excess of LiAlH_4 leads to a decrease in yield of diphenyltindihydride and the formation of deeply orange solutions, which are sensitive to air and H_2O . In terms of this thesis, the optimal stoichiometric ratio was found to be $\text{Ar}_2\text{SnH}_2:\text{LiAlH}_4 = 1.0: 0.8$. The side reaction when using an excess of LiAlH_4 will be discussed later in more detail (See 5.2.2 Anionic Cages).



Scheme 5.3 Reduction of Ar_2SnCl_2 with LiAlH_4 to access the corresponding Ar_2SnH_2 ($\text{Ar} = \text{Ph}$ (**26**), Mes (**27**), Tripp (**28**), Dipp (**29**), Dep (**30**)).

After 1-1.5 h reaction time, the suspension was quenched with 0.5 M aqueous H_2SO_4 and in order to remove aluminium complexes still present in the organic layer and to isolate a pure tin hydride the quenched reaction solution was washed with saturated potassium tartrate solution. Afterwards it was dried over Na_2SO_4 , filtered and the solvent was removed under reduced pressure resulting in yields from 40-84% referred to the amount of diaryltin dichloride. In earlier approaches, CaCl_2 was applied in drying the organic layer. However, in most cases the formation of a yellow solid while drying over CaCl_2 was observed and therefore lower yields were achieved with this kind of drying agent. Investigations of this side reaction will be part of future studies. No purification was necessary for the isolated hydrides except for $\text{Tripp}_2\text{SnH}_2$, which was recrystallised from *n*-pentane. All isolated diaryltin dihydrides, literature known as well as unknown structures, were investigated NMR and IR spectroscopically. Results of these examinations are summarised in Table 5.2. Diaryltindihydrides admittedly are stable against moisture, but react rapidly under ambient conditions with oxygen to the corresponding hydroxides or oxides.^[15] Yet, increasing stability of discussed diaryltin dihydrides against oxygen and higher temperatures was observed with increasing sterical bulk of the aryl substituent.

Table 5.2 Overview of ^{119}Sn NMR Shifts [ppm] and ^1J (^1H , $^{119/117}\text{Sn}$) [Hz] of discussed diaryltin dihydrides in C_6D_6 . Values of literature known compounds are in accordance to references.^[84–86]

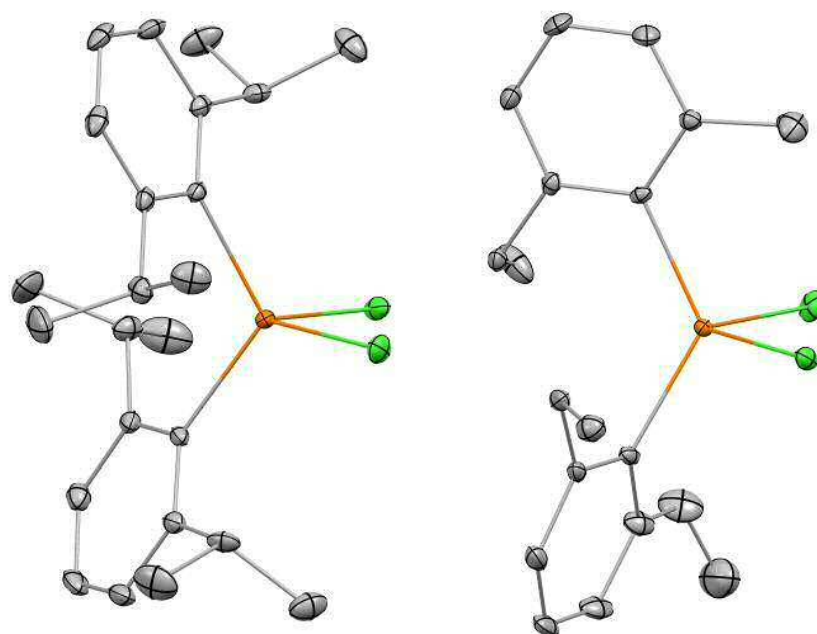
	^{119}Sn Shift	^1J (^1H , ^{119}Sn)	^1J (^1H , ^{117}Sn)	(Sn-H)
	[ppm]	[Hz]	[Hz]	[cm^{-1}]
Ph_2SnH_2 (26)	-234.08	1926.7	1840.4	-
Mes_2SnH_2 (27)	-352.82	1846.3	1764.8	1862
$\text{Tripp}_2\text{SnH}_2$ (28)	-352.29	1820.0	1736.8	1860
$\text{Dipp}_2\text{SnH}_2$ (29)	-355.41	1835.0	1753.3	1852
Dep_2SnH_2 (30)	-352.20	1843.8	1762.7	1846

5.1.2 X-Ray Crystallography

Although diaryltin dichlorides and dihydrides are a widely known class of compounds, still some of the isolated compounds have not been structurally investigated by X-Ray crystallography. This section summarises the crystallographic data of diaryltin dichlorides **24** and **25** as well as solid diaryltin dihydrides **28**, **29** and **30**, whose solid state structures have not been examined so far. More detailed information about measurements and refinement for presented compounds are depicted in the Appendix. All bond lengths and angles of presented diaryltin dichlorides fall into the known range. Their values are summarised in Table 5.3. In each case, the tin atom is found in a distorted tetrahedral environment covalently bound to two chlorines and two aryl substituents. (Figure 5.2) Notable, there is a total absence of intermolecular $\text{Cl}\cdots\text{Sn}$ interactions in all isolated structures. Both $\text{Dipp}_2\text{SnCl}_2$ (**24**) and $\text{Dep}_2\text{SnCl}_2$ (**25**) display slightly elongated average Sn–C bonds (2.145(1) and 2.157(3) Å), compared to compounds with no or less sterically demanding ortho-alkyl groups of the aryl substituent like Ph_2SnCl_2 (2.112(5) Å)^[87] and $\text{Mes}_2\text{SnCl}_2$ (2.117(2) Å)^[88]. As expected, Cl–Sn–Cl angles of **24** (94.40(3)°) and **25** (97.86(3)°) are also smaller than the respective angles in already mentioned compounds (Ph_2SnCl_2 : 101.7(1)°, $\text{Mes}_2\text{SnCl}_2$: 100.3(2)°). Tendencies of Sn–C bond lengths and Cl–Sn–Cl angles fit to the values of other diaryltin dichlorides featuring aryl groups with bulky ortho-substituents as $\text{Tripp}_2\text{SnCl}_2$ (2.147(4) Å and 98.0(1)°)^[89] and $\text{Mes}^*_2\text{SnCl}_2$ ($\text{Mes}^* = 2,4,6\text{-Tri-}t\text{-butylphenyl}$, 2.198(4) Å and 95.5(1)°)^[90]. No clear trend between sterical bulkiness of the aryl substituent and the C–Sn–C angle is observable.

Table 5.3 Selected bond lengths (Å) and angles (°) of discussed Ar_2SnCl_2 (Ar = Dipp, Dep).

	Space group	Sn–C [Å] (avg.)	Sn–Cl [Å] (avg.)	C–Sn–C [°]	Cl–Sn–Cl [°]
Dipp₂SnCl₂ (24)	P2 ₁ /c	2.145(1)	2.359(5)	119.4(1)	94.40(3)
Dep₂SnCl₂ (25)	C2/c	2.157(3)	2.361(7)	125.0(1)	97.86(3)

**Figure 5.2** Crystal Structures of discussed Ar_2SnCl_2 (Ar = Dipp (**24**, left), Dep (**25**, right)). All non-hydrogen atoms shown as 30% shaded ellipsoids. Hydrogen atoms are omitted for clarity.

Similar to already discussed chlorides, in all presented diaryltin dihydrides the tin is found in a distorted tetrahedral environment. (Figure 5.3) All hydrogen atoms bound to tin were located in the difference map. In Table 5.4 selected bond lengths and angles of all investigated hydrides are summarised. Due to high reactivity towards oxygen, there is only limited number of crystallographic data for tin hydrides available in literature and only two comparable structures such as Ph_2SnH_2 (crystallised from an *in situ* technique in a capillary) and Me_2SnH_2 are known.^[91,92]

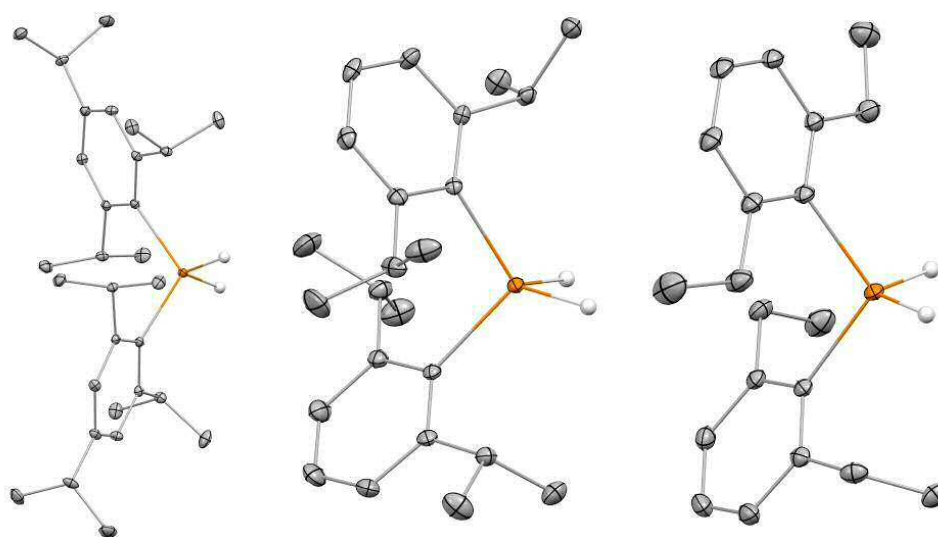


Figure 5.3 Structures of presented diaryltin dihydrides **28** (left), **29** (middle) and **30** (right). Ellipsoids possess a probability of 30%. Hydrogen atoms except Sn-H atoms are omitted for clarity.

The Sn–H bond lengths of presented structures compare nicely to Ph_2SnH_2 (1.65(6) Å avg.) and Mes_2SnH_2 (1.67(2) Å avg.), but as already discussed for corresponding chlorides again no trend between steric bulkiness of the aryl moiety and the C–Sn–C angle is legible. (Ph_2SnH_2 : 114.4(7)°; Mes_2SnH_2 : 111.07(4)°) As isolated diaryltin dihydrides show similar H–Sn–H angles as Ph_2SnH_2 (105.0(2)°) featuring a less bulkier organic moiety, no linear correlation of the steric pressure of the aryl substituents can be observed. The Sn–C bond lengths deviate only slightly from those of Ph_2SnH_2 (2.134(19) Å) and Mes_2SnH_2 (2.154(1) Å).^[91,92]

Table 5.4 Selected bond lengths (Å) and angles (°) of presented Ar_2SnH_2 (Ar = Tripp, Dipp, Dep) compared to those of literature known structures of Ph_2SnH_2 and Mes_2SnH_2 .^[91,92]

	Space group	Sn–C [Å] (avg.)	Sn–H [Å] (avg.)	C–Sn–C [°]	H–Sn–H [°]
Ph_2SnH_2 ^[91]	P2 ₁	2.134(19)	1.65(6)	114.4(7)	105.0(2)
Mes_2SnH_2 ^[92]	C2/c	2.154(1)	1.669(2)	111.07(4)	103.1(1)
Tripp₂SnH₂ (28)	P2 ₁ /n	2.166(1)	1.62(2)	116.19(5)	105.0(9)
Dipp₂SnH₂ (29)	Pca2 ₁	2.169(7)	1.70(8)	108.19(8)	103(1)
Dep₂SnH₂ (30)	P-1	2.163(2)	1.60(8)	111.24(6)	107(1)

Compared to diaryltin dichlorides, Sn-C bond lengths are only slightly elongated in corresponding tin dihydrides. Nevertheless, substituting the chlorine atoms by hydrogens can have a huge influence on the C-Sn-C angle as seen in $\text{Dep}_2\text{SnCl}_2$ (**25**) with an C-Sn-C angle of $125.0(1)^\circ$ whereas the corresponding hydride **30** displays a C-Sn-C angle of $111.24(6)^\circ$. A similar but not as strong trend is observable for $\text{Tripp}_2\text{SnCl}_2$ ($120.4(2)^\circ$)^[89] and TrippSnH_2 ($116.19(5)^\circ$) as well as for $\text{Dipp}_2\text{SnCl}_2$ ($119.4(1)^\circ$) and $\text{Dipp}_2\text{SnH}_2$ ($108.19(8)^\circ$).

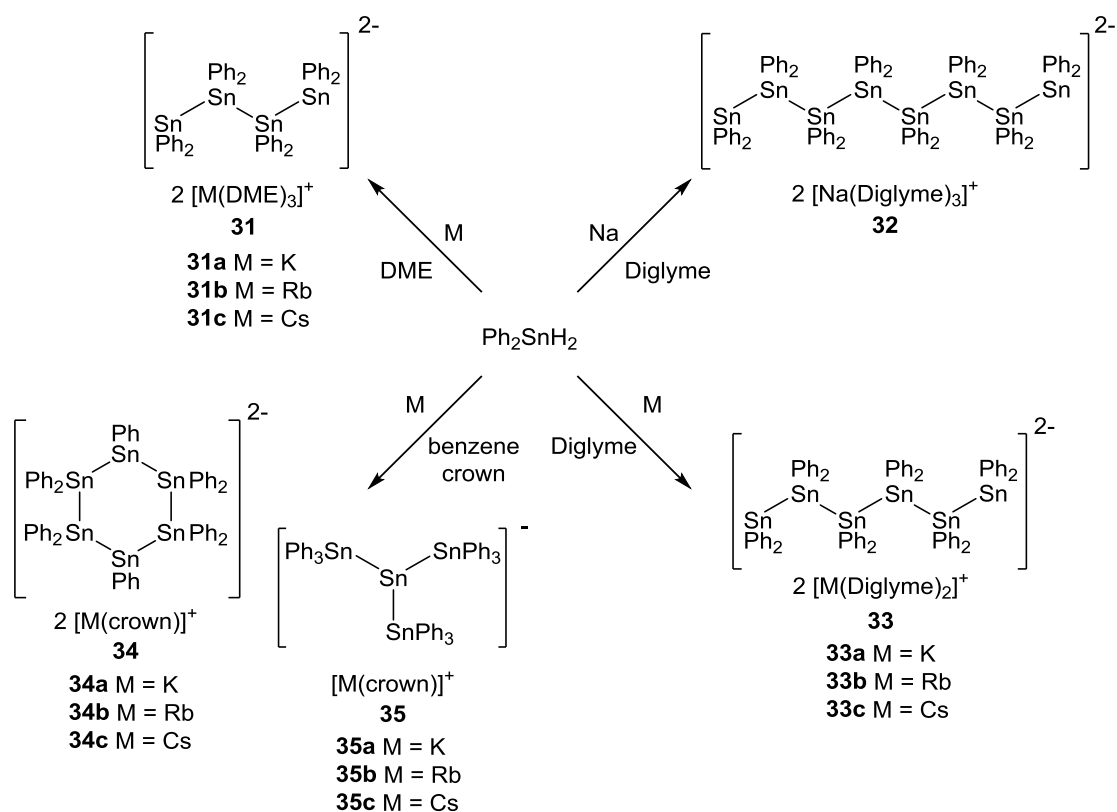
5.2 Anionic Compounds

5.2.1 Anionic Chains and Rings

Based on the earlier metalation approaches of triorganotin hydrides with strong lithium bases, GRIGNARD reagents and metal hydrides, the reactivity of diaryltin dihydrides towards alkaline metals and strong bases was investigated in various solvents.^[26,27,93] Results and observations will be summarised and discussed in this section.

5.2.1.1 Synthesis

Addition to diphenyltin dihydride to small pieces of alkaline metals (Na, K, Rb or Cs) well suspended in solvents like DME, diglyme and benzene/crown ether, immediately resulted in colour change to yellow, later orange or red, and vigorous hydrogen formation. As expected, colour change and evolution of hydrogen appeared more quickly for higher alkaline metals. Progress of the reaction seemed also to be more quickly in solvents like diglyme and DME than in a mixture of benzene/crown ether. After a few days from these reactions the products crystallised upon storage at room temperature and were identified by X-Ray crystallography. Depending on the solvent and to some extent on the metal, different compounds were isolated from these reactions. (Scheme 5.4) For applied alkaline metals in DME, the α, ω -dianionic tetrastannide **31** was obtained as orange crystals. Using sodium in diglyme gave the structural related octastannide **32**, which was isolated as dark, nearly black, shiny crystals. In contrast to sodium, the application of K, Rb and Cs in diglyme under same conditions led to the hexastannide **33** in good yields. Latter compound forms dichroic, green and red, crystals. In contrast to ethers, use of aromatic solvents like benzene mixed with the corresponding crown ether, resulted in the mixture of a dianionic cyclic species **34** and branched tetrastannide **35**. Phenyl group migration from a tin atom onto another has to occur for the formation of $[\text{Sn}_6\text{Ph}_{10}]^{2-}$ **34** (ratio of Sn:Ph < 2) and $[\text{Sn}_4\text{Ph}_9]^-$ **35** (ratio of Sn:Ph > 2) compounds. Already before terms of this thesis, similar results were found for lithium and lithium organyls as a metalation reagent.^[94] Additionally, compound **34** was also gained as a lithium derivative from reactions of diphenyltin dihydride and lithium diethylamide. Except for reactions in benzene, the described procedures result mostly in defined products without formation of elemental tin or any other byproducts. Nevertheless, mixtures of products were observed when using not analytically pure or already aged starting material. Especially the presence of residual aluminium species originating from the synthesis of the starting material using LiAlH_4 is critical.



Scheme 5.4 Summary of the reactions of Ph_2SnH_2 with alkaline metals in different solvents. The desired product can be accessed through choosing the respective solvent and/or metal. This reaction approach gives access to a rich variety of compounds.

Product mixtures were also noticed when the formal electron demand for the chain formation, which depends on the chain length, was not fulfilled and not enough reducing metal was used. This was especially crucial for the formation of **31**. As an excess of alkaline metal did not show any influence on the reaction outcome, it has proven itself to use up to double of calculated amount of alkaline metal. Only a few comparable compounds e.g. $[\text{Li}(\text{NH}_3)_4]_2[\text{Sn}_2\text{Ph}_4]$ and $[\text{K}_2(\text{NH}_3)_{12}][\text{Sn}_6\text{Ph}_{12}]$ were isolated years ago from reaction solutions of Ph_2SnCl_2 in liquid ammonia under reductive conditions. Some of these reactions also require the addition of ZINTL ions to form these dianionic compounds.^[34,36] Compared to this high effort methods, our room temperature route towards this rich variety of compounds is easy applicable and the product can be directed by choosing the respective solvent and/or the metal.

5.2.1.2 X-Ray Crystallography

All discussed anionic oligostannides have been structurally investigated by X-Ray crystallography. In this section the crystallographic data of these compounds will be discussed. Analysis of structure will mainly focus on the tin backbone. Since the tin backbone's structure is generally speaking unaffected by the nature of the counterion, values for the potassium derivatives will be shown representative for the isolated structures **31**, **33**, **34** and **35**. The sodium oligostannide **32** will be compared to these. Table 5.5 summarises the structural properties of discussed structures and related literature compounds. More detailed information about measurements and refinement for presented compounds is provided in the Appendix.

A common feature of all non-cyclic and non-branched compounds **31**, **33** and **32** is the all trans zig-zag arrangement of the tin-backbone. Additionally, in each compound the tin chain does not display significant twisting and all tin atoms lie in approximately one plane. Only a maximum deviation of 15° from the ideal dihedral angle of 180° is observed in solid state. (Figure 5.4) This arrangement was already suggested to be ideal for σ -conjugation by theoretical calculations and explains the intensive colouring of these compounds.^[45] In all cases Sn–Sn–Sn angles with values $122.82(2)$ - $140.36(1)^\circ$ are extremely widened compared to the ideal tetrahedral angle of 109.5° . In contrast, angle sums of anionic tin centres display much lower values than expected for an ideal tetrahedral arrangement ($3 \cdot 109.5^\circ = 328.5^\circ$). This observation implies a high s orbital character of the lone pair and high p character of bonding orbitals. In accordance with this observation are also the slight elongated bonds of the anionic tin centres compared to bond lengths of tetravalent tin atoms. (Table 5.5)

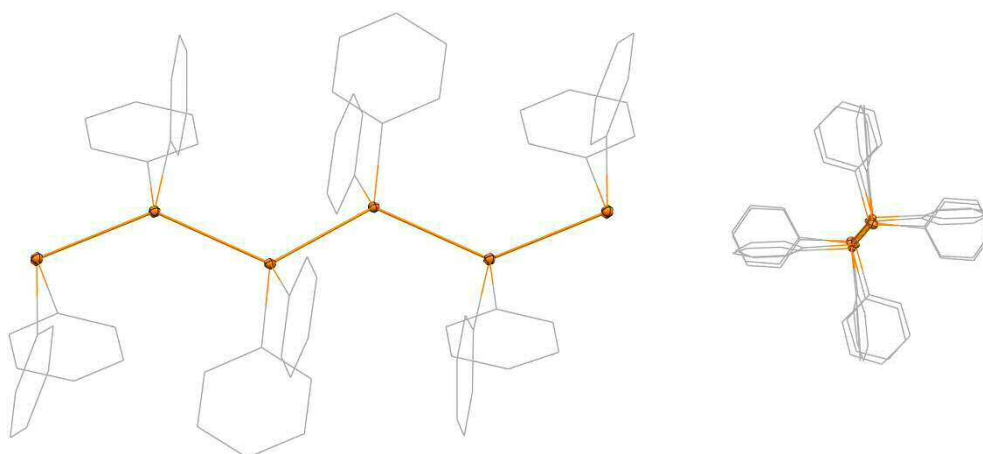


Figure 5.4 Alignment of the tin backbone of $[\text{K}(\text{diglyme})_2]_2[\text{Sn}_6\text{Ph}_{12}]$ (**33a**) (left) and $[\text{Na}(\text{diglyme})_2]_2[\text{Sn}_8\text{Ph}_{16}]$ (**32**) (right). The tin atoms arrange in an ideal all trans zig zag arrangement and all lie in approximately one plane.

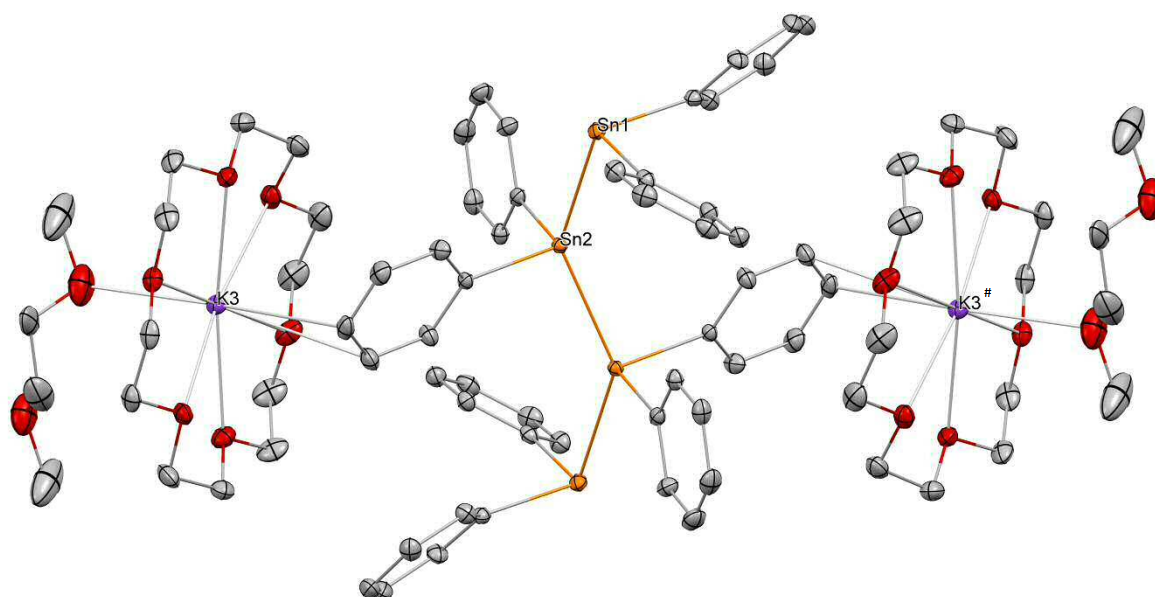


Figure 5.5 Molecular structure of $[\text{K}(\text{DME})(18\text{cr}6)]_2[\text{Sn}_4\text{Ph}_8]$ (**31a**). Hydrogens are omitted for clarity. Ellipsoids are displayed with 30% probability. **31a** forms a coordination polymer in solid state. The oxygen atom of the DME molecules interacts with the potassium ions of the next unit. Selected bond lengths [Å] and angles [°]: Sn1-Sn2 2.875(1), Sn2-Sn2# 2.8449(3), Sn1-C1 2.217(5), Sn1-C7 2.216(4), Sn2-C13 2.19(5), Sn2-C19 2.187(4), Sn1-Sn2-Sn2# 140.36(1), Sn2-Sn1-C1 103.2(1), Sn2-Sn1-C7 94.8(1), C1-Sn1-C7 94.8(1), C13-Sn2-C19 99.9(1).

Table 5.5 Overview of average bond lengths [Å] and angles [°] of discussed dianionic compounds and similar literature compounds. Values are shown for the corresponding potassium compounds of **31**, **33**, **34** and **35**.^e

	$\text{Sn}^- - \text{Sn}$	$\text{Sn} - \text{Sn}$	$\text{Sn}^- - \text{C}$	$\text{Sn} - \text{C}$	$\text{Sn} - \text{Sn} - \text{Sn}$	$\Sigma \text{Y} - \text{Sn}^- - \text{Z}$
	[Å] (avg.)	[Å] (avg.)	[Å] (avg.)	[Å] (avg.)	[°] (avg.)	[°]
$[\text{Sn}_2\text{Ph}_4]^{2-}$ [34]	2.9048		2.2214	-	-	287.85
$[\text{Sn}_2\text{Ph}_4]^{2-}$ [36]	2.9088		2.2570	-	-	291.20
$[\text{Sn}_4\text{Ph}_8]^{2-}$ (31)	2.8751(3)	2.8449(3)	2.2169(5)	2.1894(5)	140.36(1)	300.2(3)
$[\text{Sn}_6\text{Ph}_{12}]^{2-}$ [36]	2.8688	2.8308	2.2176	2.1779	126.96	295.13
$[\text{Sn}_6\text{Ph}_{12}]^{2-}$ (33)	2.8789(1)	2.8200(1)	2.213(1)	2.170(6)	129.49	294.4(1)
$[\text{Sn}_8\text{Ph}_{16}]^{2-}$ (32)	2.8724(6)	2.8300(5)	2.211(2)	2.166(9)	125.65(8)	288.2(6)
$[\text{Sn}_6\text{Ph}_{10}]^{2-}$ (34)	2.8626(5)	2.825(3)	2.23(1)	2.189(6)	124.98(2)	290.7(5)
$[\text{Sn}_4\text{Ph}_9]^-$ (35)	2.8162(5)	-	-	2.167(9)	-	292.17(3)

^e As webCCDC data bank gives only limited access to X-Ray data, literature values are here presented without standard deviation.

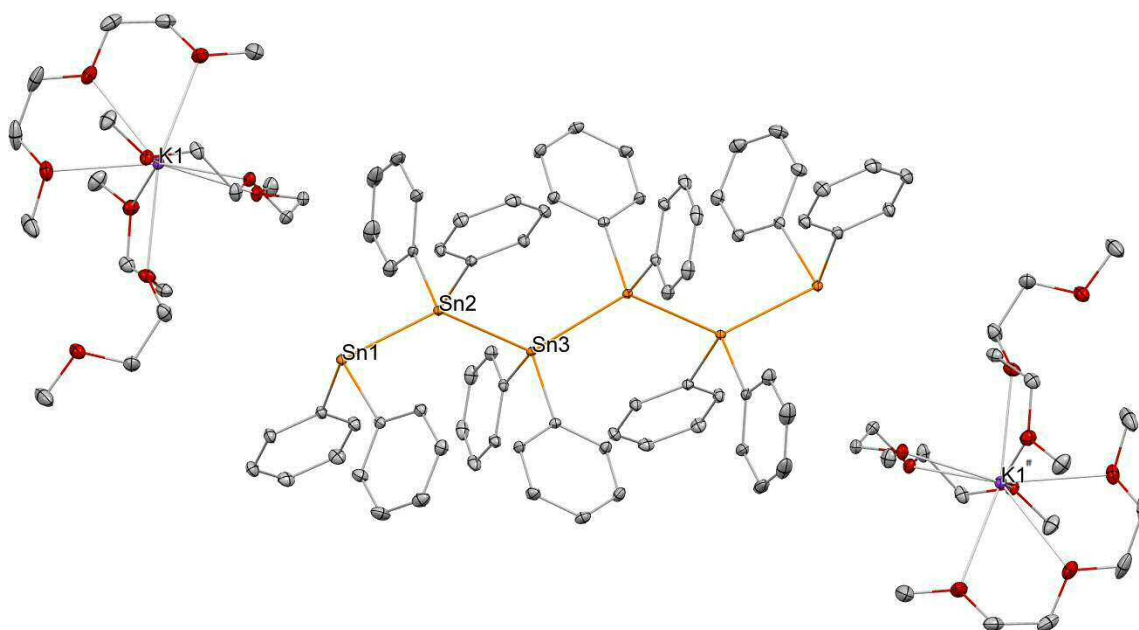


Figure 5.6 Molecular structure of $[\text{K}(\text{diglyme})_2][\text{Sn}_6\text{Ph}_{12}]$ (**33a**). Hydrogens are omitted for clarity. Ellipsoids possess a probability of 30%. Selected distances [\AA] and angles [$^\circ$]: Sn1-Sn2 2.8789(1), Sn2-Sn3 2.8258(1), Sn1-C1 2.217(1), Sn1-C7 2.209(1), Sn2-C13 2.178(1), Sn2-C19 2.174(1), Sn3-C25 2.173(1), Sn3-C31 2.157(1), Sn1-Sn2-Sn3 133.51, Sn2-Sn1-C1 97.89(3), Sn2-Sn1-C7 99.87(3), C1-Sn1-C7 99.87(3), C13-Sn2-C19 102.53(4).

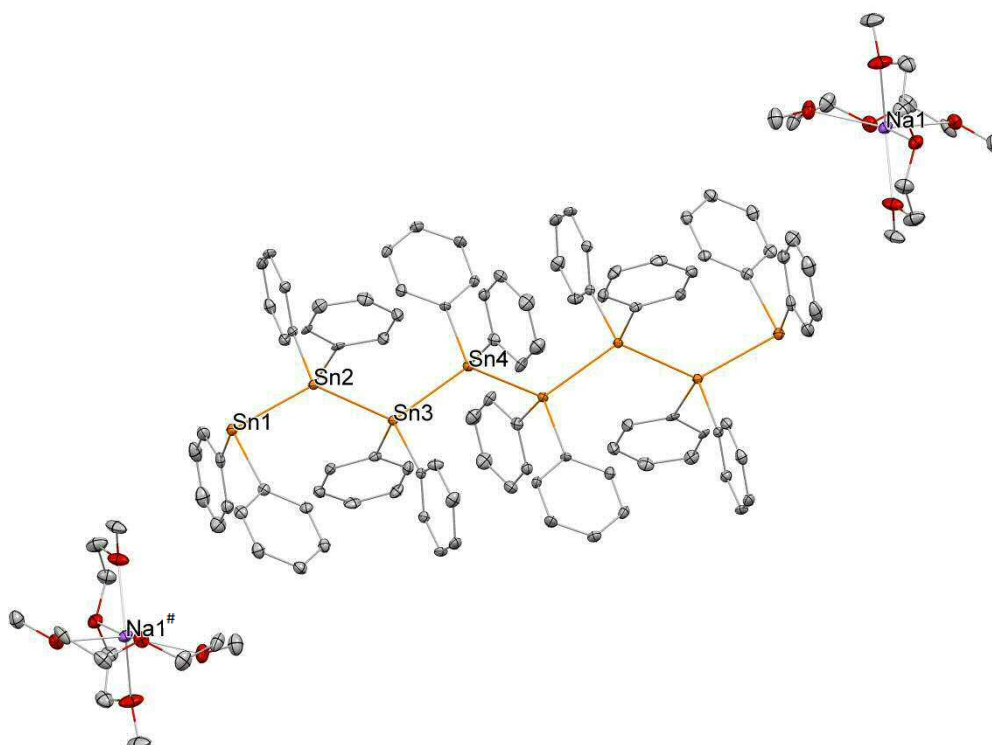


Figure 5.7 Molecular structure of $[\text{Na}(\text{diglyme})_2][\text{Sn}_8\text{Ph}_{16}]$ (**32**). Hydrogens are omitted for clarity. Ellipsoids are drawn with 30% probability. Selected distances [\AA] and angles [$^\circ$]: Sn1-Sn2 2.8724(6), Sn2-Sn3 2.8421(5), Sn3-Sn4 2.8274(6), Sn1-C1 2.218(7), Sn1-C7 2.203(6), Sn2-C13 2.178(5), Sn2-C19 2.173(7), Sn1-Sn2-Sn3 129.92(2), Sn2-Sn3-Sn4 122.82(2), C1-Sn1-C7 96.5(2), Sn2-Sn1-C1 97.8(2), Sn2-Sn1-C7 93.9(2), C13-Sn2-C19 101.7(2).

In contrast to most isolated structures of chain shaped oligostannides, a direct contact of the tin anion and the potassium cation is observable in the solid state structure of **34a** (3.667(5) Å) as well as **35a** (3.6889(5) Å). (Figure 5.8 and Figure 5.9) A similar interaction can also be found in the corresponding structures of potassium's higher homologues **34b** and **34c**. Common feature of all these compounds is also the chair conformation of the cyclic tin backbone with phenyl groups in the axial position at the anionic tin atom. Here again, the tricoordinate, anionic tin atom Sn3 displays a pyradimialised structure with an angle sum of 290.7(5)°, deviating from the ideal tetrahedral angle sum of 328.5°. Also Sn-Sn as well as Sn-C distances of the anionic tin centre (2.852(5)-2.872(2) Å and 2.23(1) Å) are slightly elongated to corresponding bonds of tetravalent tin atoms (2.825(3) Å and 2.18(1)-2.202(7) Å).

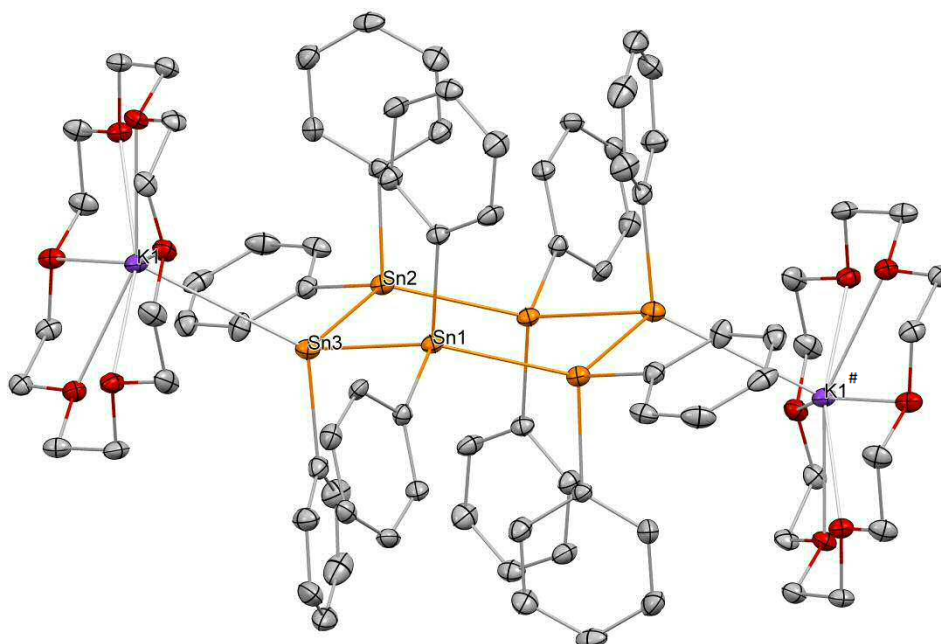


Figure 5.8 Molecular structure of $[\text{K}(\text{18crown6})]_2[\text{Sn}_6\text{Ph}_{10}]$ (**34a**). Hydrogens are omitted for clarity. Ellipsoids possess a probability of 30%. Selected bond lengths [Å] and angles [°]: Sn1-Sn3 2.872(2), Sn2-Sn3 2.852(5), Sn1-C7 2.18(1), Sn1-C13 2.193(8), Sn3-C1 2.23(1), Sn3...K 3.667(5), Sn1-Sn3-Sn2 94.51(2), C7-Sn1-C13 103.6(3), Sn1-Sn3-C1 95.9(2), Sn2-Sn3-C1 100.3(2).

The central tin atom in **35a** with Sn-Sn bond lengths from 2.8117(2) to 2.8251(2) Å deviates with an angle sum of 292.17(3)° from the ideal tetrahedral structure. Also for the corresponding Cs compound there is a direct contact between the tin anion and the counterion observable.

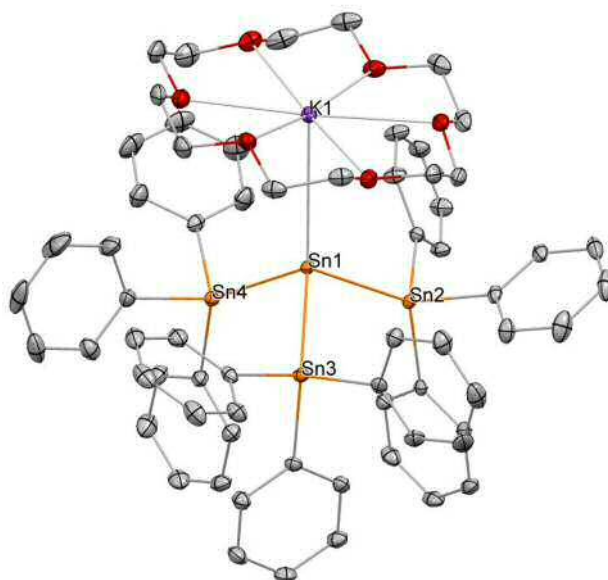


Figure 5.9 Molecular structure of $[K(18cr6)][Sn_4Ph_9]$ (**35a**). Hydrogens are omitted for clarity. Ellipsoids are drawn with a probability of 30%. In solid state a coordination polymer is formed through an interaction of the potassium with the a phenyl group of the next $[Sn_4Ph_9]^-$ unit. Selected distances [Å] and angles [°]: Sn1-Sn2 2.8251(2), Sn1-Sn3 2.8119(2), Sn1-Sn4 2.8117(2), Sn1...K1 3.6889(5), Sn2-Sn1-Sn3 96.89(1), Sn2-Sn1-Sn4 99.85, Sn3-Sn1-Sn4 99.85(1).

5.2.1.3 Spectroscopical data

Attempts of recording convincing ^{119}Sn NMR spectra of discussed dianionic chains failed, so far. Most common deuterated solvents turned out to be ineligible as the targeted compound often degraded upon solving through redistribution to a mixture of tin-containing products. Acetonitrile- d_3 seemed promising as no such visible degradation appeared after dissolution. However, no sufficient data was collected as these compounds show extremely broad signals and therefore no coupling constants are legible. Despite, values of the observed broad signals should be mentioned here: The tin backbone of $[Sn_4Ph_8]^{2-}$ (**31**) shows to broad singlets at -94 and -175 ppm. In accordance with these values, broad resonances are found at -92, -178 and -198 ppm for $[Sn_6Ph_{12}]^{2-}$ (**33**) and at -93, -177 and -178 ppm (2x) for $[Sn_8Ph_{16}]^{2-}$ (**32**). For cyclic $[Sn_6Ph_{10}]^{2-}$ (**34**) also broad signals at -140 and -190 ppm are detected. By comparison of these spectra, broader signals appear to be observed, the longer the chain grows. Theoretical calculations showed that dianionic tin chains possess a high degree of freedom in solution, which is even higher when the chain grows, and therefore are likely to move fluctuatingly. Broad signals may originate from the strong dependence of the NMR resonance on the conformation and the fluctuating movement of these compounds in solution. A more rigid systems like the monoanionic, branched $[Sn_4Ph_9]^-$ (**35**) shows precise resonances at -98 and -1066 ppm with coupling constants $^1J_{Sn,117/119Sn} = 6780/7097$ Hz and $^2J_{Sn,117Sn} = 866$ Hz in acetonitrile- d_3 . Considering this assumption, low temperature NMR analysis may facilitate the record of more satisfying data. As the dissolved compound recrystallised from acetonitrile, breakdown of

the chain in solution is excluded. In all spectra, the nature of the counterion did not show any effect on the tin backbone and stated ^{119}Sn resonances were found for all alkaline metal derivatives.

Due to σ -conjugation, all discussed anionic compounds exhibit intensive colourfulness and therefore were also investigated UV/Vis spectroscopically. Absorption spectra of the shortest dianionic chain $[\text{Sn}_4\text{Ph}_8]^{2-}$ (**31**) exhibits a maxima at 408 nm. Absorption spectra of $[\text{Sn}_6\text{Ph}_{10}]^{2-}$ (**34**) and $[\text{Sn}_4\text{Ph}_9]^-$ (**35**) exhibit similar shape and similar absorption maxima (417 and 405 nm) as **31**. As already indicated by the dichroic colouring of its crystals, two maxima at 390 and 446 nm are observable for hexastannide $[\text{Sn}_6\text{Ph}_{12}]^{2-}$ (**33**). Compared to latter transitions, two of three absorption maxima of $[\text{Sn}_8\text{Ph}_{16}]^{2-}$ (**32**) at 480 and 571 nm show a higher bathochromic shift. The third absorption maxima at 380 nm is slightly hypsochromically shifted compared to the one with highest energy of **33** (390 nm). Values of absorption maxima and UV/Vis spectra are summarised in Table 5.6 and Figure 5.10.

Table 5.6 Overview of absorption maxima of compounds $[\text{Sn}_4\text{Ph}_8]^{2-}$ (**31**), $[\text{Sn}_6\text{Ph}_{12}]^{2-}$ (**33**), $[\text{Sn}_8\text{Ph}_{16}]^{2-}$ (**32**), $[\text{Sn}_6\text{Ph}_{10}]^{2-}$ (**34**) and $[\text{Sn}_4\text{Ph}_9]^-$ (**35**).

	λ_{max} [nm]		λ_{max} [nm]
$[\text{Sn}_4\text{Ph}_8]^{2-}$ (31)	408	$[\text{Sn}_6\text{Ph}_{12}]^{2-}$ (33)	390, 446
$[\text{Sn}_6\text{Ph}_{10}]^{2-}$ (34)	417	$[\text{Sn}_8\text{Ph}_{16}]^{2-}$ (32)	380, 480, 571
$[\text{Sn}_4\text{Ph}_9]^-$ (35)	405		

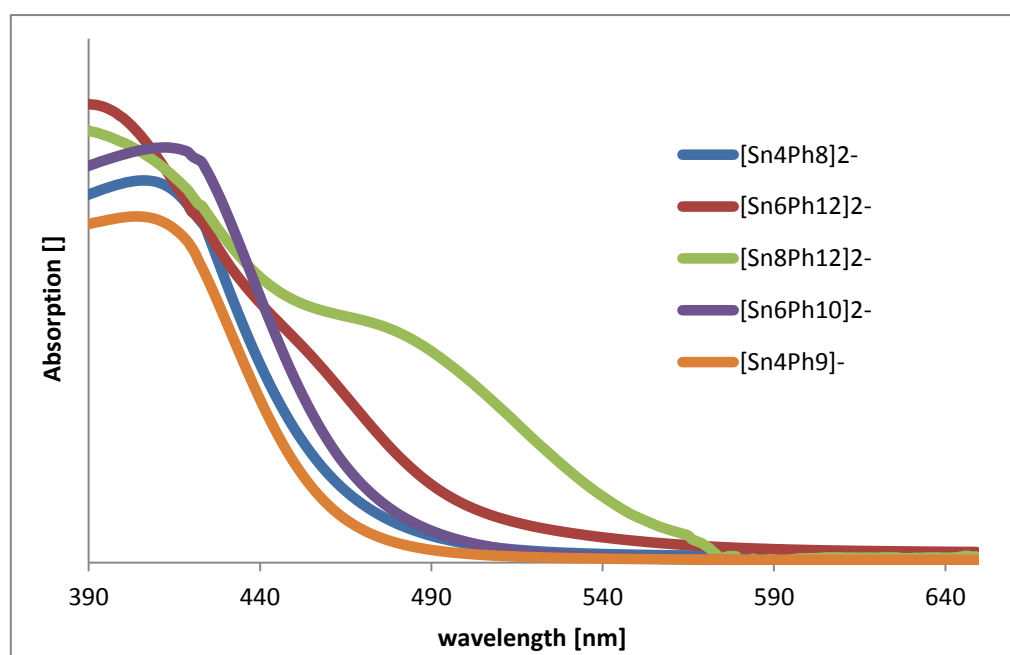
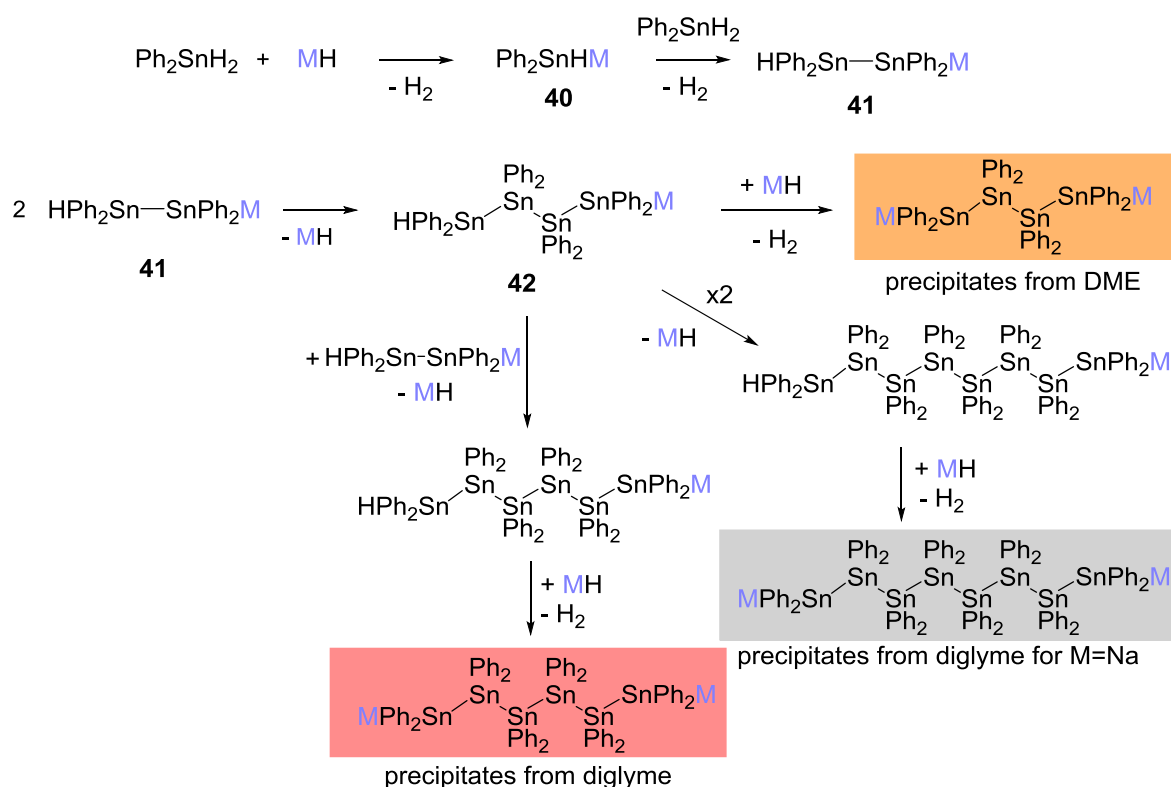


Figure 5.10 Combined UV/VIS absorption spectra of $[\text{Sn}_4\text{Ph}_8]^{2-}$ (**31**), $[\text{Sn}_6\text{Ph}_{12}]^{2-}$ (**33**), $[\text{Sn}_8\text{Ph}_{16}]^{2-}$ (**32**), $[\text{Sn}_6\text{Ph}_{10}]^{2-}$ (**34**) and $[\text{Sn}_4\text{Ph}_9]^-$ (**35**).

Although the corresponding intermediates of tin were never isolated, the fact, that all discussed dianionic compounds exhibit an even number of tin atoms, emphasises our hypothesis that the monoanionic dimer **39** plays also a crucial role in the formation of described anionic tin oligomers. Therefore, we propose the following mechanism based on these observations: Initially, the tin dihydride reacts with the metalation reagent and forms a monoanion **40**, which forms a metalated distannane **41** in a second step with a second equivalent of diphenyltin dihydride. Then, two of the so-formed highly reactive tin distannide will form the tetrastannide **42**. Further steps depend on the solvent as well as the metal. In DME **42** will further react to the α,ω -dianionic tetrastannide. When sodium is used in diglyme, two tetrastannides may form the linear octastannide. In reactions with sodium's higher homologues, the hexastannide is eventually formed in the reaction of a tetrastannide **42** and a distannane **41**.



Scheme 5.7 Overview of proposed reaction mechanism. The chosen solvent directs the outcome of the reaction.

The chosen solvent strongly determines the thermodynamically favoured and accordingly isolated compound and depends to a lesser extent on the metal. Outcome of reactions with $p\text{Tol}_2\text{SnH}_2$ and $p\text{Anis}_2\text{SnH}_2$ under same conditions, correlating nicely to the oligostannides derived from diphenyltin dihydride, also implies neglectable influence of the organic substituent on the tin centre. Using alkyl instead of aryl substituents never led to pure and well-defined products.^[94]

5.2.1.5 Derivatisation

Polymerisation of diphenyltin dihydride using transition metal catalysts, heat or amine bases is a widely applied method for the syntheses of tin oligo- and polymers, which are promising materials for future applications because of σ -conjugation.^[8] Isolated compounds can be considered as functional subunits of these σ -conjugated materials and allow fine tuning of their properties through further derivatisation. Their anionic functionality allows capping their ends with neutral species, incorporation into other chain or ring systems by e.g conversion with electrophiles. (Figure 5.11)

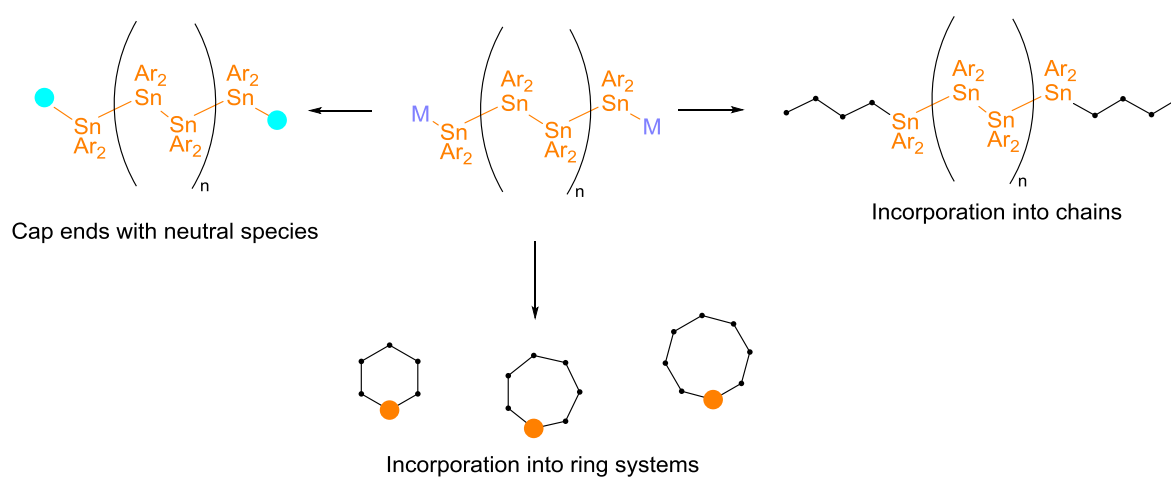
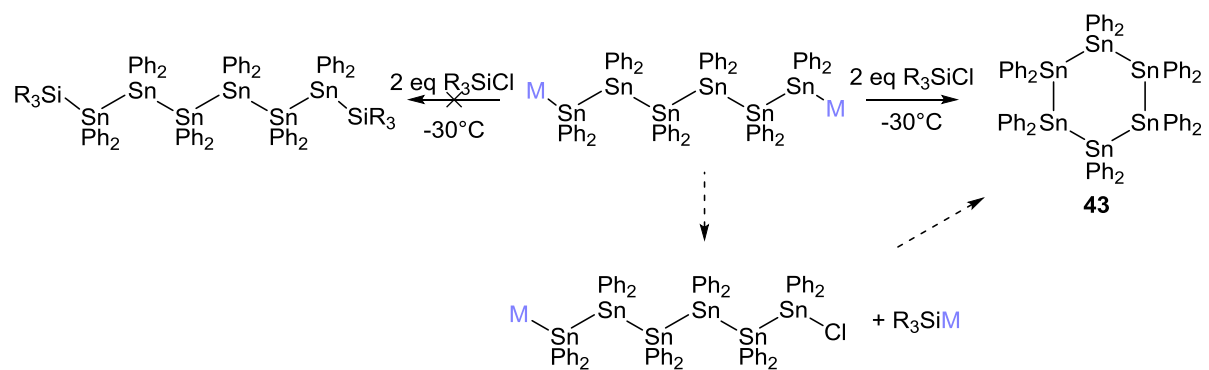


Figure 5.11 Potential reactions of α, ω -dianionic chains. Their functionality allows the chains to be capped with neutral species, incorporated into chains or into ring systems.

Initial experiments for the derivatisation of discussed anionic species were conducted with **33** as it is easily accessible in good yields and at no time cocrystallisation of any byproduct was observed. The anionic compound was dissolved in acetonitrile, precooled to -30°C and the silylchlorides (R_3SiCl ; $\text{R} = \text{TMS}$ or $i\text{Pr}$) as electrophilic species also diluted in acetonitrile was added slowly at low temperature. The colour change to yellow indicated an ongoing reaction. However, from all reaction solutions only the ring closure product **43** was isolated, presumably formed *via* a metal-halogen exchange and intramolecular ring closure. (Scheme 5.8) In future approaches, reactions of transition metal complexes, alternatively to silyl chlorides, with anionic chain species to form coordination polymers will be investigated. As ring formation as a side reaction is not possible for anionic rings, their conversion with these electrophiles will be examined in further studies.



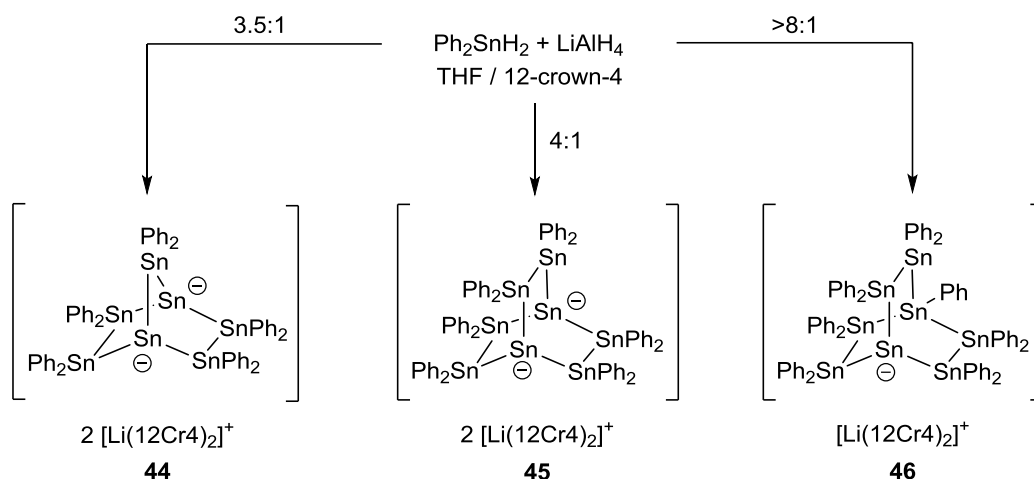
Scheme 5.8 Derivatization attempt of **33** with R_3SiCl ($R = TMS$ or iPr) does not give the intended product. The isolated product **43** of these reactions is likely formed *via* a metal-halogen exchange and a subsequent intramolecular ring closure.

5.2.2 Anionic Cages

As already discussed in section 5.1.1, low yields and the formation of orange solutions were observed when using an excess of LiAlH_4 in the reduction of Ph_2SnCl_2 in Et_2O as already mentioned earlier. Since we wanted to have a closer look on this possible side reaction, we decided to convert defined stoichiometric amounts of Ph_2SnH_2 (**26**) and LiAlH_4 . Here, Et_2O as a solvent was replaced by THF because of its lower volatility and therefore is more convenient to work with. Additionally, for these reactions purchased, grey LiAlH_4 was additionally recrystallised from Et_2O and was used as a pure, colourless crystalline solid for these reactions to guarantee an exact stoichiometry. To support crystallisation of reaction products, corresponding amounts of the crown ether 12-crown-4 were added.

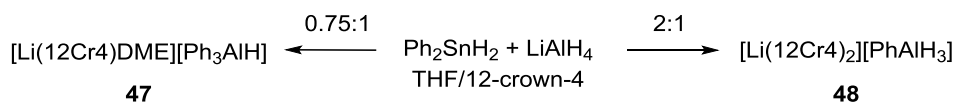
5.2.2.1 Synthesis

For all reactions with a moderate excess of LiAlH_4 , reaction solutions also turned orange similar to reductions when using a surplus of reducing agent. Accompanied slight formation of hydrogen was observed and after a few days a colourless, fluffy precipitate, confirmed by IR to be AlH_3 , was separated from these orange solutions. NMR spectroscopically also benzene was identified as a byproduct. In initial experiments, using no defined stoichiometry orange crystals of **44** and red crystals of **45** were obtained next to each other after cooling to -30°C . Crystals obtained for both compounds were suitable for X-Ray crystallography, which revealed the structure of the isolated products. Since in these initial approaches no direct correlation between number of electrons, formally introduced with LiAlH_4 , could be identified, it was assumed that the amount of lithium cations may govern the resulting compound and $[\text{AlH}_4]^-$ plays only a role in bond formation, but does not influence the resulting structure. Considering this assumption, we applied ratios of LiAlH_4 to diphenyltin dihydride, which represent the ratio of lithium ions to tin atoms in the isolated cages, and could isolate pure products from these reactions: Application of 3.5 eq Ph_2SnH_2 referred to 1 equivalent LiAlH_4 gave the dianionic, bicyclic [2.2.1] tin cage **44**. The molar ratio of $\text{Ph}_2\text{SnH}_2:\text{LiAlH}_4=4:1$ provided a dianionic [2.2.2] bicyclic compound **45**. Whereas a 8:1 ratio yielded the structural related monoanion **46**, which shows structural similarities to MeLi18 accessed *via* the reaction of a pentastanna[1.1.1]propellane with MeLi as discussed in section 4.3.4.2. In Scheme 5.9 the relation between the applied stoichiometric ratio and the reaction product is illustrated. Also anionic cyclic and non-cyclic tin oligomers, compounds already discussed in 5.2.1 Anionic Chains and Rings, sometimes cocrystallised with described cages as byproducts.



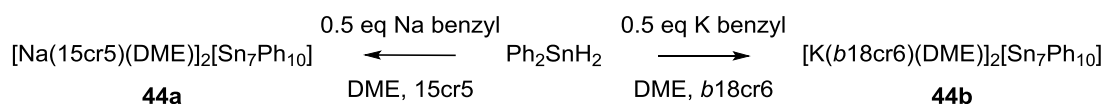
Scheme 5.9 Reaction of Ph_2SnH_2 with $LiAlH_4$ in various stoichiometric ratios. Above structures were isolated in moderate yields from reactions with stated $Ph_2SnH_2:LiAlH_4$ molar ratio. H_2 , benzene and AlH_3 as side products were identified by NMR or IR spectroscopy. Compound **44** was isolated as orange crystals. While **45** displays red colour and **46** is yellow.

When using a higher excess of $LiAlH_4$ under same conditions as in the above described reactions, again evolution of H_2 was observed, but also the formation of a grey solid, presumed to be elemental tin. Also benzene was formed in this reaction as evidenced by 1H NMR spectroscopy. After removal of the resulting tin, the phenylated aluminum compounds **47** and **48** were isolated as colourless crystals from the stoichiometric ratios declared in Scheme 5.10. Herein, the remarkable aspect is the phenyl group migration, which was already observed from one tin to another in the reactions of Ph_2SnH_2 with alkaline metals, from the tin onto the aluminium. Similar compounds featuring more sterically demanding compounds have been isolated so far in the conversion of an aryl lithium compound with $LiAlH_4$ or AlH_3NMe_3 .^[95,96] The reverse direction, organogroup migration from aluminium compounds onto other main group metal centres, is a popular way for the synthesis of organo main group metal compounds.^[97]



Scheme 5.10 Higher Excess of $LiAlH_4$ leads to formation of hydrogen, benzene, elemental tin and phenylated aluminum compounds **47** and **48**.

In the quest of a possible alternative reagent to $LiAlH_4$, we considered the use of strong bases e.g. sodium and potassium benzyl as coupling reagents. Conversion of diphenyltin dihydride with 0.5 eq of sodium or potassium benzyl gave indeed the corresponding structural analogue of **44**. (Scheme 5.11)



Scheme 5.11 Reactions of Ph_2SnH_2 with Potassium and Potassium benzyl in presence of the corresponding crown ether in DME.

Anionic functionality of discussed cages also allows the further derivatisation similar to presented anionic linear oligomers.

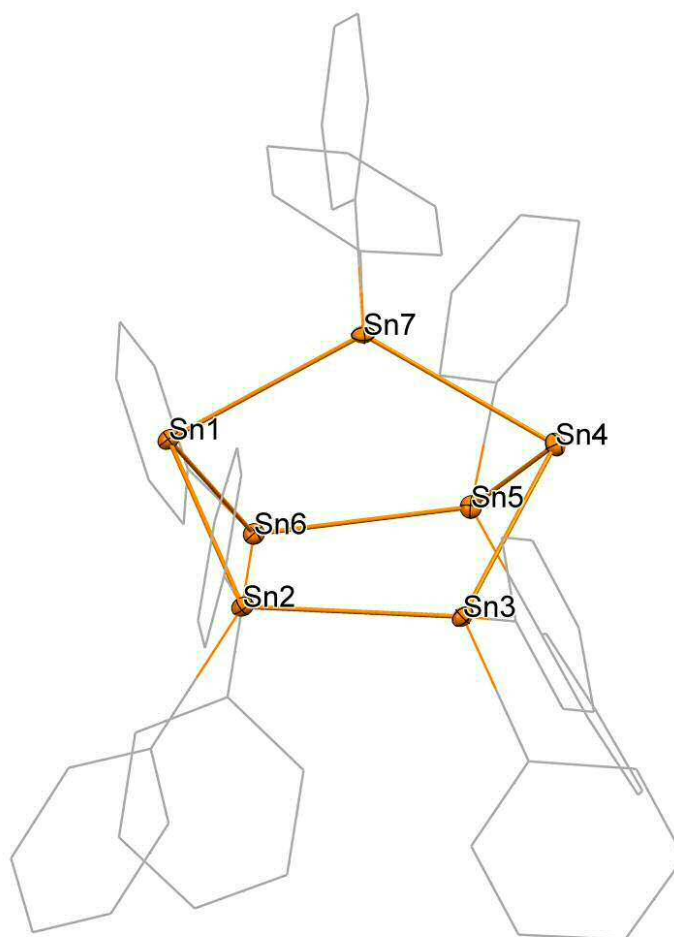
5.2.2.2 X-Ray Crystallography

All presented cages were analysed by X-Ray crystallography and their structural properties will be discussed in this section. Again discussion of structural characteristics will mainly focus on the tin backbone. Also structures of presented phenylated aluminum compounds will be discussed here. For more detailed information about measurements and refinement see the Appendix.

Characteristics of tin backbones in **44**, **44a** and **44b** are fairly comparable and similar trends can be observed in all these compounds. Due to the strained [2.2.1] bicyclic system, the bridging tin atom Sn7 in **44** shows slightly extended bond lengths (2.934(5) and 2.851(6) Å) compared to the average $\text{Sn}^{\text{b}}-\text{Sn}$ distance of 2.849(9) Å. (Figure 5.12) Same tendency is also found for **44a** (2.8868(7) and 2.8782(4) Å vs. 2.862(2) Å) and **44b** (2.8780 Å vs. 2.843(8) Å). Also Sn–Sn–Sn bond angles of the bridging tin atoms show similar extended values (120.91(2)-123.1(2)°) compared to the ideal tetrahedral angle of 109.5 and angles of the non-charged tin atoms (110.28(2)-114.1(1)°) in all of these compounds, which may also explain the highly lowfield shifted ^{119}Sn NMR resonance of this tin nucleus. Similar to already discussed anionic chain and ring systems, the angle sums of anionic bridgehead atoms in **44**, **44a** as well as **44b** also show lower values (263.79(6)-267.13(6)°) than expected for an atom with ideal tetrahedral environment ($3 \cdot 109.5^\circ = 328.5^\circ$). Again, this implies the high s orbital character of the lone pair and a large p orbital character of bonding orbitals. In accordance with this observation, also bond lengths of these anionic tin centres are slightly extended compared to bond distances between neutral Sn atoms. For a summary of these values see Table 5.7.

Table 5.7 Summary of structural properties of $[\text{Sn}_7\text{Ph}_{10}]^{2-}$ anions of **44**, **44a** and **44b**. Bridgehead tin atoms are here denoted as Sn^b . Bridging tin atoms are denoted as Sn^c .

	Space Group	$\text{Sn}^b\text{--Sn}$ [Å] (avg.)	$\text{Sn}^c\text{--Sn}^b$ [Å]	$\text{Sn}\text{--Sn}$ [Å]	Σ $\text{Sn}\text{--Sn}^b\text{--Sn}$ [°]	$\text{Sn}\text{--Sn}^c\text{--Sn}$ [°]
$\text{Li}_2[\text{Sn}_7\text{Ph}_{10}]$ (44)	P-1	2.849(9)	2.934(5)	2.850(4)	264.4(1)	123.1(2)
			2.851(6)	2.795(4)	264.1(6)	
$\text{Na}_2[\text{Sn}_7\text{Ph}_{10}]$ (44a)	P2 ₁ /c	2.862(2)	2.8868(7)	2.8370(6)	267.13(6)	120.91(2)
			2.8782(4)	2.8612(5)	263.79(6)	
$\text{K}_2[\text{Sn}_7\text{Ph}_{10}]$ (44b)	P3 ₁ 21	2.843(8)	2.8780	2.824(1)	265.93(3)	121.72

**Figure 5.12** Molecular structure of the $[\text{Sn}_7\text{Ph}_{10}]^{2-}$ backbone in $[\text{Li}(\text{12cr4})_2][\text{Sn}_7\text{Ph}_{10}]$ (**44**). Hydrogen atoms are omitted for clarity. Ellipsoids are drawn with 30% probability. Selected distances [Å] and angles [°]: Sn1–Sn7 2.934(5), Sn1–Sn2 2.833(2), Sn1–Sn6 2.862(3), Sn2–Sn3 2.850(4), Sn6–Sn5 2.795(4), Sn2–Sn1–Sn6 94.77(8), Sn2–Sn1–Sn7 84.0(1), Sn6–Sn1–Sn7 85.6(1), Sn1–Sn2–Sn3 114.1(1), Sn2–Sn3–Sn4 112.7(1), Sn3–Sn4–Sn5 94.6(2), Sn3–Sn4–Sn7 85.9(2), Sn5–Sn4–Sn7 83.6(2), Sn1–Sn6–Sn5 110.5(1), Sn1–Sn7–Sn4 123.1(2).

Same structural peculiarity does apply for the anionic bridgehead tin centres in dianionic **45** and in monoanionic **46**, but not for the neutral bridgehead atom in **46**. Herein, differences in hybridisation of the two bridgehead atoms Sn1 and Sn4 are evidenced by the notable difference in Sn–Sn^b–Sn angle sums. The anionic tin centre Sn1 displays an angle sum of 287.84(7)°, indicating a high s orbital character of the lone pair, in contrast to the tetrasubstituted Sn4 with an Sn–Sn^b–Sn angle sum of 318.54(4)°. Latter corresponds rather to an ideal sp³ hybridisation. Also bond length tendencies correspond to this observation. (Figure 5.14, Table 5.8) Noteworthy, in **46** tin centres alpha to the anionic bridgehead tin atom (Sn1) possess widened Sn–Sn–Sn angles (117.40(9)-122.17(9)°) like all bridging atoms in the tin backbone of **45** (120.49(2)-124.58(2)°). In contrast, Sn–Sn–Sn angles of tin centres in beta position display values closer to those of an ideal tetrahedron (105.49(8)-110.47(8)°).

Table 5.8 Comparison of structural properties for the bridgehead atoms in [Li(12cr4)₂][Sn₈Ph₁₂] (**45**) and [Li(12cr4)₂][Sn₈Ph₁₃] (**46**). (Figure 5.13 and Figure 5.14)

		Sn ^b –Sn [Å] (avg.)	Σ Sn–Sn ^b –Sn [°]
[Li(12cr4)₂][Sn₈Ph₁₂] (45)	Sn1	2.839(9)	276.05(6)
	Sn8	2.818(7)	274.06(6)
[Li(12cr4)₂][Sn₈Ph₁₃] (46)	Sn1	2.850(9)	287.84(7)
	Sn4	2.784(9)	318.54(4)

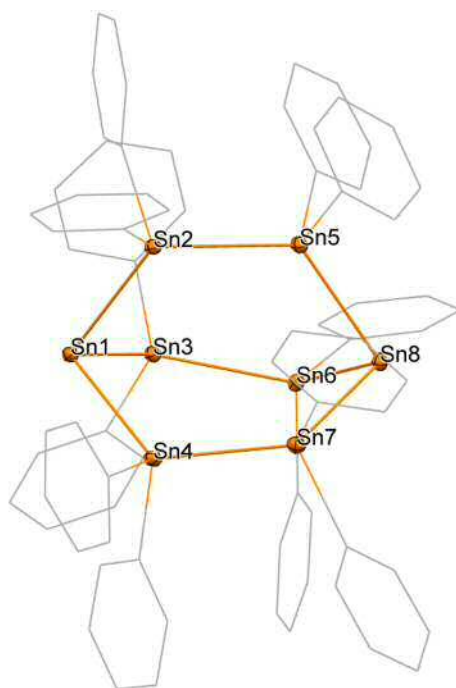


Figure 5.13 Molecular structure of the $[\text{Sn}_8\text{Ph}_{12}]^{2-}$ anion in $[\text{Li}(12\text{cr}4)_2][\text{Sn}_8\text{Ph}_{12}]$ (**45**). Hydrogen atoms are omitted for clarity. Ellipsoids are drawn with 30% probability. Selected distances [Å] and angles [°]: Sn1-Sn2 2.8253(7), Sn1-Sn3 2.8407(7), Sn1-Sn4 2.8382(8), Sn2-Sn5 2.8316(8), Sn3-Sn6 2.8065(8), Sn4-Sn7 2.7887(8), Sn5-Sn8 2.8253(7), Sn6-Sn8 2.8242(8), Sn7-Sn8 2.8253(7), Sn2-Sn1-Sn4 91.42(2), Sn2-Sn1-Sn3 93.35(2), Sn1-Sn2-Sn5 120.49(2), Sn1-Sn3-Sn6 121.18(2), Sn1-Sn4-Sn7 123.15(2), Sn2-Sn5-Sn8 124.58(2).

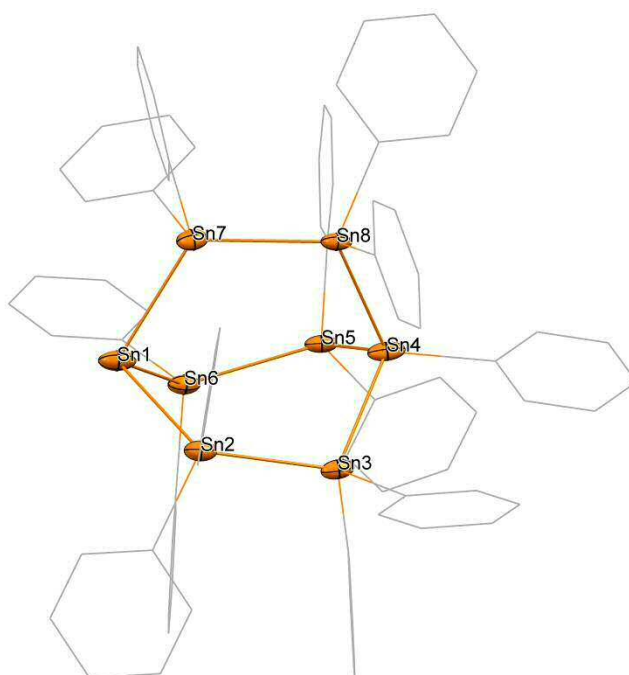


Figure 5.14 Molecular structure of the $[\text{Sn}_8\text{Ph}_{13}]^-$ backbone in $[\text{Li}(12\text{cr}4)_2][\text{Sn}_8\text{Ph}_{13}]$ (**46**). Hydrogen atoms are omitted for clarity. Ellipsoids are drawn with 30% probability. Selected distances [Å] and angles [°]: Sn1-Sn2 2.853(4), Sn1-Sn6 2.861(3), Sn1-Sn7 2.838(2), Sn2-Sn3 2.811(3), Sn4-Sn3 2.789(2), Sn4-Sn5 2.778(3), Sn4-Sn8 2.787(2), Sn5-Sn6 2.827(3), Sn7-Sn8 2.8318(3), Sn2-Sn1-Sn6 96.98(9), Sn2-Sn1-Sn7 95.50(9), Sn6-Sn1-Sn7 95.34(9), Sn1-Sn2-Sn3 117.40(9), Sn2-Sn3-Sn4 110.47(8), Sn3-Sn4-Sn5 106.88(8), Sn3-Sn4-Sn8 105.24(8), Sn5-Sn4-Sn8 106.40(8), Sn4-Sn5-Sn6 105.49(8), Sn1-Sn6-Sn5 122.17(9), Sn1-Sn7-Sn8 121.85(9), Sn4-Sn8-Sn7 106.61(8).

Structural data of the phenylated aluminum compounds $[\text{Li}(\text{12cr4})][\text{Ph}_3\text{AlH}]$ (**47**), $[\text{Li}(\text{12cr4})][\text{PhAlH}_3]$ (**48**) and structural related literature compounds are summarised in Table 5.9. Bond angles correspond well to values of an ideal tetrahedron and found bond lengths mostly fit to values of presented literature known compounds. Yet, some differences are observable. For example, Al–H bond distance of **47** (1.66(2) Å) is slightly longer compared to the Al–H bond distance in $\text{K}[\text{Pfp}_3\text{AlH}]$ (1.59(4) Å)^[98], but considerably longer than in e.g. dimeric $[\text{AlH}_3(\text{THF})]_2$ (1.39(4) and 1.55(3) Å)^[99]. In compound **48**, a slightly shorter Al–C bond is observed (2.022(4) Å) than in $[\text{Mes}^*\text{AlH}_3]^-$ having a more sterically demanding aryl substituent (2.0301(5) Å)^[95]. Same holds for the Al–H distances (1.46(4)-1.50(5) Å) in **48** compared to $[\text{Mes}^*\text{AlH}_3]^-$ (1.539(57)-1.601(50) Å)^[95]. Molecular structures of discussed phenylated aluminum compounds are illustrated in Figure 5.15 and Figure 5.16.

Table 5.9 Comparison of the structural data of **47** and **48** to $[\text{Pfp}_3\text{AlH}]^-$ (Pfp = Pentafluorophenyl) and $[\text{Mes}^*\text{AlH}_3]^-$ (Mes* = 2,4,6-*t*-Bu₃C₆H₂).

	Space group	Al–C [Å]	Al–H [Å]	C–Al–C [°]	C–Al–H [°]	H–Al–H [°]
$[\text{Pfp}_3\text{AlH}]^-$ ^[98]		2.016(3)		111.4(1)	109(2)	
	C2/c	2.024(3)	1.59(4)	111.7(1)	110(2)	-
$[\text{Ph}_3\text{AlH}]^-$ (47)		2.015(3)		107.5(1)	107(2)	
		2.022(3)		111.0(1)	105.6(8)	
	P2 ₁ /c	2.010(2)	1.66(2)	109.7(1)	110.3(8)	-
$[\text{Mes}^*\text{AlH}_3]^-$ ^[95]		2.006(3)		109.5(1)	110.7(8)	
			1.556(54)		113.1(19)	107.9(28)
	P2 ₁ /c	2.0301(5)	1.539(57)	-	113.1(18)	102.6(26)
			1.601(50)		110.0(16)	109.6(28)
$[\text{PhAlH}_3]^-$ (48)			1.46(4)		108(2)	107(2)
	Pbca	2.022(4)	1.50(5)	-	114(2)	110(2)
			1.50(5)		110(2)	107(2)

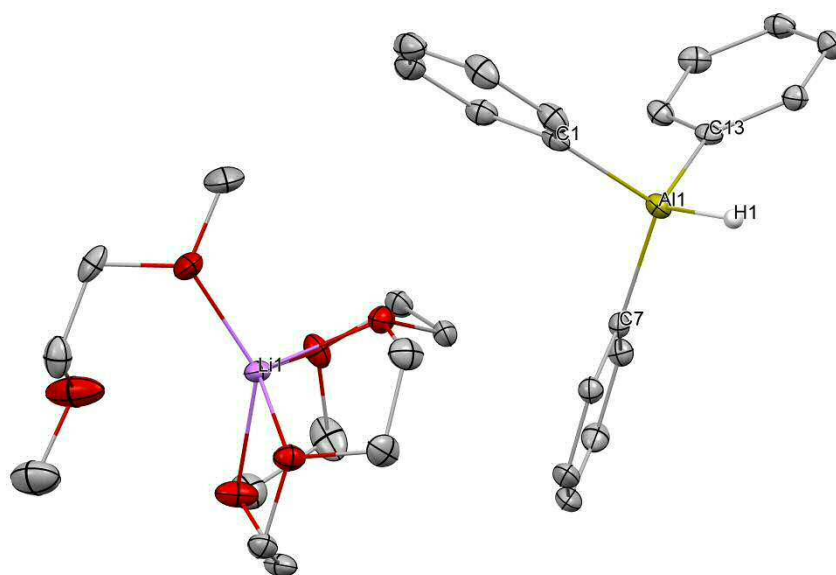


Figure 5.15 Molecular structure of $[\text{Li}(12\text{cr}4)(\text{DME})][\text{Ph}_3\text{AlH}]$ (**47**). Hydrogens except Al–H atoms are omitted for clarity. Ellipsoids are drawn with 30% probability. Selected distances [\AA] and angles [$^\circ$]: Al1–C1 2.022(3), Al1–C7 2.010(2), Al1–C13 2.006(3), Al1–H1 1.66(2), C1–Al1–C7 111.0(1), C1–Al1–C13 109.7(1), C7–Al1–C13 109.5(1), C1–Al1–H1 105.6(8), C7–Al1–H1 110.3(8), C13–Al1–H1 110.7(8).

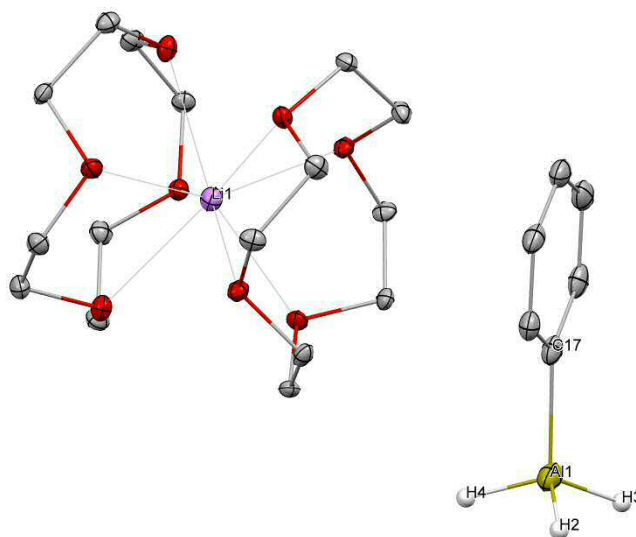


Figure 5.16 Molecular structure of $[\text{Li}(12\text{cr}4)_2][\text{PhAlH}_3]$ (**48**). Hydrogens except Al–H atoms are omitted for clarity. Ellipsoids possess a probability of 30%. Selected bond lengths [\AA] and angles [$^\circ$]: Al1–C17 2.022(4), Al1–H2 1.46(4), Al1–H3 1.50(5), Al1–H4 1.50(5), C17–Al1–H2 108(2), C17–Al1–H3 114(2), C17–Al1–H4 110(2), H2–Al1–H3 107(2), H2–Al1–H4 110(2), H3–Al1–H4 107(2).

5.2.2.3 Spectroscopical Data

All mentioned anionic cages **44**, **45** and **46** were investigated ^{119}Sn NMR spectroscopically. Due to the same degradation issues as described for dianionic chains in common NMR solvents, acetonitrile- d_3 again was the deuterated solvent of choice. In this solvent it was possible to record reasonable spectra with nice coupling pattern as illustrated e.g. for **44** in Figure 5.17. Most resonances fall into the expected range. Exception in this observation is the bridging atom of **44**, which also exhibits structural particularities because of the strained bicyclic [2.2.1] system as already discussed in section 5.2.2.2 X-Ray crystallography. The unusual structural properties result in a highly lowfield shifted resonance at +200.28 ppm compared to the non-anionic tin centres in **44** displaying a ^{119}Sn NMR shift of +35.64 ppm. Latter values are also exceedingly lowfield shifted compared to corresponding tin atoms in **45** and **46** (-183.18 to -316.81 ppm). Resonances in ^{119}Sn NMR and observed coupling constants of all these compounds are summarised in Table 5.10. Due the “roof” effect and low solubility, most $J(^{119}\text{Sn}, ^{119}\text{Sn})$ coupling constants in **45** could not be detected.

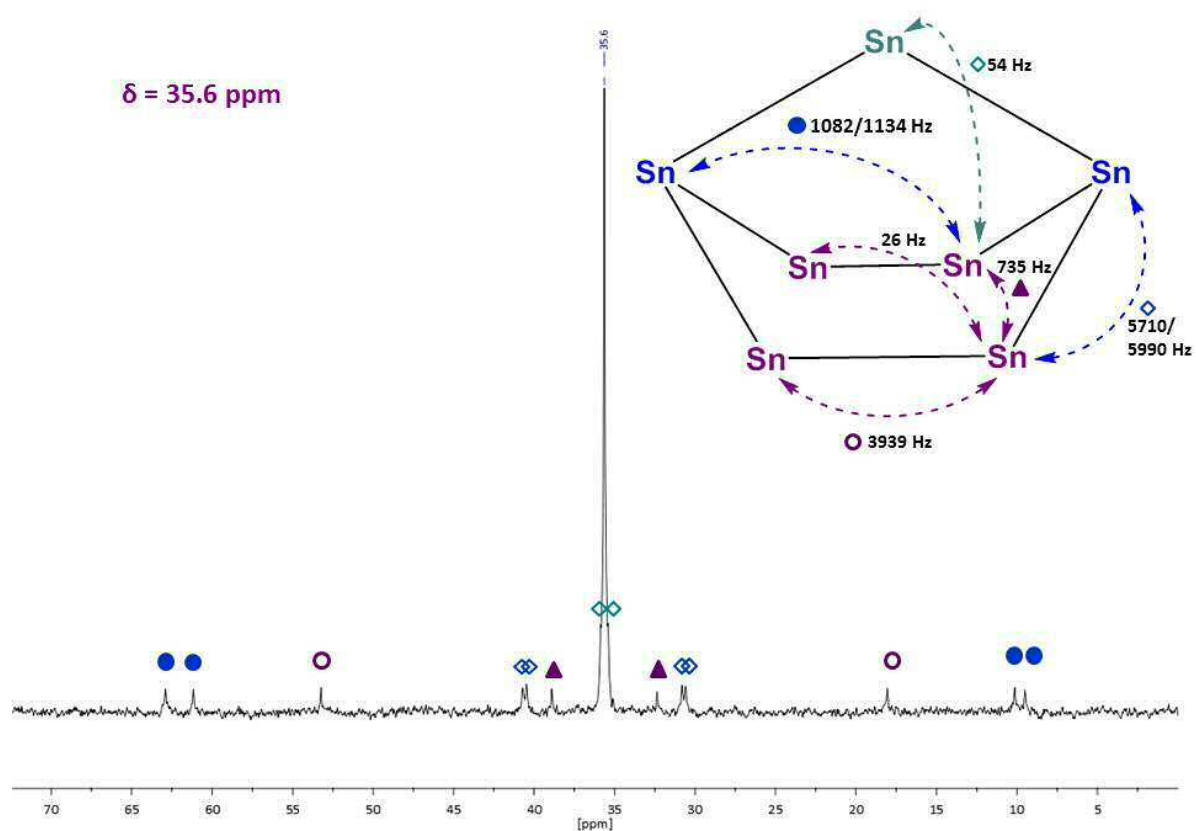
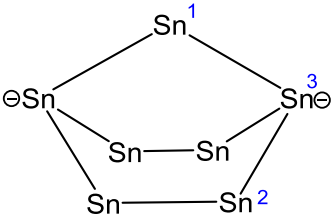
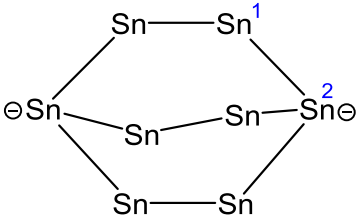


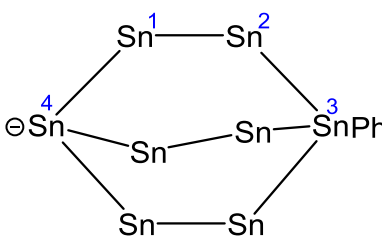
Figure 5.17 Coupling pattern of the shift at 35.6 ppm in the ^{119}Sn NMR spectra of in $[\text{Li}(\text{12cr4})_2][\text{Sn}_7\text{Ph}_{10}]$ (**44**).

Table 5.10 Summary of ^{119}Sn resonances [ppm] and coupling constants [Hz] of **44**, **45** and **46** in CD_3CN .

	^{119}Sn Shift		
	[ppm]		
	¹ 200.28	$^1J (^{119}\text{Sn}, ^{117/119}\text{Sn}) = 4426/4636 \text{ Hz}$ $^2J (^{119}\text{Sn}, \text{Sn}^f) = 54 \text{ Hz}$	
	² 35.64	$^1J (^{119}\text{Sn}, ^{117/119}\text{Sn}) = 5710/5990 \text{ Hz}$ $^1J (^{119}\text{Sn}, ^{117}\text{Sn}) = 3939 \text{ Hz}$ $^2J (^{119}\text{Sn}, ^{117/119}\text{Sn}) = 1082/1134 \text{ Hz}$ $^2J (^{119}\text{Sn}, ^{117}\text{Sn}) = 735 \text{ Hz}$ $^2J (^{119}\text{Sn}, \text{Sn}^f) = 54 \text{ Hz}$ $^3J (^{119}\text{Sn}, ^{117}\text{Sn}) = 26 \text{ Hz}$	
	³ -857.73	$^1J (^{119}\text{Sn}, ^{117/119}\text{Sn}) = 5710/5990 \text{ Hz}$ $^1J (^{119}\text{Sn}, ^{117/119}\text{Sn}) = 4426/4636 \text{ Hz}$ $^2J (^{119}\text{Sn}, ^{117/119}\text{Sn}) = 1082/1134 \text{ Hz}$	
		¹ -316.81	$^1J (^{119}\text{Sn}, ^{117}\text{Sn}) = 5020 \text{ Hz}$ $^1J (^{119}\text{Sn}, ^{117}\text{Sn}) = 3610 \text{ Hz}$ $^2J (^{119}\text{Sn}, ^{117/119}\text{Sn}) = 770/807 \text{ Hz}$ $^2J (^{119}\text{Sn}, ^{117}\text{Sn}) = 240 \text{ Hz}$ $^3J (^{119}\text{Sn}, ^{117}\text{Sn}) = 17 \text{ Hz}$
		² -586.97	$^1J (^{119}\text{Sn}, ^{117}\text{Sn}) = 5020 \text{ Hz}$ $^2J (^{119}\text{Sn}, ^{117/119}\text{Sn}) = 770/807 \text{ Hz}$

^f Coupling constants $J (^{119}\text{Sn}, ^{117}\text{Sn})$ and $J (^{119}\text{Sn}, ^{119}\text{Sn})$ are not resolved.

Continuation of **Table 5.10** Summary of ^{119}Sn resonances [ppm] and coupling constants [Hz] of **44**, **45** and **46** in CD_3CN .

		^{119}Sn Shift	
		[ppm]	
 <p>[Sn₈Ph₁₃]⁻ (46)</p>		$^1J(^{119}\text{Sn}, ^{117}\text{Sn}) = 6126 \text{ Hz}$	
			$^1J(^{119}\text{Sn}, ^{119}\text{Sn}) = 6422 \text{ Hz}$
	¹ -183.18		$^2J(^{119}\text{Sn}, \text{Sn}) = 708 \text{ Hz}$
			$^2J(^{119}\text{Sn}, \text{Sn}^{\text{g}}) = 548 \text{ Hz}$
			$^2J(^{119}\text{Sn}, ^{117}\text{Sn}) = 2274 \text{ Hz}$
			$^1J(^{119}\text{Sn}, ^{117/119}\text{Sn}) = 1020/1170 \text{ Hz}$
	² -238.75		$^1J(^{119}\text{Sn}, ^{117/119}\text{Sn}) = 916/957 \text{ Hz}$
			$^2J(^{119}\text{Sn}, \text{Sn}^{\text{g}}) = 131 \text{ Hz}$
			$^1J(^{119}\text{Sn}, \text{Sn}^{\text{g}}) = 1170 \text{ Hz}$
	³ -471.10		$^2J(^{119}\text{Sn}, \text{Sn}^{\text{g}}) = 548 \text{ Hz}$
			$^3J(^{119}\text{Sn}, \text{Sn}^{\text{g}}) = 170 \text{ Hz}$
			$^1J(^{119}\text{Sn}, ^{117}\text{Sn}) = 6126 \text{ Hz}$
⁴ -758.24		$^1J(^{119}\text{Sn}, ^{119}\text{Sn}) = 6422 \text{ Hz}$	
		$^3J(^{119}\text{Sn}, \text{Sn}^{\text{g}}) = 170 \text{ Hz}$	

^g Coupling constants $J(^{119}\text{Sn}, ^{117}\text{Sn})$ and $J(^{119}\text{Sn}, ^{119}\text{Sn})$ are not resolved.

5.3 Clusters and molecules with non-classical bond situation

Phenyl group migration was described in the formation of compounds discussed in earlier sections of this chapter. Considering this observation, addition of a reactive, low valent species to solutions of diaryltin dihydrides may force aryl group migration while forming Sn-Sn bonds and thereby encloses eventually the synthesis of molecular tin cages. Deployment of low valent species in this reaction introduces simultaneously already naked tin centres for the formation of metalloid tin clusters. Since cages and clusters are likely to form the bulk metal due to their metastability, more sterically demanding substituents than a phenyl group were introduced on the tin centre for kinetic stabilisation of such compounds. Chosen aryl substituents and synthesis of starting material for these reactions was discussed in 5.1 Diaryltin dichlorides and dihydrides. Results of subsequent conversions of these tin hydrides will be discussed in this subchapter.

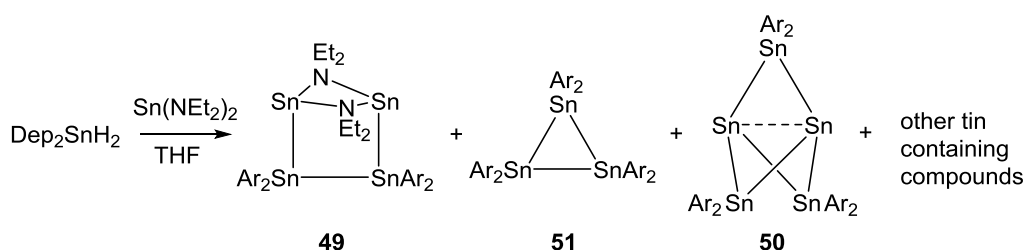
5.3.1 Synthesis

Initial experiments applying diphenyltin dihydrides and LAPPERT's stannylene in toluene led to a single tin containing product, which displays a triplet at -137.04 ppm ($J = 153$ Hz) with a ratio 1:4:1 in $^{119}\text{Sn}\{^1\text{H}\}$ NMR. However, the detected product has not been identified, so far. Identification for products of more sterically demanding phenyl substituents is summarised in the following.

5.3.1.1 Reactions of Dep_2SnH_2

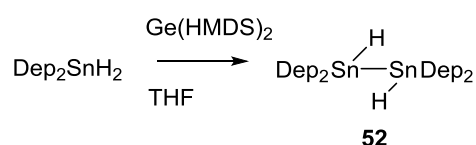
Equimolar conversion of Dep_2SnH_2 and $\text{Sn}(\text{NEt}_2)_2$ in THF quickly led to a dark brownish solution. After two days ^{119}Sn NMR investigation (a small amount of C_6D_6 was added to the NMR sample for locking) indicated the formation of the pentastanna[1.1.1]propellane Sn_5Dep_6 (354.99 and -1760.39 ($J_{\text{Sn},^{119}\text{Sn}} = 4174$ Hz, $J_{\text{Sn},^{117}\text{Sn}} = 3990$ Hz) ppm) and decastanna[5]prismane $(\text{DepSn})_{10}$ (-24.44 ppm).^[9,59] Additional shifts were found at 868.7 and -116.2 ppm, which could not be assigned. Thin layer chromatography of the reaction solution (*n*-heptane/toluene = 10/1) showed a spot with the characteristic violet colour of the propellane. Upon narrowing of the reaction solution brown crystals precipitated, which turned out the suitable for X-Ray crystallography. This analysis method revealed the structure **49**, which may play a role as an intermediate in the formation of other compounds. Unassigned ^{119}Sn NMR resonances at 868.7 and -116.2 in the reaction solution are likely to originate from **49**. For purification the narrowed reaction solution was applied onto a silica gel column (*n*-heptane/toluene = 10/1 to 5/1). From fractions of this column two additional products were isolated as depicted in Scheme 5.12. Already presumed pentastanna[1.1.1]propellane **50** was isolated and structurally confirmed from the first violet fraction. Also the cyclic $(\text{Dep}_2\text{Sn})_3$ (**51**) was characterised by X-Ray crystallography, after isolating from the following second fraction. Discussion of these compounds'

structural characteristics can be found in section 5.3.2 X-Ray Crystallography. Other tin containing compounds found in ^{119}Sn NMR analysis could not be confirmed structurally or not assigned, so far.



Scheme 5.12 Overview of products in the reaction of Dep_2SnH_2 with $\text{Sn}(\text{NEt}_2)_2$.

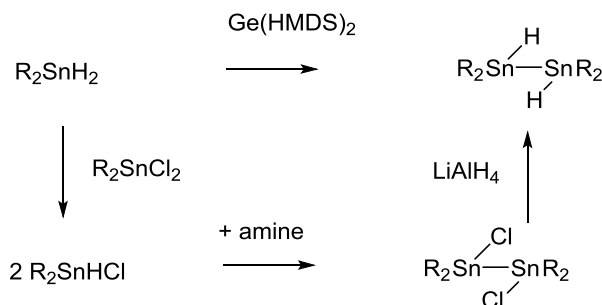
Under similar conditions, application of $\text{Sn}(\text{HMDS})_2$ instead of $\text{Sn}(\text{NEt}_2)_2$ resulted first in a yellow solution, which then turned slowly overnight brownish red. The solution was investigated ^{119}Sn NMR spectroscopically after two days. Additional to shifts again indicating pentastanna[1.1.1]propellane **50** (354.31 and -1757.93 ppm, also indicated by thin layer chromatography displaying a violet spot), plenty of peaks were found in the range of -100 to -300 ppm (-128.47, -145.58, -157.07, -175.79, -203.61, -243.22 and -297.47 ppm). Due to the presence of unconsumed starting material Dep_2SnH_2 , the reaction was stirred for another six days and again investigated spectroscopically. Most of the former found shifts disappeared and only two of them were still present at -157.07 and -203.61 ppm. Additionally, another shift at -74.10 appeared. Shifts in the named region are often found for neutral cyclic oligomers.^[100] It is also presumed that the disappeared shifts possibly are oligomers, which are formed intermediately and are consumed while forming the final products. In contrast to these reactions with LAPPERT's stannylene, the main product was identified in the reaction with LAPPERT's germylene according to ^{119}Sn NMR. In the reaction of Dep_2SnH_2 with $\text{Ge}(\text{HMDS})_2$ tin bond formation occurs and mainly the dimeric $(\text{Dep}_2\text{SnH})_2$ (**52**) is formed. The role of the germanium or respectively the resulting germanium compound has not been resolved so far. Sole evidence is given by ^1H NMR analysis, which shows additional shifts around 0 ppm. This observation indicates the formation of other amine and amide compounds during this reaction.



Scheme 5.13 Conversion of Dep_2SnH_2 and a equimolar amount of $\text{Ge}(\text{HMDS})_2$ leads to the tin-tin bond coupling product **52**.

Due to its remaining functionalities, compound **52** is an appealing dimeric building block for further modification. Yet, synthesis of functional distannanes e.g. $(t\text{Bu}_2\text{SnH})_2$ included a multi-step synthesis

route starting from R_2SnH_2 or $(tBu_2SnCl)_2$ was isolated as a byproduct in the synthesis of R_2SnCl_2 and was reduced using $LiAlH_4$. The observed reactivity may enclose an alternative route for the synthesis of such dimers featuring different substituents.^[101]



Scheme 5.14 Synthesis of $(R_2HSn)_2$ using a multi-step synthesis route and the alternative route using $Ge(HMDS)_2$.

5.3.1.2 Reactions of $Tripp_2SnH_2$ and $Dipp_2SnH_2$

All reactions of $Tripp_2SnH_2$ or $Dipp_2SnH_2$ with E(II) amides were again conducted in THF, whereby latter tin hydride displays a slightly poorer solubility also in this fairly good solvent for organotin compounds. Nevertheless, both exhibit the same reactivity towards deployed E(II) amides. An overview of reaction products of these reactions is given in Scheme 5.15.

In the reaction of equimolar amounts Ar_2SnH_2 ($Ar = Tripp, Dipp$) with LAPPERT'S stannylene $Sn(HMDS)_2$, cyclic $Sn_4H_2Ar_6$ ($Ar = Tripp$ (**53**), $Dipp$ (**54**)) was isolated as a main product through crystallisation from the brownish red reaction solutions. Apparently due to the lowered solubility of the $Dipp$ substituent, the colourless product was isolated in shorter reaction times and in higher yields in the case of $Sn_4H_2Dipp_6$ (2 weeks, 58% yield). Compound **54** also exhibits a way poorer solubility in benzene, since recording of ^{13}C NMR in C_6D_6 showed almost no signals for this compound, but was satisfying in the case of **53** in the same solvent. Additionally, solubility of **54** in THF- d_8 was only moderate, but enough to do ^{13}C and ^{119}Sn NMR analysis. Both compounds are insoluble in *n*-pentane. In experiments using a molar ratio of 3 : 1 = $Ar_2SnH_2 : Sn(HMDS)_2$, which would correspond to the amount of aryl groups and tin atoms in the resulting product, lower yields were achieved. Therefore a formal excess of the tin(II) species is required in the formation of $Sn_4Ar_6H_2$ and suggests the development of other byproducts, which are so far unidentified. Spectroscopic data of both compounds are compared to related published structures in Table 5.11. Isolated compounds **53** and **54** display highly lowfield shifted ^{119}Sn NMR resonances (-166.7 and -192.9 ppm; -163.6 and -195.4 ppm) compared to $[SnHAr^*]_4$ (-324.3 ppm), but correspond nicely to the resonance of $[SnH(CH(TMS)_2)]_4$ (-198 ppm). Yet, 1H NMR shifts at 8.42 and 8.46 ppm of **53** and **54** are fairly lowfield shifted than corresponding resonances of presented literature compounds. Also lower coupling

constants $^1J(^1\text{H}, ^{119}\text{Sn})$ are observed for these novel compounds. Other values fall into the same order.

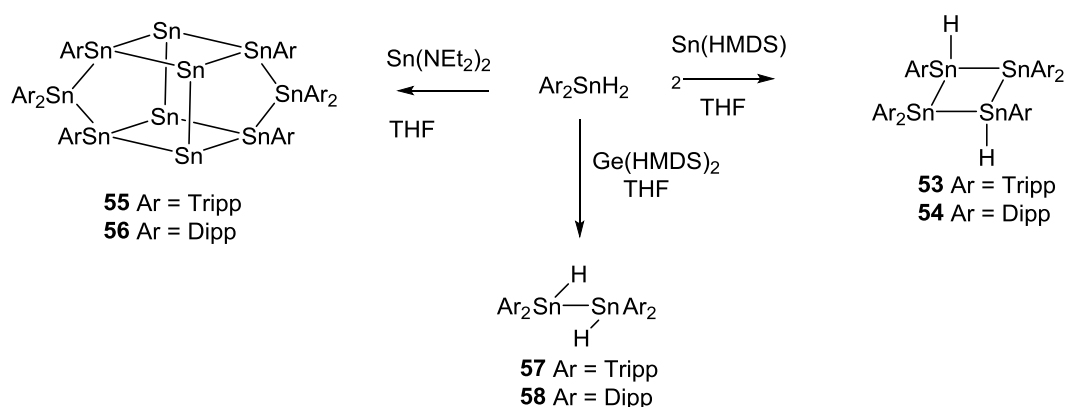
Table 5.11 Overview of spectroscopic data for 4-membered tin rings $[\text{SnHAr}^*]_4$ ($\text{Ar}^*=2,6\text{-Mes}_2\text{C}_6\text{H}_3$), $[\text{SnH}(\text{CH}(\text{TMS})_2)]_4$, $\text{Sn}_4\text{H}_2\text{Tripp}_6$ (**53**) and $\text{Sn}_4\text{H}_2\text{Dipp}_6$ (**54**) featuring hydride functionalities.

	^{119}Sn Shift	^1H Shift	$^1J(^1\text{H}, ^{119}\text{Sn})$	$^2J(^1\text{H}, ^{119}\text{Sn})$	(Sn-H)
	[ppm]	[ppm]	[Hz]	[Hz]	$[\text{cm}^{-1}]$
$[\text{SnHAr}^*]_4$ ^[81]	-324.3	3.97	1590	-	1789
$[\text{SnH}(\text{CH}(\text{TMS})_2)]_4$ ^[48]	-198	5.76	1326	-	1845
$\text{Sn}_4\text{H}_2\text{Tripp}_6$ (53)	-166.7	8.42	1177	158	1834
	-192.9				
$\text{Sn}_4\text{H}_2\text{Dipp}_6$ (54)	-163.6	8.46	1189	138	1838
	-195.4				

Application of the more labile Sn(II) amide species $\text{Sn}(\text{NEt}_2)_2$ in the conversion with $\text{Tripp}_2\text{SnH}_2$ also led to the formation of colourless crystals after 9 days, which turned out to be again cyclic $\text{Sn}_4\text{H}_2\text{Tripp}_6$. In this reaction, colour change of the initial yellowish reaction solution to dark brown occurred even quicker than in reactions with LAPPERT'S stannylene. Reaction solutions of $\text{Sn}(\text{NEt}_2)_2$ also appeared always even more intense in brown colour than corresponding experiments with $\text{Sn}(\text{HMDS})_2$. Nevertheless, precipitated colourless crystals of **53** seemed to disappear slowly and additional purple crystals formed, which were suitable for single crystal X-Ray diffraction. Structural analysis revealed the formation of the metalloid tin cluster $\text{Sn}_{10}\text{Tripp}_8$ (**55**), which was just recently isolated by SCHULZ and coworkers from the reaction of $(\text{Tripp}_2\text{Sn})_2$ with a Mg(I) reductant.^[51] In ^{119}Sn NMR spectra of the reaction solution (small amount of C_6D_6 was added for locking) next to others at least two resonances at 136.0 and 235.8 ppm were observed, which would fit to ^{119}Sn resonances found by SCHULZ and coworkers in C_6D_6 at 134.7 and 236.7 ppm. A third shift suitable to the literature shift (358.9 ppm) was probably not found and assigned because of solvent effects. Thin layer chromatography of the reaction solutions using pure *n*-heptane as an eluent showed next to a purple coloured spot of **55** at $R_f = 0.6$ also a violet coloured spot at $R_f = 0.9$, which indicates again the formation of a pentastanna[1.1.1]propellane. All in all, disappearance of all colourless crystals and crystallisation of pure **55** took about 4 weeks. Similar observations were found for the reaction with $\text{Dipp}_2\text{SnH}_2$ and **56** could be structurally investigated by X-Ray crystallography. Since $\text{Sn}_4\text{H}_2\text{Dipp}_6$ (**54**) exhibits quite poor solubility compared to **53**, the dissolution of colourless crystals of **54** takes even longer. Heating the reaction solution to 60°C for 1 day followed by heating to 80°C for 4 days led to the dissolution of all colourless crystals and a formation of additional **56**, but also a high amount of

elemental tin was formed in this case. Entire NMR spectroscopical data could not be recorded for **55** and **56** so far, as both compounds exhibit poor solubility in all common deuterated solvents after precipitating from the reaction solution.

Reaction of LAPPERT's germylene with Ar_2SnH_2 ($\text{Ar} = \text{Tripp}$, Dipp) gave in both the corresponding structural analogues of $(\text{Dep}_2\text{SnH})_2$ (**52**), compound $(\text{Tripp}_2\text{SnH})_2$ (**57**) and $(\text{Dipp}_2\text{SnH})_2$ (**58**) as main products in this reaction after 3 days. Compound **57** was proven NMR spectroscopically by ^1H coupled ^{119}Sn NMR, whereas **58** was additionally analysed by X-Ray crystallography to verify the suggested structure. In the case of $\text{Ar} = \text{Dipp}$ the reaction seems to proceed straight forward and no additional products were detected by ^{119}Sn NMR using equimolar amounts of the starting material. For $\text{Ar} = \text{Tripp}$ an additional peak at -65.3 ppm was detected in ^{119}Sn NMR. For further investigations, the reaction of $\text{Dipp}_2\text{SnH}_2$ with $\text{Ge}(\text{HMDS})_2$ was repeated using a 1:0.5 stoichiometric ratio. In this case next to **58** also the formation of **54** was recorded by ^{119}Sn NMR.



Scheme 5.15 Overview of the reactivity of Ar_2SnH_2 ($\text{Ar} = \text{Tripp}$, Dipp) towards Sn(II) amides.

Mentioned observations in reactions of Ar_2SnH_2 with $\text{Sn}(\text{NEt}_2)_2$, the partial redissolution of $\text{Sn}_4\text{H}_2\text{Ar}_6$ ($\text{Ar} = \text{Tripp}$ (**53**), Dipp (**54**)) and the subsequent formation of $\text{Sn}_{10}\text{Tripp}_8$ ($\text{Ar} = \text{Tripp}$ (**55**), Dipp (**56**)), suggest that the four membered ring plays a crucial role in the formation of the metalloid tin clusters **55** and respectively **56**. It seems that basicity of the more stable Sn(II) species $\text{Sn}(\text{HMDS})_2$ is sufficient to form **53** and **54** in the reaction with Ar_2SnH_2 ($\text{Ar} = \text{Tripp}$, Dipp), but basicity of this amide is not strong enough for further reactions with the remaining hydride functionalities of **53** and **54**. In contrast, the more labile and more basic $\text{Sn}(\text{NEt}_2)_2$ seems to further transform the still functional $\text{Sn}_4\text{H}_2\text{Ar}_6$. In order to have a closer look on these events, conversions of isolated $\text{Sn}_4\text{H}_2\text{Dipp}_6$ (**54**) with $\text{Sn}(\text{HMDS})_2$ respectively $\text{Sn}(\text{NEt}_2)_2$ on NMR scale was watched and monitored. Addition of $\text{Sn}(\text{HMDS})_2$ to a suspension of **54** in THF did not lead to any observable change after 10 days. (Figure 5.18) By contrast, adding $\text{Sn}(\text{NEt}_2)_2$ to such a suspension resulted to a noticeable colour change after already 5 h and an intense brown colour similar to reaction solutions of $\text{Dipp}_2\text{SnH}_2$ and $\text{Sn}(\text{NEt}_2)_2$ after 5 days.

(Figure 5.19) Indeed, ^{119}Sn NMR analysis shows evidence for the formation of **56**. Additionally, briefly heating of a colourless suspension of **54** in 1, 2-dichlorobenzene resulted in a colour change to purple. Again in this solution next to resonances assigned to **54**, shifts at 332.0, 231.2 and 139.0 ppm were detected by ^{119}Sn NMR, which could indicate again the formation of **56**. For complete comprehension of these reactions, further investigations have to be done in future.



Figure 5.18 Conversion of $\text{Sn}_4\text{H}_2\text{Dipp}_6$ (**54**) with $\text{Sn}(\text{HMDS})_2$ on NMR scale in THF. Photo on the left shows the solution before addition of the tin(II) amide. Second photo shows the solution after addition of $\text{Sn}(\text{HMDS})_2$. Photo on the right shows the solution after 10 days. No colour change was observed at all.

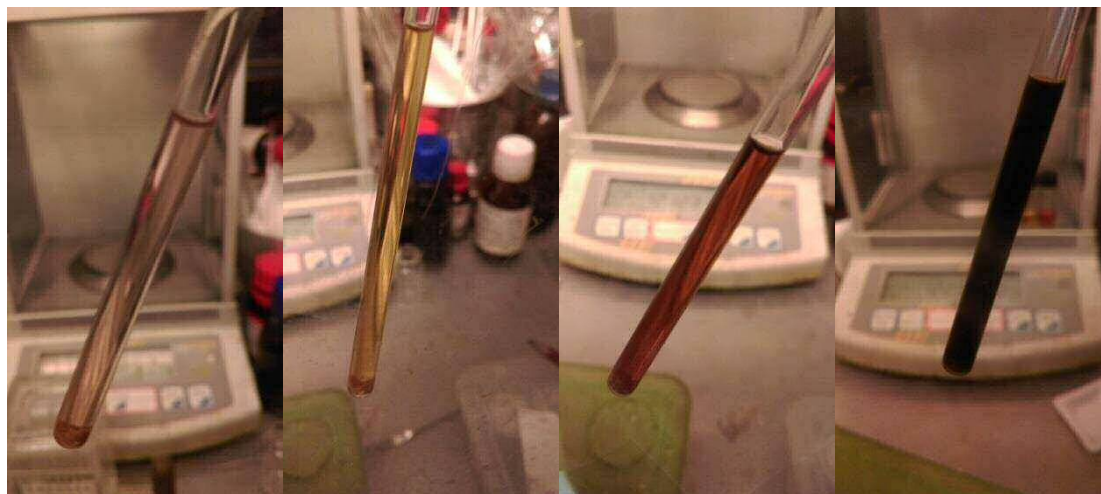


Figure 5.19 Conversion of $\text{Sn}_4\text{H}_2\text{Dipp}_6$ (**54**) with $\text{Sn}(\text{NEt}_2)_2$ on NMR scale in THF. Photo on the left shows the solution before addition of the tin(II) amide. Second photo shows the solution after addition of $\text{Sn}(\text{NEt}_2)_2$. Photos on the right show the colour change of the solution after 5 h and after 5 days.

5.3.1.3 Conclusive Considerations

In brief, reaction outcome in the conversion of Ar_2SnH_2 with E(II) amides depends strongly on the chosen low valent species, whereas the stability of the E(II) species and the basicity of amide substituents seem to direct the resulting main product. Since experiments of $\text{Tripp}_2\text{SnH}_2$ and $\text{Dipp}_2\text{SnH}_2$ show nearly identical results in contrast to Dep_2SnH_2 , the sterical demand of the *ortho* substituent may also play an important role in guiding the reaction outcome.

In order to proof the requirement of the low valent species and confirm that not potential contamination originating from the synthesis of the Sn(II) amides, like unreacted lithium amide or the hydrolysed amine, are responsible for the observed reactivity, reactions of latter compounds with $\text{Dipp}_2\text{SnH}_2$ were investigated as well. In all these experiments, no formation of a dark brown reaction solution was observed as earlier described for the reactions with Sn(II) amide species. (Figure 5.20) In the case of $(\text{CH}_3\text{Si})_2\text{NH}$, no conversion of the starting material $\text{Dipp}_2\text{SnH}_2$ was detected at all. Conversions of the same organotin hydride with lithium amides $(\text{CH}_3\text{Si})_2\text{NLi}$ and Et_2NLi resulted in yellow reaction solutions, which did not show any evidence for the formation of described neutral tin compounds, but again forming similar anionic tin species as described in section 5.2.1 Anionic Chains and Rings.



Figure 5.20 Reaction solutions of $\text{Dipp}_2\text{SnH}_2$ with $(\text{CH}_3\text{Si})_2\text{NH}$ (HMDS-H, left), $(\text{CH}_3\text{Si})_2\text{NLi}$ (HMDS-Li, middle) and Et_2NLi (right).

5.3.2 X-Ray Crystallography

In the following subchapter, structural data of previously presented compounds will be discussed. Some of the examined compounds have been already investigated by X-Ray crystallography and will be compared to data available in literature. Novel compounds will be referred to structurally related compounds. For more detailed information about measurement and refinement for discussed structures see the Appendix.

5.3.2.1 Structures derived from Dep_2SnH_2

Compound **49** was isolated from the reaction of Dep_2SnH_2 with $\text{Sn}(\text{NEt}_2)_2$ as a possible intermediate in the formation of final products. Two bridging amides connect two adjacent tin atoms (Sn1 and Sn1\#), which do not feature any organic substituents, and so form a trapezoidal shaped tin backbone with angles of $94.92(1)^\circ$ (Sn1-Sn2-Sn2\#) and 84.65° (Sn2-Sn1-Sn1\#). (Figure 5.21) Amide connected tin atoms can be considered as low valent and originate presumably from the $\text{Sn}(\text{II})$ amide starting material. An angle sum of $268.2(3)^\circ$ observable on these tin centres implies the high p character of bonding orbitals and the high s character of orbital occupied by the remaining inert lone electron pair. The Sn-Sn bond distance of these tin centres (Sn1-Sn2 $2.9300(1)$ Å) is slightly extended compared to the ones between the tetravalent tin atoms (Sn2-Sn2\# $2.8785(6)$ Å). Tin carbon bond lengths fall in between $2.207(4)$ - $2.217(5)$ Å.

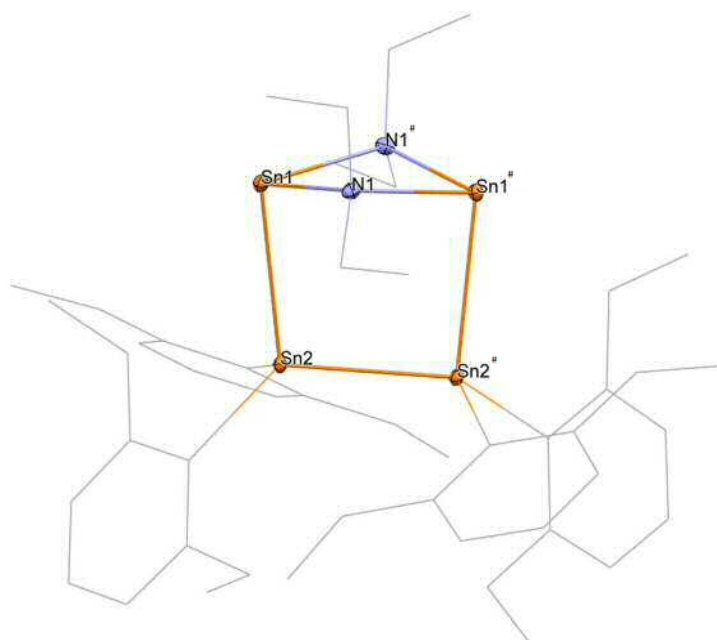


Figure 5.21 Molecular structure of $\text{Sn}_4\text{Dep}_4(\text{NEt}_2)_2$ (**49**). Hydrogen atoms are omitted for clarity. Ellipsoids possess a probability of 30%. Selected distances [Å] and angles [$^\circ$]: Sn1-Sn2 $2.9300(1)$, Sn2-Sn2\# $2.8785(6)$, Sn2-C5 $2.217(5)$, Sn2-C15 $2.207(4)$, Sn1-N1 $2.266(4)$, Sn1-N1\# $2.270(3)$, Sn1-Sn2-Sn2-Sn2\# $97.3(1)$, C5-Sn2-C15 $100.8(2)$, Sn2-Sn1-N1 $96.0(1)$, Sn2-Sn1-N1\# $91.7(1)$, N1-Sn1-N1\# $80.5(1)$.

Molecular structure of $(\text{Dep}_2\text{Sn})_3$ (**51**) was already determined by MASAMUNE and SITA.^[102] The tin backbone of this compound builds up an approximate perfect equilateral triangle with an average Sn–Sn bond length of 2.859(8) Å and an average Sn–Sn–Sn bond angle of 60.0(1)° as illustrated in Figure 5.22. This observation and all other found values are in accordance with the observations in literature. Related derivative $(\text{Tripp}_2\text{Sn})_3$ features longer Sn–Sn bond distances compared to **51**, probably because of the bigger sterical demand of the aryl group substituents.

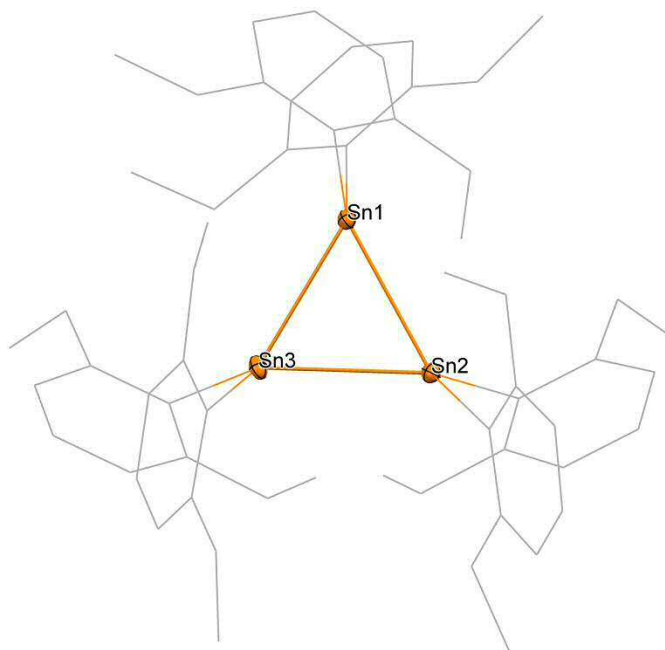


Figure 5.22 Molecular structure of $(\text{Dep}_2\text{Sn})_3$ (**51**). Hydrogen atoms are omitted for clarity. Ellipsoids are drawn with 30% probability. Selected distances [Å] and angles [°]: Sn1–Sn3 2.849(1), Sn1–Sn3 2.875(1), Sn2–Sn3 2.855(1), Sn1–C41 2.19(1), Sn2–C11 2.20(1), Sn2–Sn1–Sn3 59.84(3), Sn1–Sn2–Sn3 59.62(3), Sn1–Sn3–Sn2 60.53(3).

Initial structural investigation of **50** was also accomplished by SITA.^[59] However, in structural data available in literature next to pentastanna[1.1.1]propellane also $(\text{Dep}_3\text{Sn})_2$ cocrystallised in the unit cell. In terms of this work, a novel unit cell solely occupied by four pentastanna[1.1.1]propellanes was determined, which crystallise in the monoclinic space group $P2_1/c$. Molecular structure of **50** is illustrated in Figure 5.23. In Table 5.12 its bond distances and angles are compared to values available in literature. Except for the space group there are no structural deviations from the example in literature.

Table 5.12 Comparison of known structure of Sn₅Dep₆ and one found in terms of this thesis. Bridgehead atoms are here denoted as Sn^b.

	Space Group	Sn ^b -Sn [Å] (avg.)	Sn ^b ...Sn ^b [Å]	Sn-C [Å] (avg.)	Σ Sn-Sn ^b -Sn [°]	Sn ^b -Sn-Sn ^b [°] (avg.)
Sn ₅ Dep ₆ ^[59]	P-1	2.857(8)	3.367(3)	2.19(1)	266.55(1) 266.39(1)	72.19(6)
Sn ₅ Dep ₆ (50)	P2 ₁ /c	2.852(8)	3.373	2.188(9)	266.20(6) 265.44(6)	72.47(3)

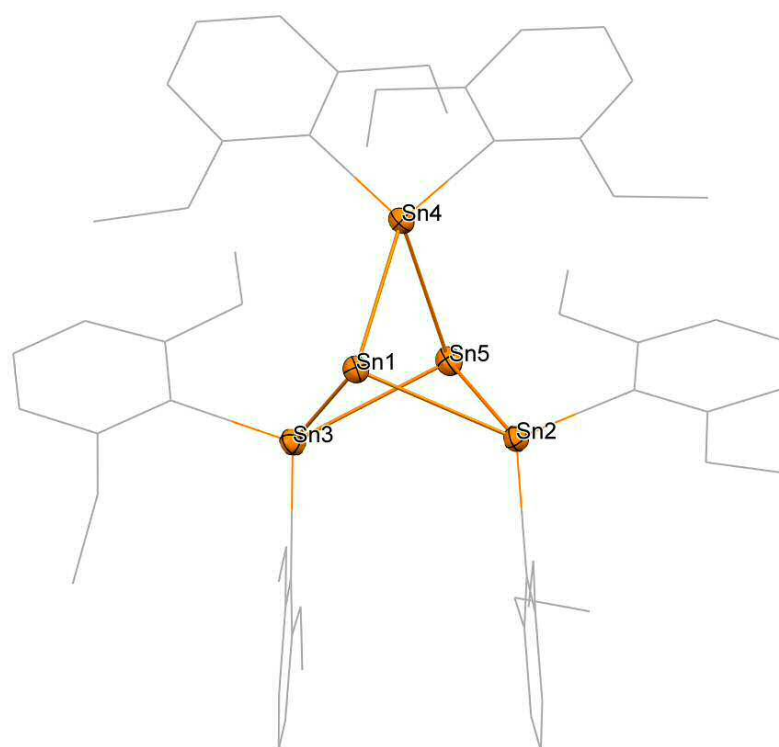


Figure 5.23 Molecular structure of pentastanna[1.1.1]propellane Sn₅Dep₆ (**50**). Hydrogen atoms are omitted for clarity. Ellipsoids are drawn with 30% probability. Selected distances [Å] and angles [°]: Sn1-Sn2 2.8531(6), Sn1-Sn3 2.8384(8), Sn1-Sn4 2.8569(7), Sn1...Sn5 3.373, Sn2-Sn5 2.8562(7), Sn3-Sn5 2.8668(7), Sn4-Sn5 2.8449(7), Sn2-SnC1 2.198(7), Sn2-C1 2.200(8), Sn2-Sn1-Sn4 90.18(2), Sn2-Sn1-Sn4 87.53(2), Sn3-Sn1-Sn4 88.49(2), Sn1-Sn2-Sn5 72.42(5), Sn1-Sn3-Sn5 72.47(2), Sn1-Sn4-Sn5 72.52(2), Sn2-Sn5-Sn3 86.93(2), Sn2-Sn5-Sn4 88.66(2), Sn3-Sn5-Sn4 89.85(2).

5.3.2.2 Structures derived from Tripp₂SnH₂ and Dipp₂SnH₂

Using Ge(HMDS)₂ as an E(II) amide species in conversion with Dipp₂SnH₂ yields yellowish, nearly colourless crystals of dimeric compound **58**, which turned out to be suitable for X-Ray crystallography. (Dipp₂SnH)₂ (**58**) crystallises in the monoclinic space group C 2/c. Its molecular structure is shown in Figure 5.24. Both tin atoms are found in a slightly distorted tetrahedral environment, covalently bound to two aryl substituents, one tin and one hydride. The Sn-H bond

exhibiting a length of 1.79(3) Å is not altered gravely from the derived diarylytin dihydride $\text{Dipp}_2\text{SnH}_2$ (**29**) (1.71(2) and 1.70(3) Å). Found Sn–Sn bond distances are slightly shorter compared to the next discussed tin rings **53** and **54**. The Sn–C bond lengths fall into the known range (2.169(3)-2.174(3) Å).

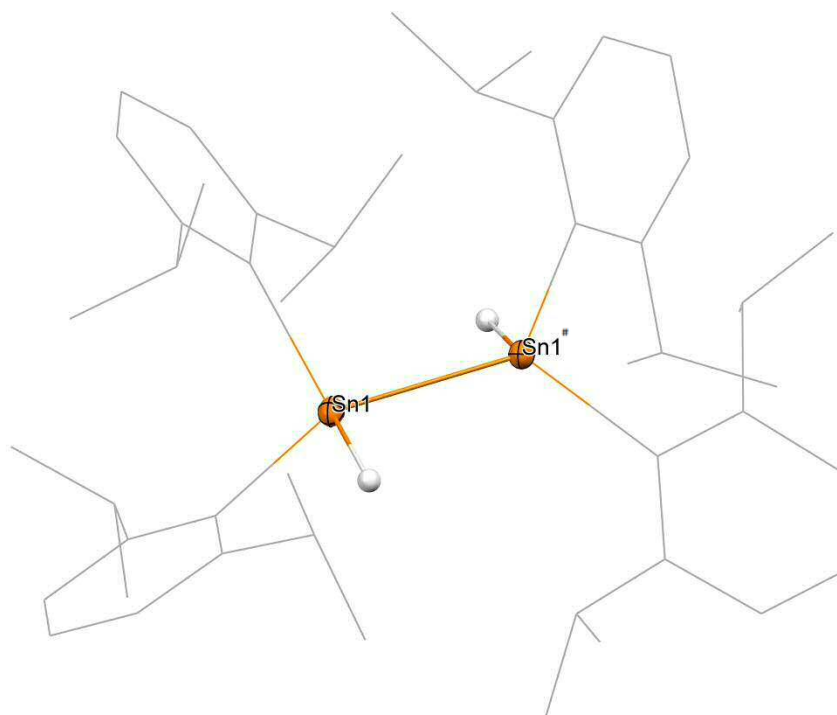


Figure 5.24 Molecular structure of $(\text{Dipp}_2\text{SnH})_2$ (**58**). Ellipsoids are shown with 30% probability. Hydrogen atoms except Sn–H atoms are omitted for clarity. Selected bond lengths [Å] and angles [°]: Sn1–Sn1# 2.7497(7), Sn1–H1 1.79(3), Sn1–C1 2.174(3), Sn1–C13 2.169(3), Sn1#–Sn1–H1 103(1), C1–Sn1–C13 105.8(1), C1–Sn1–H1 115(1).

Molecular structures of **53** and **54**, gained from approaches using $\text{Sn}(\text{HMDS})_2$, are illustrated in Figure 5.25 and Figure 5.26 respectively. All hydrogen atoms bound to tin were located in the difference map. In initial crystal structure determination experiments, colourless crystals of **53** were cooled down as usual to 100 K with a cold N_2 stream for measurement. Due to a potential phase transition during cooling down, data collected from these approaches was not sufficient. Eventually, data collected from measurements at room temperature led to satisfying results. Common characteristic in both structures is the *trans* orientation of the two remaining hydride functionalities, which may be formed owing to the sterical demand of the aryl substituents. Additionally, the tin backbone in both molecular structures builds up a flat almost perfect rhombic, nearly square shaped, structure. The Sn–Sn–Sn angles found on the tin centres still featuring a hydride functionality (95.63(1)° in **53**; 95.08(4) and 94.53(4)° in **54**) are widened compared to corresponding angles on tin atoms displaying only carbon substituents (84.37(1)° for **53**; 85.12(3) and 85.20(4)° for **54**). The average Sn–Sn bond distance in **53** (2.860(1) Å) corresponds nicely to the average Sn–Sn bond length found in **54** (2.853(8) Å).

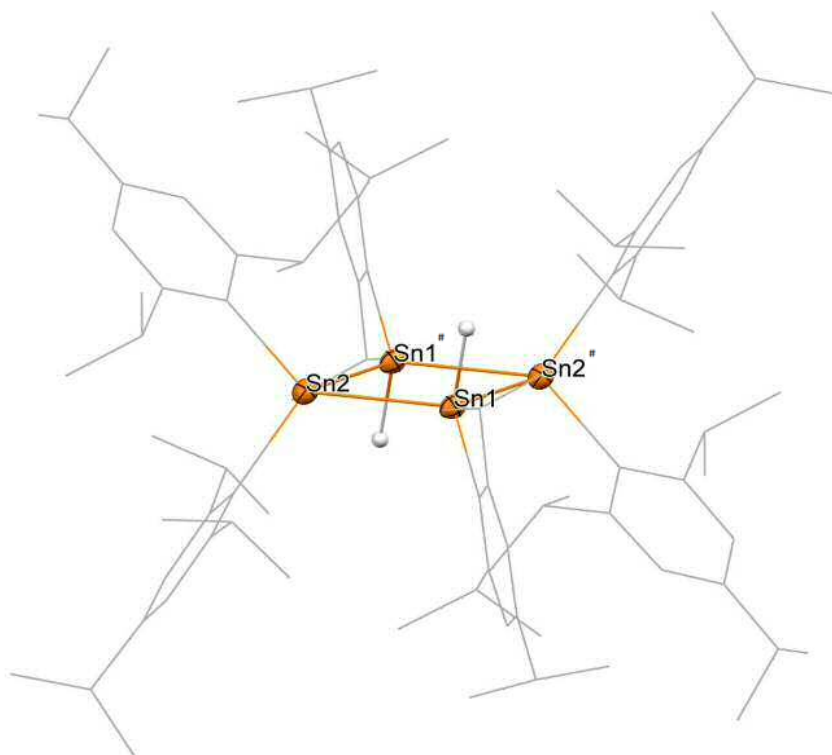


Figure 5.25 Molecular structure of $\text{Sn}_4\text{H}_2\text{Tripp}_6$ (**53**). Ellipsoids possess a probability of 30%. Hydrogen atoms except Sn-H atoms are omitted for clarity. Selected distances [\AA] and angles [$^\circ$]: Sn1-Sn2 2.8559(5), Sn1-Sn2# 2.8640(6), Sn1-H1 1.68(5), Sn1-C1 2.186(4), Sn2-C31 2.215(4), Sn2-C16 2.212(5), Sn2-Sn1-Sn2# 95.63(1), Sn1-Sn2-Sn1# 87.37(1).

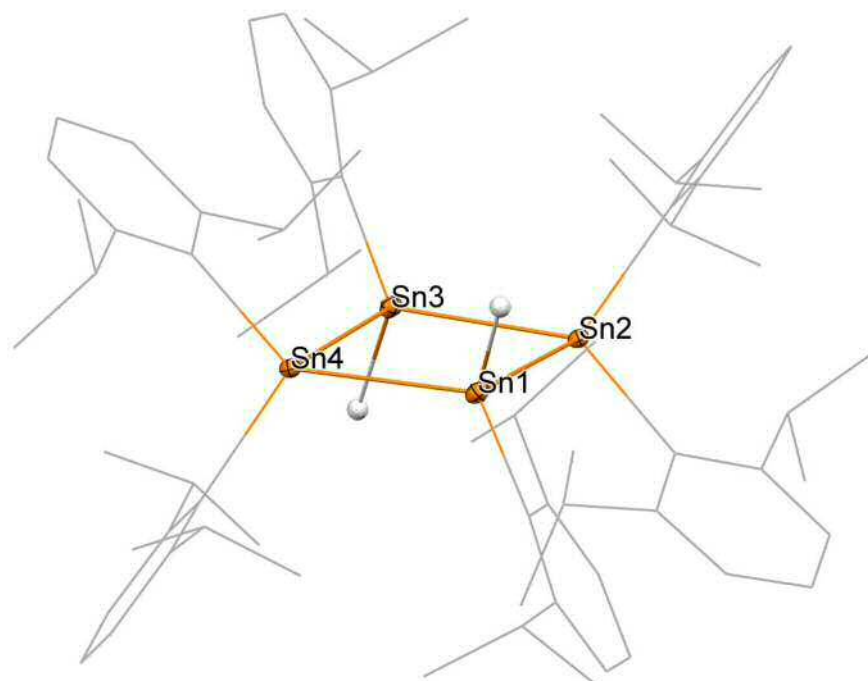


Figure 5.26 Molecular structure of $\text{Sn}_4\text{H}_2\text{Dipp}_6$ (**54**). Ellipsoids possess a probability of 30%. Hydrogen atoms except Sn-H atoms are omitted for clarity. Selected distances [\AA] and angles [$^\circ$]: Sn1-Sn4 2.842(1), Sn1-Sn2 2.853(1), Sn2-Sn3 2.857(1), Sn3-Sn4 2.863(1), Sn1-H1 1.7(1), Sn3-H2 1.9(1), Sn1-C1 2.20(1), Sn2-C13 2.213(9), Sn2-C25 2.21(2), Sn3-C37 2.204(9), Sn4-C49 2.214(9), Sn4-C61 2.21(1), Sn2-Sn1-Sn4 95.08(4), Sn1-Sn2-Sn3 85.12(3), Sn2-Sn3-Sn4 94.53(4), Sn1-Sn4-Sn3 85.50(4).

Only recently, the structurally related compounds $[\text{SnHAr}^*]_4$ and $[\text{SnH}(\text{CH}(\text{TMS})_2)]_4$ have been isolated by POWER^[81] and WESEMANN^[48]. Structural data of latter compounds are compared to the isolated structures **53** and **54** in Table 5.13. Like WESEMANN's $[\text{SnH}(\text{CH}(\text{TMS})_2)]_4$, **53** and **54** are flat, whereas $[\text{SnHAr}^*]_4$ exhibits a butterfly geometry enclosing an angle of 143.4°. Nearly all bond distances of latter are comparable to these literature values, except for the average Sn–H bond distances (1.68(5) and 1.8(1) Å), which are slightly extended compared to the found Sn–H in $[\text{SnHAr}^*]_4$ (1.451(2) Å).

Table 5.13 Summary of structural data found in the molecular structures in $[\text{SnHAr}^*]_4$ ^[81], $[\text{SnH}(\text{CH}(\text{TMS})_2)]_4$ ^[48], $\text{Sn}_4\text{H}_2\text{Tripp}_6$ (**53**) and $\text{Sn}_4\text{H}_2\text{Dipp}_6$ (**54**).

	Space Group	Sn–Sn [Å] (avg.)	Sn–C [Å] (avg.)	Sn–H [Å] (avg.)	Sn–Sn–Sn [°] (avg.)
$[\text{SnHAr}^*]_4$ ^[81]	Fddd	2.8242	2.1730(8)	1.451(2)	87.03
$[\text{SnH}(\text{CH}(\text{TMS})_2)]_4$ ^{[48], h}	P2 ₁ /c	2.8146(5)	2.186(1)	-	-
$\text{Sn}_4\text{H}_2\text{Tripp}_6$ (53)	P-1	2.860(1)	2.204(8)	1.68(5)	95.63(1) 87.37(1)
$\text{Sn}_4\text{H}_2\text{Dipp}_6$ (54)	P-1	2.853(8)	2.197(1)	1.8(1)	94.80(1) 85.31(2)

The isolated metalloid tin clusters $\text{Sn}_{10}\text{Tripp}_8$ was just recently structurally investigated.^[51] Nevertheless, structural data determined in terms of this work are compared to the ones found by WIEDERKEHR *et al.* in Table 5.14. In all cases $\text{Sn}_{10}\text{Ar}_8$ (Ar = Tripp, Dipp) crystallises in the low symmetry space group P-1. Also all bond distances and bond angles of investigated structures **55** and **56** compare nicely to the literature values for this type of cluster. Molecular structures of these compounds are depicted in Figure 5.27 and Figure 5.28 respectively. More interestingly, the inner structural motif in **55** and **56** spanned by the metalloid tin atoms resembles the motif in compound Sn_8Ar^*_4 (**16**), which was mentioned in section 4.3.4.3 Activation of Small Molecules. Viewing **16**, **55** and **56** from the side shows that a rhomboid is shaped by the metalloid tin atoms in the centre as illustrated in Figure 5.29. Structural data including selected distances and angles of this rhomboid are summarised in Table 5.15. Distances of opposed tin atoms, displaying an obtuse angle (114.68–118.14°) in this rhomboid, show a Sn···Sn distances of 3.223–32622(4) Å, which is shorter than the

^h X-Ray data of $[\text{SnH}(\text{CH}(\text{TMS})_2)]_4$ was not available in webCCDC database and structural information was only mentioned with restrictions in published literature.

$\text{Sn}^b \cdots \text{Sn}^b$ distance in already discussed pentastanna[1.1.1]propellane Sn_5Dep_6 (3.367(3) Å). The nature of bonding between these bridgehead atoms in Sn_5Dep_6 has not been clarified, so far. Nevertheless, it has been agreed that interaction between these atoms is required to some extent.^[74] Comparable distances between two metalloids tin atoms in **16**, **55** as well as **56** suggests a similar bonding situation. By all means, nature of bonding in isolated structures cannot be described with classical bond models. Due to the structural relations between isolated metalloids clusters and **16**, a similar activation of small molecules as published for latter might be possible and will be part of future investigations.^[81]

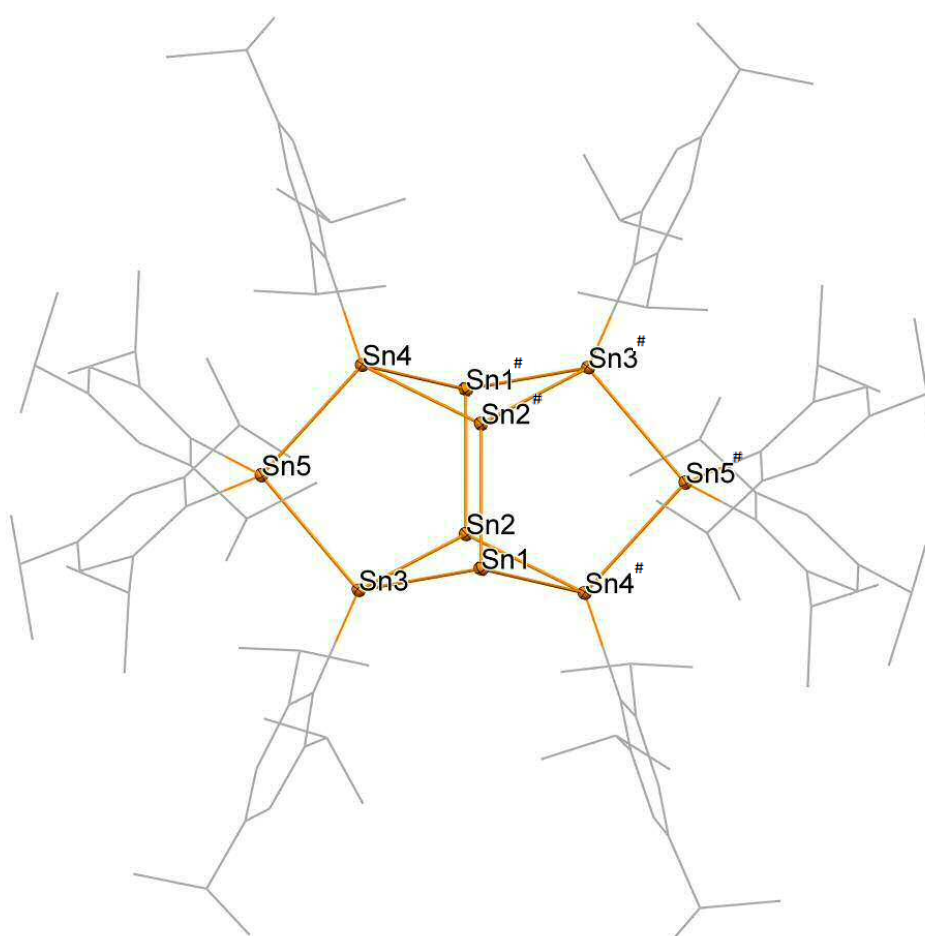


Figure 5.27 Molecular structure of $\text{Sn}_{10}\text{Tripp}_8$ (**55**). Hydrogen atoms are omitted for clarity. Ellipsoids possess a probability of 30%. Selected distances [Å] and angles [°]: Selected distances [Å] and angles [°]: Sn1-Sn2# 2.8748(5), Sn1-Sn3 2.8875(5), Sn1-Sn4# 2.8864(5), Sn2 \cdots Sn2# 3.2385(5), Sn2-Sn3 2.8161(5), Sn2-Sn4# 2.8014(5), Sn3-Sn5 2.8574(4), Sn4-Sn5 2.8512(5), Sn3-C1 2.202(4), Sn4-C16 2.197(4), Sn5-C31 2.206(4), Sn5-C46 2.196(5), Sn3-Sn1-Sn4# 96.52(1), Sn3-Sn2-Sn4# 100.16(1), Sn1-Sn3-Sn2 72.46(1), Sn1#-Sn4-Sn2# 72.69(1), Sn3-Sn5-Sn4 97.57(1).

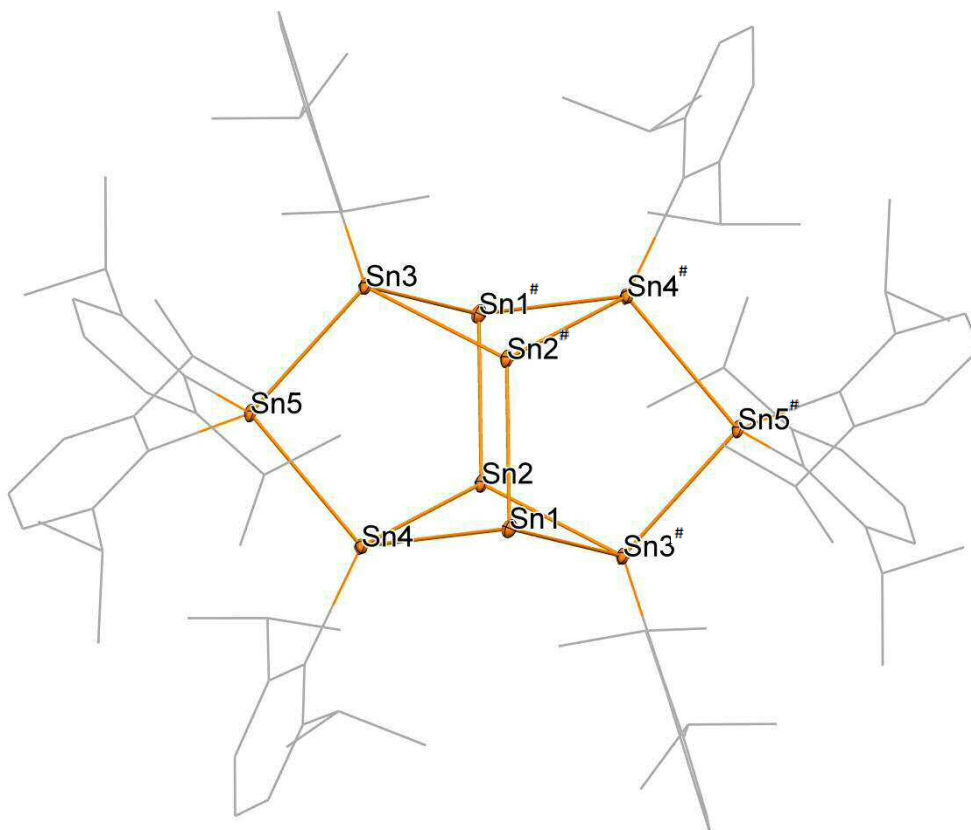


Figure 5.28 Molecular structure of $\text{Sn}_{10}\text{Dipp}_8$ (**56**). Hydrogen atoms are omitted for clarity. Ellipsoids possess a probability of 30%. Selected distances [Å] and angles [°]: Sn1-Sn2# 2.8876(6), Sn1-Sn3# 2.8843(5), Sn1-Sn4 2.8829(4), Sn2...Sn2# 3.2622(4), Sn2-Sn3# 2.8327(4), Sn2-Sn4 2.8164(6), Sn3-Sn5 2.8572(5), Sn4-Sn5 2.8535(4), Sn3-C1 2.200(3), Sn4-C13 2.192(3), Sn5-C25 2.205(3), Sn5-C37 2.200(3), Sn3#-Sn1-Sn4 97.73(1), Sn3#-Sn2-Sn4 100.51(1), Sn1-Sn3#-Sn2 72.06(1), Sn1-Sn4-Sn2 72.32(1), Sn3-Sn5-Sn4 97.40(1).

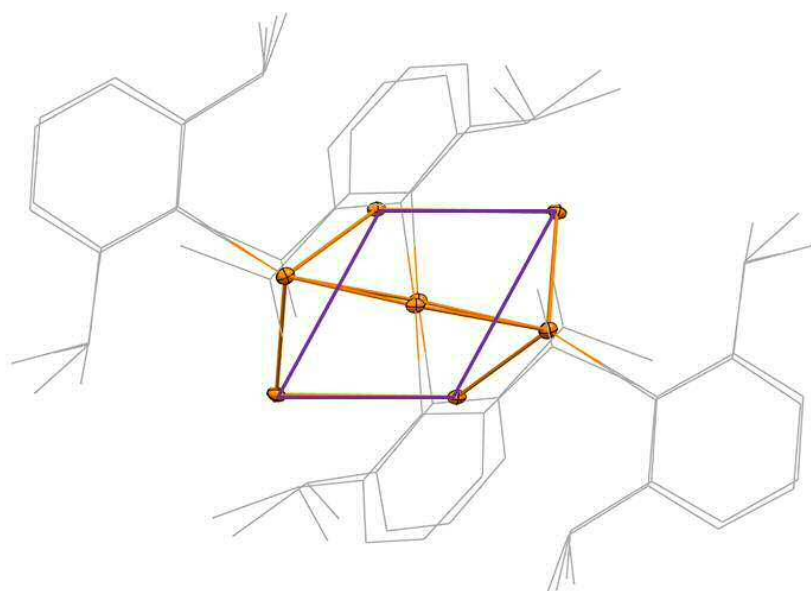


Figure 5.29 Compound Sn_8Dipp_8 (**56**) viewed from the side. The rhomboid spanned by the metalloid tin atoms is highlighted in violet.

Table 5.14 Comparison of published structure for $\text{Sn}_{10}\text{Tripp}_8$ ^[51] and structurally investigated $\text{Sn}_{10}\text{Tripp}_8$ (55) and $\text{Sn}_{10}\text{Dipp}_8$ (56). Metalloid tin centres are denoted as Sn^0 .

	$\text{Sn}^0\text{-Sn}$ [Å](avg.)	Sn-Sn [Å](avg.)	$\text{Sn}^0\text{-Sn}^0$ [Å]	$\text{Sn}^0\cdots\text{Sn}^0$ [Å]	Sn-Sn-Sn [°]	$\text{Sn-Sn}^0\text{-Sn}$ [°]	$\text{Sn}^0\text{-Sn-Sn}^0$ [°]
$\text{Sn}_{10}\text{Tripp}_8$ ^[51]	2.8513(6)	2.8579(3)	2.8757(9)	3.2638(9)	98.03(2)	100.43 97.10	71.90 72.20(2)
$\text{Sn}_{10}\text{Tripp}_8$ (55)	2.8479(1)	2.8543(2)	2.8748(5)	3.2385(5)	97.57(1)	96.52(1) 100.16(1)	72.69(1) 72.46(1)
$\text{Sn}_{10}\text{Dipp}_8$ (56)	2.8541(3)	2.8555(2)	2.8876(6)	3.2622(4)	97.40(1)	97.73(1) 100.51(1)	72.32(1) 72.06(1)

Table 5.15 Structural motif built by metalloid tin atoms in $\text{Sn}_{10}\text{Tripp}_8$ (55) and $\text{Sn}_{10}\text{Dipp}_8$ (56) compared to the metalloid tin cluster Sn_8Ar^* ₄ ($\text{Ar}^* = \text{Ar}^* = 2,6\text{-Mes}_2\text{C}_6\text{H}_3$)^[103].

	$\text{Sn}^1\text{-Sn}^2$ [Å]	$\text{Sn}^1\cdots\text{Sn}^{2\#}$ [Å]	$\text{Sn}^0\cdots\text{Sn}^0$ [Å]	$\text{Sn}^1\text{-Sn}^2\text{-Sn}^{1\#}$ [°]
Sn_8Ar^* ^[103]	2.853	3.107(2)	3.223	114.68
$\text{Sn}_{10}\text{Tripp}_8$ (55)	2.8748(5)	3.372	3.2385(5)	118.14
$\text{Sn}_{10}\text{Dipp}_8$ (56)	2.8876(6)	3.363	3.2622(4)	117.63(1)

$\text{Sn}^{2\#}\text{---Sn}^{1\#}$
 $\text{Sn}^1\text{---Sn}^2$

Therewith, it was shown that diaryltin dihydrides in the reaction with low valent group 14 amides give access to non-cyclic, cyclic and oligocyclic molecular compounds, including structures featuring non-classical bonding. In further investigations, fine tuning of applied reaction conditions regarding solvent, temperature and stoichiometry will be of central interest. Additionally, altering the aryl substituent on the tetravalent tin centre could enclose even more structural possibilities. Since this approach was proven to be convenient route granting access to a wide variety of compounds, its principle could also be extended to other main group as well as transition metal amides or even alcoholates.

7 Experimental Section

7.1 Materials and Methods

All manipulations involving air or moisture sensitive compounds were either performed under a nitrogen atmosphere using standard Schlenk tube techniques or were carried out in a nitrogen flushed Glovebox UNILAB supplied by M.Braun. The solvents bis(2-methoxyethyl)ether (dried over Potassium) as well as acetonitrile (dried over phosphorus pentoxide) were distilled prior to use. All other dried and deoxygenated solvents were obtained from an Innovative Technology solvent drying system. These solvents were used without any further purification except for THF applied in various Grignard reactions, which was additionally dried over LiAlH_4 and freshly distilled prior use.

SnCl_4 anhydrous (98% v/v) purchased from Alfa Aesar was distilled and stored under nitrogen. Anhydrous SnCl_2 was obtained by dehydration of the corresponding dihydrate according to literature.^[104] For the conversions with organotin hydrides, purchased LiAlH_4 was recrystallised from Et_2O . All other chemicals from commercial sources were used as purchased from chemical suppliers. Elemental analysis was performed with an Elementar Vario MICRO cube. Melting point measurements were carried out by threefold determination with a Buechi 535 or a Electrothermal Mel-Temp instrument.

7.1.1 NMR Spectroscopy

^1H (300.22 MHz), ^{13}C (75.5 MHz), ^{29}Si (59.64 MHz) as well as ^{119}Sn (111.92 MHz) NMR spectra were recorded on a Varian Mercury 300 MHz spectrometer from Varian at 25°C if not otherwise stated. Chemical shifts are given in ppm relative to TMS regarding ^1H , ^{13}C and ^{29}Si and in case ^{119}Sn relative to Me_4Sn . Spectra were referenced to solvent residual signals. Coupling constants (^nJ) are reported in Hertz (Hz).

7.1.2 ATR-FTIR

All IR measurements were measured fast under ambient conditions on an *ALPHA-P* device from Bruker in transmission modus. The letters s (strong), m (medium) and w (weak) are used to indicate the intensity of the transmission bands.

7.1.3 UV/VIS

All UV/VIS measurements were performed in quartz glass cuvettes with a thickness of 1 cm on a Cary 60 UV-VIS device from Agilent Technologies. If not otherwise stated, measurements were done in absorption mode. Analysis of measured results was done with Spekwin32. Dry acetonitrile was used as solvent in all cases. Absorption maxima are given in nm.

7.1.4 Mass Spectrometry

Mass spectrometry measurements were performed using a “Waters GCT Premier” system after ionization with an EI ionization source ($E = 70$ eV). The measured compounds were directly injected as solution (DI) in THF. The reported values for a given species are denoted as mass to charge ratio, accompanied by the corresponding calculated values.

7.1.5 Crystal Structure Determination

For single crystal X-ray diffractometry all suitable crystals were covered with a layer of silicone oil. A single crystal was selected, mounted on a glass rod on a copper pin, and placed in the cold N_2 stream provided by an Oxford Cryosystems cryometer ($T=100$ K, if not otherwise stated). XRD data collection was performed on a Bruker APEX II diffractometer with use of Mo $K\alpha$ radiation ($\lambda = 0.71073$ Å) and a CCD area detector. Empirical absorption corrections were applied using SADABS.^[105,106] The structures were solved with use of either direct methods or the Patterson option in SHELXS and refined by the full-matrix least-squares procedures in SHELXL.^[107,108] The space group assignments and structural solutions were evaluated using PLATON.^[109,110] Non-hydrogen atoms were refined anisotropically. Hydrogen atoms next to the heavy atom Sn were found on the difference Fourier map, however it should be noted that a common problem exists with locating light atoms (hydrogens) next to heavy atoms because of their poor scattering abilities. All other hydrogen atoms were located in calculated positions corresponding to standard bond lengths and angles.

7.2 Synthesis

7.2.1 Synthesis of Aryl bromides

Synthesis of MesBr (59)

To a mixture of 280 mL mesitylene (241 g, 2.0 mol, 1.0 eq) and the same volume of H₂O in 3-necked round bottom flask 100 mL bromine (312 g, 1.95 mol, 0.97 eq) were added dropwise over a period of 180 min at 0°C. The resulting pale orange emulsion was stirred for 17 h at rt. The phases were then separated and the organic phase was washed with saturated NaHCO₃ solution (3x200 mL). The combined organic layers were dried over Na₂SO₄, filtered and the solvent was removed under reduced pressure to give a yellow liquid. The crude product was purified by vacuum distillation (90°C, 10 mbar).

Yield: 240.3 g (60%), colourless clear liquid. ¹H NMR (300.22 MHz, CDCl₃) δ 6.91 (s, 2 H; H^{Ar}), 2.40 (s, 6 H; *o*-CH₃), 2.26 (s, 3 H; *p*-CH₃) ppm. ¹³C NMR (75.5 MHz, CDCl₃) δ 137.99 (C^{Ar}), 136.36 (C^{Ar}), 129.15 (C^{Ar}), 124.32 (C^{Ar}), 23.83 (*o*-CH₃), 20.79 (*p*-CH₃) ppm.

Synthesis of TrippBr (60)^[111]

At 0°C a solution of 20.5 mL bromine (64.0 g, 0.401 mol, 0.97 eq) in 50 mL CCl₄ was added slowly to a suspension of 100 mL 1,3,5-triisopropylbenzene (84.5 g, 0.413 mol, 1.0 eq) and 3.3 g iron powder in 50 mL CCl₄ in a 3-necked round bottom flask. After the reaction was stirred for 22 h incomplete conversion was detected by ¹H-NMR and additional 4 mL bromine (12.5 g, 78.0 mmol, 0.19 eq) in 10 mL CCl₄ were added at 0°C. The reaction was stirred additional 20 h. After full conversion, the reaction was cooled to 0°C and was quenched with NaOH solution (200 mL, prepared from 40 g NaOH in 250 mL H₂O dest.). The phases were separated and the organic layer was washed with H₂O dest. (2x200 mL), then dried over Na₂SO₄, filtered and the solvent was removed under reduced pressure. The redish brown liquid crude product was purified by vacuum distillation (130°C, 11 mbar).

Yield: 112.0 g (96%), colourless clear liquid. ¹H NMR (300.22 MHz, CDCl₃) δ 7.01 (s, 2 H; H^{Ar}), 3.51 (septet, ³J_{H,H} = 6.8 Hz, 2 H; 2xCH(CH₃)₂), 2.89 (septet, ³J_{H,H} = 6.8 Hz, 1 H; CH(CH₃)₂), 1.27 (d, ³J = 6.8 Hz, 18 H; 6xCH₃) ppm. ¹³C NMR (75.5 MHz, CDCl₃) δ 147.95 (C^{Ar}), 147.53 (C^{Ar}), 123.74 (C^{Ar}), 122.43 (C^{Ar}), 34.20 (CH), 33.70 (CH), 24.18 (CH₃), 23.26 (CH₃) ppm.

Synthesis of DippBr (61)

In a 4 L 3-necked round bottom flask equipped with a reflux condenser and two 250 mL dropping funnels a solution of 96 mL CHBr₃ (277.4 g, 1.10 mol, 1.1 eq) in 500 mL DME was heated up to 60°C. Simultaneously 125 mL isobutyl nitrite (108.8 g, 1.05 mol, 1.05 eq) in 125 mL DME and 188 mL

2,6-diisopropylaniline (176.7 g, 1.0 mol, 1.0 eq) in 188 mL DME were added dropwise over a period of 2.5 h at 60°C. The solution turned brown and slight bubble formation was observed. After full supplementation, the reaction was stirred for 6.5 h at 60°C. As incomplete conversion was detected by ^1H NMR, additional 70 mL isobutyl nitrite (60.9 g, 0.59 mol, 0.6 eq) in 50 mL DME were added and stirred additionally for 15 h at 50°C. Subsequent the reaction was heated to 100°C for 2 h. After full conversion was detected by ^1H NMR, solvent was removed under reduced pressure to give a redish brown liquid. The crude product was purified by vacuum distillation. (94°C, 5 mbar)

Yield: 126.5 g (53%), slightly yellow liquid. ^1H NMR (300.22 MHz, CDCl_3) δ , 7.39-7.33 (m, 1 H; H^{Ar}), 7.25 (d, $^3J_{\text{H,H}} = 7.9$ Hz, 2 H; $2\times\text{H}^{\text{Ar}}$), 3.64 (septet, $^3J_{\text{H,H}} = 6.9$ Hz, 2 H; $2\times\text{CH}$), 1.37 (d, $^3J_{\text{H,H}} = 6.9$ Hz, 12 H; $4\times\text{CH}_3$) ppm. ^{13}C NMR (75.5 MHz, CDCl_3) δ 147.89 (C^{Ar}), 127.49 (C^{Ar}), 126.68 (C^{Ar}), 124.28 (C^{Ar}), 33.72 (CH), 23.20 (CH_3) ppm.

Synthesis of DepBr (62)

A similar procedure as for DippBr (61) was applied for the synthesis of 2-bromo-1,3-diethylbenzene. Over a period of 6 h, 164.7 mL 2,6-diethylaniline (149.24 g, 1.00 mol, 1.0 eq) in 85 mL DME and 130 mL isobutyl nitrite (113.4 g, 1.10 mol, 1.1 eq) in 120 mL DME were added simultaneously *via* a dropping funnel to a solution of 96 mL bromoform (277.4 g, 1.10 mol, 1.1 eq) in 500 mL DME heated up to 60°C. After full supplementation, the reaction was stirred at rt for 16 h. As incomplete conversion was detected by ^1H NMR, the brown reaction solution was again heated to 60°C and additional 24 mL isobutyl nitrite (20.88 g, 20.2 mmol, 0.2 eq) diluted in 50 mL DME were added. After additional 16 h at room temperature, the solvent was removed under reduced pressure and the brown liquid was purified by vacuum distillation (70°C, 2 mbar).

Yield: 110.0 g (52%), yellow liquid. ^1H NMR (300.22 MHz, CDCl_3) δ 7.23-7.09 (m, 1 H; H^{Ar}), 7.10 (d, $^3J_{\text{H,H}} = 7.5$ Hz, 2 H; $2\times\text{H}^{\text{Ar}}$), 2.83 (q, $^3J_{\text{H,H}} = 7.5$ Hz, 4 H; $2\times\text{CH}_2$), 1.27 (t, $^3J_{\text{H,H}} = 7.5$ Hz, 6 H; $2\times\text{CH}_3$) ppm. ^{13}C NMR (75.5 MHz, CDCl_3) δ 143.95 (C^{Ar}), 127.26 (C^{Ar}), 127.05 (C^{Ar}), 126.54 (C^{Ar}), 30.36 (CH_2), 14.45 (CH_3) ppm.

7.2.2 Synthesis of Ar_2SnCl_2

Synthesis of Ph_2SnCl_2 (21) ^[82]

In a Schlenk flask 44.3 g Ph_3SnCl (114.9 mmol, 2.0 eq) and 6.7 mL tin (IV) chloride (14.94 g, 57.3 mmol, 1.0 eq) were mixed neat. After a brownish liquid was formed, the reaction was slowly heated to 110°C for 3 h. Conversion was monitored by NMR in CDCl_3 and if necessary additional tin (IV) chloride or triphenyltin chloride was added. After cooling down to rt, the formed solid was extracted with 150 mL *n*-heptane and the remaining light grey solid was separated from the colourless clear solution by filtration. The filtrate was concentrated and cooled to -30°C to give a colourless solid, which was isolated through suction.

Yield: 54.38 g (92%) m.p.^{exp} 39-41°C (m.p.^{lit} 42-44°C [112]). ¹H NMR (300.22 MHz, CDCl₃) δ 7.70-7.73 (m, 4 H; 4xH^{Ar}), 7.54-7.56 (m, 6 H; 6xH^{Ar}) ppm. ¹³C NMR (75.5 MHz, CDCl₃) δ 137.10 (C^{Ar}), 135.22 (²J_{C,Sn}= 62.8 Hz; C^{Ar}), 131.99 (C^{Ar}), 129.87 (³J_{C,Sn}= 85.3 Hz; C^{Ar}) ppm. ¹¹⁹Sn NMR (111.92 MHz, CDCl₃) δ -27.20 ppm.

Synthesis of Mes₂SnCl₂ (22)

In a 3-necked round bottom flask 4.25 mL SnCl₄ (9.48 g, 9.48 mmol, 1.0 eq) dissolved in 200 mL toluene were cooled to -50°C. Dropwise a Grignard solution, prepared from 15.95 g MesBr (80.1 mmol, 2.2 eq) and 2.16 g Mg turnings (88.8 mmol, 2.44 eq) in 100 mL dry THF, was added slowly at -50°C. After full supplementation, the yellowish suspension was allowed to warm up to rt overnight. Afterwards the reaction was refluxed for 2 h. Solvent was removed under reduced pressure to give an off-white solid. ¹¹⁹Sn NMR of the crude product in CDCl₃ revealed the 3 species Mes₂SnCl₂ (-51.08 ppm), Mes₂SnClBr (-96.17 ppm) and Mes₂SnBr₂ (-146.22 ppm). For workup the off-white solid was dissolved in 200 mL DCM and 50 mL THF. 200 mL aqueous HCl (1.0 M) were added and the two phase mixture was stirred for 1 h. This procedure was repeated a second time. The combined aqueous layers were reextracted with DCM (2x100 mL) Combined organic layers were washed with brine (1x200 mL), dried over Na₂SO₄ and filtered. The solvent was removed under reduced pressure to give an off-solid. The crude product was purified by recrystallization from DCM/*n*-heptane.

Yield: 4.01 g (26 %), colourless solid. m.p.^{exp} 181-183°C (m.p.^{lit} 185°C [113]). ¹H NMR (300.22 MHz, CDCl₃) δ 6.93 (s, 4 H; 4xH^{Ar}), 2.55 (s, 12 H; 4xo-CH₃), 2.30 (s, 6 H; 2xp-CH₃) ppm. ¹³C NMR (75.5 MHz, CDCl₃) δ 143.69 (C^{Ar}), 141.54 (C^{Ar}), 139.28 (C^{Ar}), 129.70 (C^{Ar}), 24.86 (CH₃), 21.26 (CH₃) ppm. ¹¹⁹Sn NMR (111.92 MHz, CDCl₃) δ -50.91 ppm.

Synthesis of Tripp₂SnCl₂ (23)

In a 3-necked round bottom flask 4.25 mL SnCl₄ (9.48 g, 9.48 mmol, 1.0 eq) dissolved in 150 mL *n*-heptane were cooled to -50°C. Dropwise a Grignard solution, prepared from 22.68 g TrippBr (80.1 mmol, 2.2 eq) and 2.16 g Mg turnings (88.8 mmol, 2.44 eq) in 100 mL dry THF, was added slowly at -50°C. After full supplementation, the colourless suspension was allowed to warm up to rt overnight. Afterwards the reaction was refluxed 3 h. Solvent was removed under reduced pressure to give an off-white solid. ¹¹⁹Sn NMR of the crude product in CDCl₃ revealed the 3 species Tripp₂SnCl₂ (-65.62 ppm), Tripp₂SnClBr (-115.64 ppm) and Tripp₂SnBr₂ (-170.87 ppm). For workup the off-white solid was dissolved in 200 mL DCM and 40 mL THF. 200 mL aqueous HCl (1.0 M) were added and the two phase mixture was stirred for 1 h. This procedure was repeated a second time. The combined aqueous layers were reextracted with DCM (2x100 mL) Combined organic layers were washed with

brine (1x200 mL), dried over Na₂SO₄ and filtered. The solvent was removed under reduced pressure to give a colourless solid. Crystals suitable for X-Ray crystallography were obtained by recrystallisation from *n*-pentane.

Yield: 19.30 g (90%), colourless solid. m.p.^{exp} 142-144 °C. ¹H NMR (300.22 MHz, CDCl₃) δ 7.05 (s, ⁴J_{H,Sn} = 38.0 Hz, 4 H; 4xH^{Ar}), 3.27 (qu, ³J_{H,H} = 6.7 Hz, 4 H; 4xCH), 2.88 (qu, ³J_{H,H} = 7.0 Hz, 2 H; 2xCH), 1.43 – 0.99 (m, 36 H; 12xCH₃) ppm. ¹³C NMR (75.5 MHz, CDCl₃) δ 154.19 (²J_{C,Sn} = 66.0 Hz; C^{Ar}), 152.33 (C^{Ar}), 139.99 (C^{Ar}), 123.00 (³J_{C,Sn} = 77.6 Hz; C^{Ar}), 37.46 (³J_{C,Sn} = 49.7 Hz; CH), 34.42 (CH), 24.91 (CH₃), 23.96 (CH₃) ppm. ¹¹⁹Sn NMR (111.92 MHz, CDCl₃) δ -64.76 ppm.

Synthesis of Dipp₂SnCl₂ (24)

In a 3-necked round bottom flask 4.25 mL SnCl₄ (9.48 g, 9.48 mmol, 1.0 eq) dissolved in 150 mL *n*-heptane were cooled to -50°C. Dropwise a Grignard solution, prepared from 19.32 g DippBr (80.1 mol, 2.2 eq) and 2.16 g Mg turnings (88.8 mmol, 2.44 eq) in 100 mL dry THF, was added slowly at -50°C. After full supplementation, the brownish suspension was allowed to warm up to rt overnight. Afterwards the reaction was refluxed for 3 h. Solvent was removed under reduced pressure to give a brownish solid. ¹¹⁹Sn NMR of the crude product in CDCl₃ revealed the 3 species Dipp₂SnCl₂ (-70.06 ppm), Dipp₂SnClBr (-120.35 ppm) and Dipp₂SnBr₂ (-175.75 ppm). For workup the brownish solid was dissolved in 200 mL DCM and 40 mL THF. 200 mL aqueous HCl (1.0 M) were added and the two phase mixture was stirred for 1 h. This procedure was repeated a second time. The combined aqueous layers were reextracted with DCM (2x100 mL). Combined organic layers were washed with brine (1x200 mL), dried over Na₂SO₄ and filtered. The solvent was removed under reduced pressure to give a brownish solid. The crude product was purified by recrystallisation from a mixture of *n*-heptane. Crystals suitable for X-Ray crystallography were obtained by recrystallisation from *n*-pentane.

Yield: 5.78 g (31%), colourless solid. m.p.^{exp} 196-198°C. ¹H NMR (300.22 MHz, CDCl₃) δ 7.42 (t, ³J_{H,H} = 7.6 Hz, 2 H; 2xH^{Ar}), 7.23 (d, ³J_{H,H} = 7.6 Hz, 4 H; 4xH^{Ar}), 3.29 (qu, ³J_{H,H} = 6.7 Hz, 4 H; 4xCH), 1.21 (d, ³J_{H,H} = 6.7 Hz, 24 H; 8xCH₃) ppm. ¹³C NMR (75.5 MHz, CDCl₃) δ 154.19 (C^{Ar}), 142.71 (C^{Ar}), 131.66 (C^{Ar}), 124.89 (³J_{C,Sn} = 74.8 Hz; C^{Ar}), 37.58 (³J_{C,Sn} = 51.0 Hz; CH), 24.81 (CH₃) ppm. ¹¹⁹Sn NMR (111.92 MHz, CDCl₃) δ -70.07 ppm.

Synthesis of Dep₂SnCl₂ (25)

In a 3-necked round bottom flask 4.25 mL SnCl₄ (9.48 g, 9.48 mmol, 1.0 eq) dissolved in 150 mL *n*-heptane were cooled to -50°C. Dropwise a Grignard solution, prepared from 17.07 g DepBr (80.1 mmol, 2.2 eq) and 2.16 g Mg turnings (88.8 mmol, 2.44 eq) in 100 mL dry THF, was added slowly at -50°C. After full supplementation, the brownish suspension was allowed to warm up to rt

overnight. Afterwards the reaction was refluxed for 3 h. Solvent was removed under reduced pressure to give a brownish solid. ^{119}Sn NMR of the crude product in CDCl_3 revealed the 3 species $\text{Dep}_2\text{SnCl}_2$ (-65.38 ppm), $\text{Dep}_2\text{SnClBr}$ (-112.81 ppm) and $\text{Dep}_2\text{SnBr}_2$ (-164.90 ppm). For workup the brownish solid was dissolved in 200 mL DCM and 40 mL THF. 200 mL aqueous HCl (1.0 M) were added and the 2 phase mixture was stirred 1 h. This procedure was repeated a second time. The combined aqueous layers were reextracted with DCM (2x100 mL). The combined organic layers were washed with brine (1x200 mL), dried over Na_2SO_4 and filtered. The solvent was removed under reduced pressure to give a brownish solid. The crude product was purified by recrystallisation from a mixture of *n*-heptane. Crystals suitable for single crystal X-Ray diffractometry were obtained by recrystallisation from *n*-pentane.

Yield: 10.88 g (66%), colourless solid. m.p.^{exp} 69-70°C (m.p.^{lit} 67.5-68.5°C [102]). ^1H NMR (300.22 MHz, CDCl_3) δ 7.38 (t, $^3J_{\text{H,H}} = 7.5$ Hz, 2 H; $2x\text{H}^{\text{Ar}}$), 7.18 (d, $^3J_{\text{H,H}} = 7.5$ Hz, 4 H; $4x\text{H}^{\text{Ar}}$), 2.91 (q, $^3J_{\text{H,H}} = 7.2$ Hz, 8 H; $2x\text{CH}_2$), 1.23 (t, $^3J_{\text{H,H}} = 7.2$ Hz, 12 H; $4x\text{CH}_3$) ppm. ^{13}C NMR (75.5 MHz, CDCl_3) δ 149.90 (C^{Ar}), 142.73 (C^{Ar}), 131.54 (C^{Ar}), 127.47 ($^3J_{\text{C,Sn}} = 74.5$ Hz; C^{Ar}), 31.70 ($^3J_{\text{C,Sn}} = 48.8$ Hz; CH_2), 16.77 (CH_3) ppm. ^{119}Sn NMR (111.92 MHz, CDCl_3) δ -65.36 ppm.

7.2.3 Synthesis of Ar_2SnH_2

In a 250 mL round-bottom Schlenk flask LiAlH_4 was suspended in Et_2O and cooled down to 0°C. At 0°C diaryltin dichloride was added in portions. After the reaction was stirred for 1 h at 0°C, it was poured slowly onto degassed H_2SO_4 (0.5 M) *via* a canula, which was also cooled to 0°C. The phases were separated, the organic layer was washed with degassed, saturated Potassium tartrate solution, dried over Na_2SO_4 and filtered. The solvent was removed to give a colourless to brownish oil or solid.

Synthesis of Ph_2SnH_2 (26)

1.80 g LiAlH_4 (47.3 mmol, 0.82 eq) in 200 mL Et_2O , 20.00 g Ph_2SnCl_2 (58.2 mmol, 1.0 eq), turned brownish, 75 mL degassed H_2SO_4 (0.5 M) for quenching, 2x 150 mL degassed saturated Potassium tartrate solution. The resulting colourless oil was used without further purification.

Yield: 13.51 g (84%), colourless oil. ^1H NMR (300.22 MHz, C_6D_6) δ 7.37 (s, $^3J_{\text{H,Sn}} = 54.6$ Hz, 4 H; $4x\text{H}^{\text{Ar}}$), 7.08-7.07 (m, 6 H; $6x\text{H}^{\text{Ar}}$) 6.05 (s, $^1J_{\text{H,119Sn}} = 1926.7$ Hz, $^1J_{\text{H,117Sn}} = 1840.4$ Hz, 2 H, SnH_2) ppm. ^{13}C NMR (75.5 MHz, C_6D_6) δ 137.87 ($^2J_{\text{C,Sn}} = 40.5$ Hz, C^{Ar}), 135.54 (C^{Ar}), 129.26 (C^{Ar}), 128.95 (C^{Ar}) ppm. ^{119}Sn NMR (111.92 MHz, C_6D_6) δ -234.08 ($^1J_{\text{Sn,H}} = 1927$ Hz) ppm.

Synthesis of Mes₂SnH₂ (27)

0.37 g LiAlH₄ (0.95 mmol, 0.81 eq) in 150 mL Et₂O, 5.00 g Mes₂SnCl₂ (11.7 mmol, 1.0 eq), turned grey, 35 mL degassed H₂SO₄ (0.5 M) for quenching, 2x 75 mL degassed saturated Potassium tartrate solution. The resulting colourless solid was used without further purification.

Yield: 2.26 g (54%), colourless solid. m.p.^{exp} 140-143°C (m.p.^{lit} 133-135°C^[85]). ¹H NMR (300.22 MHz, C₆D₆) δ 6.75 (s, ⁴J_{H,Sn} = 18.28 Hz, 4 H; 4xH^{Ar}), 5.94 (s, ¹J_{H,119Sn} = 1846 Hz, ¹J_{H,117Sn} = 1765 Hz, 2 H; SnH₂), 2.36 (s, 12 H; 4xo-CH₃) 2.11 (s, 6 H; 2xp-CH₃) ppm. ¹³C NMR (75.5 MHz, C₆D₆) δ 144.87 (C^{Ar}), 138.67 (C^{Ar}), 135.13 (C^{Ar}), 129.16 (C^{Ar}), 25.99 (³J_{C,Sn} = 43.6 Hz, o-CH₃), 21.0 (p-CH₃) ppm. ¹¹⁹Sn NMR (111.92 MHz, C₆D₆) δ -352.82 (¹J_{Sn,H} = 1846 Hz) ppm. ATR-FTIR 1862 (s; ν_s SnH) cm⁻¹.

Synthesis of Tripp₂SnH₂ (28)

0.98 g LiAlH₄ (25.8 mmol, 0.86 eq) in 125 mL Et₂O, 18.00 g Tripp₂SnCl₂ (30.2 mmol, 1.0 eq), turned brownish, 50 mL degassed H₂SO₄ (0.5 M) for quenching, 2x 150 mL degassed saturated Potassium tartrate solution. The resulting brownish solid was purified by recrystallisation from *n*-pentane. Crystals suitable for single crystal X-Ray diffraction were also obtained by recrystallisation from *n*-pentane.

Yield: 7.15 g (45%), colourless solid. m.p.: 55-57°C. ¹H NMR (300.22 MHz, C₆D₆) δ 7.14 (s, 4 H; 4xH^{Ar}), 6.23 (s, ¹J_{H,119Sn} = 1820 Hz, ¹J_{H,117Sn} = 1737 Hz, 2 H; SnH₂), 3.40-3.29 (m, 4 H; 4xCH), 2.78 (qu, ³J_{H,H} = 7.0 Hz, 2 H; 2xCH), 1.22 (t, ³J_{H,H} = 6.5 Hz, 36 H; 12xCH₃) ppm. ¹³C NMR (75.5 MHz, C₆D₆) δ 155.72 (C^{Ar}), 150.39 (C^{Ar}), 135.94 (C^{Ar}), 121.62 (J_{C,Sn} = 45.6 Hz; C^{Ar}), 38.22 (CH), 34.72 (CH), 24.77 (CH₃), 24.24 (CH₃) ppm. ¹¹⁹Sn NMR (111.92 MHz, C₆D₆) δ -352.29 (¹J_{Sn,H} = 1820 Hz) ppm. ATR-FTIR 1860 (s; ν_s SnH) cm⁻¹.

Synthesis of Dipp₂SnH₂ (29)

1.20 g LiAlH₄ (31.6 mmol, 0.81 eq) in 150 mL Et₂O, 20.00 g Dipp₂SnCl₂ (39.1 mmol, 1.0 eq), turned brownish, 60 mL degassed H₂SO₄ (0.5 M) for quenching, 2x 150 mL degassed saturated Potassium tartrate solution. The resulting off-white oil solidified after cooling to -30°C. Crystals suitable for single crystal X-Ray diffraction were obtained by recrystallisation from *n*-pentane.

Yield: 14.15 g (82%), off-white solid. m.p.: 41-43°C. Anal. Calcd. for C₂₄H₃₆Sn: C, 65.03; H, 8.19. Found: C, 64.73; H, 7.73. ¹H NMR (300.22 MHz, C₆D₆) δ 7.26-7.21 (m, 2 H; 2xH^{Ar}), 7.15-7.05 (m, 4 H; 4xH^{Ar}), 6.22 (s, J_{H,119Sn} = 1835 Hz, J_{H,117Sn} = 1753 Hz, 2 H; SnH₂), 3.27 (septett, ³J_{H,H} = 6.7 Hz, 4 H; 4xCH), 1.15 (d, J_{H,H} = 6.7 Hz, 24 H; 8xCH₃) ppm. ¹³C NMR (75.5 MHz, C₆D₆) δ 155.56 (C^{Ar}), 138.77 (C^{Ar}), 130.09 (C^{Ar}), 123.51 (³J_{C,Sn} = 44.0 Hz; C^{Ar}), 38.27 (³J_{C,Sn} = 41.0 Hz; CH), 24.65 (CH₃) ppm. ¹¹⁹Sn NMR (111.92 MHz, C₆D₆) δ -355.41 (J_{Sn,H} = 1835 Hz) ppm. MS (DI-EI): calcd for [M⁺]: 443.1765; found: 443.1792. ATR-FTIR 1852 (s; ν_s SnH) cm⁻¹.

Synthesis of Dep₂SnH₂ (30)

0.81 g LiAlH₄ (21.1 mmol, 0.81 eq) in 100 mL Et₂O, 12.00 g Dep₂SnCl₂ (26.3 mmol, 1.0 eq), turned brownish, 40 mL degassed H₂SO₄ (0.5 M) for quenching, 2x 100 mL degassed saturated Potassium tartrate solution. Crystals suitable for single crystal X-Ray diffraction were obtained by recrystallisation from *n*-pentane.

Yield: 4.12 g (40%), colourless solid at -30°C. m.p.: about rt. Anal. Calcd. for C₂₀H₂₈Sn: C, 62.05; H, 7.29. Found: C, 61.62; H, 7.10. ¹H NMR (300.22 MHz, C₆D₆) δ 7.11 (t, ³J_{H,H} = 7.4 Hz, 2 H; 2xH^{Ar}), 6.94 (d, ³J_{H,H} = 7.7 Hz, 4 H; 4xH^{Ar}), 6.03 (s, J_{H,119Sn} = 1844 Hz, J_{H,117Sn} = 1763 Hz, 2 H; SnH₂), 2.70 (q, ³J_{H,H} = 7.3 Hz, 8 H; 4xCH₂), 1.06 (t, ³J_{H,H} = 7.3 Hz, 12 H; 4xCH₃) ppm. ¹³C NMR (75.5 MHz, C₆D₆) δ 151.41 (²J_{C,Sn} = 32.1 Hz; C^{Ar}), 138.27 (C^{Ar}), 129.81 (C^{Ar}), 126.15 (³J_{C,Sn} = 43.7 Hz; C^{Ar}), 33.26 (³J_{C,Sn} = 40.2 Hz; CH₂), 16.76 (CH₃) ppm. ¹¹⁹Sn NMR (111.92 MHz, C₆D₆) δ -352.20 (¹J_{Sn,H} = 1844 Hz) ppm. MS (DI-EI): calcd for [M⁺]: 387.1138; found: 387.1162. ATR-FTIR 1846 (s; ν_s SnH) cm⁻¹.

7.2.4 Synthesis of Sn(II) and Ge(II) amides**Synthesis of Sn(N(SiMe₃)₂)₂ (63)** ^[114]

In a Schlenk flask 1.89 g SnCl₂ (10.0 mmol, 1.0 eq) and 3.34 g Lithium bis(trimethylsilyl)amide (95%, 20.0 mmol, 2.0 eq) were dissolved in 100 mL THF at 0°C. The yellow suspension was stirred for 1 h at 0°C and was then allowed to warm up to rt. After 20 h the solvent was removed under reduced pressure, the remaining solid was extracted with *n*-pentane and filtered. Again, the solvent was removed under reduced pressure to give an orange oil.

Yield: 2.59 g (59%), orange oil. ¹H NMR (300.22 MHz, C₆D₆) δ 0.29 (s, 36 H; 12xCH₃) ppm. ¹¹⁹Sn NMR (111.92 MHz, C₆D₆) δ 84.35 ppm. ²⁹Si DEPT NMR (59.64 MHz, C₆D₆) δ -2.26 ppm.

Synthesis of Ge(N(SiMe₃)₂)₂ (64) ^[114]

In a Schlenk flask 3.10 g GeCl₂·Dioxane (13.4 mmol, 1.0 eq) and 4.71 g Lithium bis(trimethylsilyl)amide (95%, 26.8 mmol, 2.0 eq) were dissolved in 100 mL Et₂O at 0°C. The yellow suspension was stirred for 4 h at 0°C and was then allowed to warm up to rt. After 3 h at rt the solvent was removed under reduced pressure. The yellowish solid was extracted with 100 mL *n*-pentane and filtered. The solvent was again removed under reduced pressure to give a yellow solid.

Yield: 3.48 g (66%), yellow solid. m.p.^{exp} 33-34°C (m.p.^{lit} 32-33°C ^[114]). ¹H NMR (300.22 MHz, C₆D₆) δ 0.31 (s, 36 H; 12xCH₃) ppm. ¹³C (75.5 MHz, C₆D₆) δ 5.40 (¹J_{C,Si} = 55.6 Hz; CH₃) ppm. ²⁹Si DEPT NMR (59.64 MHz, C₆D₆) δ 0.94 ppm.

Synthesis of Sn(NEt₂)₂ (65)

In a Schlenk tube 3.56 g anhydrous SnCl₂ (18.8 mmol, 1.0 eq) and 3.06 g Lithium diethylamide (97%, 37.5 mmol, 2.0 eq) were dissolved in 100 mL Et₂O at -20°C. The brown suspension was stirred for 2 h at -20°C and was then allowed to warm up to rt. After 22 h the solvent was removed under reduced pressure, the remaining brownish grey solid was extracted with 100 mL *n*-pentane and filtered. The solvent was removed under reduced pressure to give brown oil.

Yield: 3.68 g (75%), brown oil. ¹H NMR (300.22 MHz, C₆D₆) δ 3.52 (q, ³J_{H,H} = 6.9 Hz, 8 H; 4xterm-NCH₂CH₃), 3.37 – 3.01 (m, 8 H; 4xμ₂-NCH₂), 1.20 (t, ³J_{H,H} = 6.9 Hz, 12 H; 4xCH₃), 0.99 (t, ³J_{H,H} = 7.1 Hz, 12 H; 4xCH₃) ppm. ¹³C (75.5 MHz, C₆D₆) δ 44.71 (CH₂), 42.84 (CH₂), 17.41 (CH₃), 11.92 (CH₃) ppm. ¹¹⁹Sn NMR (111.92 MHz, C₆D₆) δ 103.82 ppm.

7.2.5 Synthesis of R₃SiCl

Synthesis of (Me₃Si)₃SiCl (66) ^[115,116]

To a suspension of 75 g Tetrakis(trimethylsilyl)silane (0.234 mol, 1.0 eq) in 150 mL DME, 24.4 g Potassium *t*-butoxide (0.238 mol, 1.02 eq) were added in portions. The reaction turned redish orange and then brown. Full conversion was monitored by ²⁹Si DEPT NMR and if necessary additional Potassium *t*-butoxide was added. After full conversion was detected, the reaction solution was poured slowly into 400 mL degassed aqueous H₂SO₄ (1.0 M) and 250 mL Et₂O *via* a canula. The aqueous layer was reextracted with Et₂O (1x250 mL). The combined organic layers were washed with Brine (1x250 mL), dried over Na₂SO₄, filtered and the solvent was removed under reduced pressure. The yellow crude oil was then in portions added to 250 mL degassed CCl₄ (dried over Na₂SO₄) in a 3-necked round bottom flask equipped with a reflux condenser. The reaction heated automatically and cooled down after 3 h. The solvent was then removed under reduced pressure after all in all 15 h. The crude product was purified by recondensation.

Yield: 52.54 g (79%), colourless oily soild. ¹H NMR (300.22 MHz, CD₃CN) δ 0.26 (s, 27 H; 9xCH₃) ppm. ¹³C (75.5 MHz, CDCl₃) δ 0.52 ppm. ²⁹Si DEPT NMR (59.64 MHz, CD₃CN) δ -11.57 ppm.

Synthesis of *i*Pr₃SiCl (67)

In a 3-necked round bottom flask 40 mL triisopropylsilane (30.92 g, 195 mmol) were dissolved in 125 mL degassed CCl₄ (dried over Na₂SO₄) and a catalytic amount of PtCl₂ was added. The reaction was heated to reflux and turned black after 1.5 h. As full conversion was detected by ¹³C NMR after 12 h the reaction suspension was filtered to remove the black catalyst and solvent was removed under reduced pressure. The crude product was purified by vacuum distillation (61°C, 5 mbar).

Yield: 28.23 g (75%), colourless clear liquid. ¹H NMR (300.22 MHz, CDCl₃) δ 1.24 – 1.09 (m, 21 H) ppm. ¹³C (75.5 MHz, CDCl₃) δ 17.63 (CH), 13.65 (CH₃) ppm. ²⁹Si DEPT NMR (59.64 MHz, CDCl₃) δ 35.74 ppm.

7.2.6 Synthesis of Anionic Chains and Rings

7.2.6.1 Reactions of Ph_2SnH_2 with Alkaline metals

Synthesis of $[\text{Sn}_4\text{Ph}_8][\text{M}(\text{DME})_3]_2$ (M = K (**31a**), Rb (**31b**), Cs (**31c**))

24 mg K (0.61 mmol, 0.6 eq) were added to 275 mg Ph_2SnH_2 (1.00 mmol, 1.0 eq) dissolved in 10 mL DME. Evolution of hydrogen was observed and the reaction turned yellow, then orange and finally red. After 3 h no bubble formation was noticed anymore and after 2 days the product crystallised as orange suitable for X-Ray crystallography. A similar procedure for the corresponding Rubidium (51 mg Rb) and Caesium (80 mg Cs) compound was applied.

Yield: orange crystals. ^{119}Sn NMR (111.92 MHz, CD_3CN) δ -94 (broad), -175 (broad) ppm. UV-VIS (CH_3CN) λ 408 nm.

Synthesis of $[\text{Sn}_6\text{Ph}_{12}][\text{M}(\text{Dyglme})_3]_2$ (M = K (**33a**), Rb (**33b**), Cs (**33c**))

19 mg K (0.49 mmol, 0.5 eq) were added to 275 mg Ph_2SnH_2 (1.00 mmol, 1.0 eq) dissolved in 10 mL diglyme. Evolution of hydrogen was observed and the reaction turned yellow, then orange and finally red. After 3 h no bubble formation was noticed anymore and after 2 days the product crystallised as dichroic, green and red, crystals. These turned out to be suitable for single crystal X-Ray diffraction. A similar procedure for the corresponding Rubidium (41 mg Rb) and Caesium (64 mg Cs) compound was applied.

Yield: 79 mg (19%), dichroic, green and red crystals. ^{119}Sn NMR (111.92 MHz, CD_3CN) δ -92 (broad), -178 (broad), -198 (broad) ppm. UV-VIS (CH_3CN) λ 390, 446 nm.

Synthesis of $[\text{Sn}_8\text{Ph}_{16}][\text{Na}(\text{Diglyme})_2]_2$ (**32**)

10 mg Na (0.43 mmol, 0.4 eq) were added to 275 mg Ph_2SnH_2 (1.00 mmol, 1.0 eq) dissolved in 10 mL diglyme. Formation of hydrogen was observed and the reaction turned first orange and then red. After 3 h no bubble formation was noticed anymore and after 3 days the product was yielded as black, shiny crystals, which were suitable for X-Ray crystallography.

Yield: 343 mg (91%), black, green shiny crystals. m.p.: decomposition from 250°C. Anal. Calcd. for $\text{C}_{132}\text{H}_{164}\text{Na}_2\text{O}_{18}\text{Sn}_8$: C, 52.25; H, 5.45. Found: C, 51.68; H, 6.12. ^{119}Sn NMR (111.92 MHz, CD_3CN) δ -93 (broad), -177 (broad), -178 (broad, 2x) ppm. UV-VIS (CH_3CN) λ 380, 480, 571 nm.

Synthesis of $[\text{M}(\text{crown})]_2[\text{Sn}_6\text{Ph}_{10}]$ (M = K (**34a**), Rb (**34b**), Cs (**34c**)) and synthesis of $[\text{M}(\text{crown})][\text{Sn}_4\text{Ph}_9]$ (M = K (**35a**), Rb (**35b**), Cs (**35c**))

30 mg K (0.77 mmol, 0.8 eq) were added to a solution of 275 mg Ph_2SnH_2 (1.00 mmol, 1.0 eq), 352 mg 18-crown-6 (1.33 mmol, 1.3 eq) in 10 mL benzene. Sparse evolution of hydrogen was observed and the reaction turned slowly orange. The products were isolated as orange-yellow

crystals, which turned out to be suitable for X-Ray crystallography. A similar procedure for the corresponding Rubidium (68 mg, 576 mg dibenzo-18-crown-6) and Caesium (106 mg Cs, 423 mg 18-crown-6) compound was applied.

Analytical data for $[\text{Sn}_6\text{Ph}_{10}]^{2-}$ (**34**): orange-yellow crystals. ^{119}Sn NMR (111.92 MHz, C_6D_6) δ -140 (broad, 4xSn), -190 (broad, 2xSn) ppm. UV-VIS (CH_3CN) λ 417 nm.

Analytical data for $[\text{Sn}_4\text{Ph}_9]^-$ (**34**): ^{119}Sn NMR (111.92 MHz, CD_3CN) δ -196 ($^1J_{\text{Sn},117} = 1590$ Hz, $^1J_{\text{Sn},117} = 1665$ Hz), -1073 ($^1J_{\text{Sn},117} = 1590$ Hz, $^1J_{\text{Sn},117} = 1665$ Hz) ppm. UV-VIS (CH_3CN) λ 405 nm.

7.2.6.2 Reactions of Ph_2SnH_2 with Lithium Amides

Synthesis of $[\text{Sn}_6\text{Ph}_{10}][\text{Li}(\text{THF})_4]_2$ (**34d**)

8 mg Et_2NLi were added to 28 mg Ph_2SnH_2 dissolved in 2 mL THF and while adding the reaction turned orange. The product was isolated as red crystals suitable for X-Ray crystallography from the orange reaction solution.

7.2.6.3 Derivatisation of Anionic Structures

Reaction of $[\text{Sn}_6\text{Ph}_{12}][\text{Na}(\text{DME})_3]_2$ and $(\text{Me}_3\text{Si})_3\text{SiCl}$

28 mg $(\text{Me}_3\text{Si})_3\text{SiCl}$ in 3 mL acetonitrile was added dropwise to 106 mg of $[\text{Sn}_6\text{Ph}_{12}][\text{Na}(\text{DME})_3]_2$ in 8 mL at -30°C . The red solution changes its colour to yellow and after a while a yellow solid precipitates. The reaction was kept at -30°C for 12 h. Only the cyclic $\text{Sn}_6\text{Ph}_{12}$ was isolated from the yellow precipitate as well as the supernatant solution.

7.2.7 Synthesis of Anionic Cages

7.2.7.1 Reactions of Ph_2SnH_2 with LiAlH_4

Synthesis of $[\text{bicylco}[2.2.1]\text{Sn}_7\text{Ph}_{10}][\text{Li}(\text{12cr4})_2]_2$ (**44**)

275 mg Ph_2SnH_2 (1.00 mmol, 3.5 eq) were slowly added to a solution of 10.9 mg LiAlH_4 (0.29 mmol, 1.0 eq) and 102 mg 12-crown-4 (0.58 mmol, 2.0 eq) in 10 mL THF. The solution turns slowly yellow and a slight evolution of hydrogen is observed. After a few hours the reaction turned orange. Occurring insoluble solids were removed *via* centrifugation. The product was isolated as orange crystals after cooling the solution to -30°C suitable for X-Ray crystallography.

Yield: orange crystals. ^{119}Sn NMR (111.92 MHz, CD_3CN) δ 200.28 ($^1J_{\text{Sn},117/119\text{Sn}} = 4426/4636$ Hz, $^2J_{\text{Sn},\text{Sn}} = 54$ Hz; $\text{Sn}^- - \text{Ph}_2\text{Sn} - \text{Sn}^-$), 35.64 ($^1J_{\text{Sn},117/119\text{Sn}} = 5710/5990$ Hz, $^1J_{\text{Sn},117\text{Sn}} = 3939$ Hz, $^2J_{\text{Sn},117/119\text{Sn}} = 1082/1134$ Hz, $^2J_{\text{Sn},117\text{Sn}} = 735$ Hz, $^2J_{\text{Sn},\text{Sn}} = 54$ Hz, $^3J_{\text{Sn},\text{Sn}} = 26$ Hz; $\text{Sn}^- - \text{Ph}_2\text{Sn} - \text{Ph}_2\text{Sn} - \text{Sn}^-$), -857.73 ($^1J_{\text{Sn},117/119\text{Sn}} = 5710/5990$ Hz, $^1J_{\text{Sn},117/119\text{Sn}} = 4426/4636$ Hz, $^2J_{\text{Sn},117/119\text{Sn}} = 1082/1134$; $\text{Sn}^- - \text{Ph}_2\text{Sn} - \text{Ph}_2\text{Sn} - \text{Sn}^-$) ppm.

Synthesis of [bicyclo[2.2.2]Sn₈Ph₁₂][Li(12cr4)₂] (45)

275 mg Ph₂SnH₂ (1.00 mmol, 4.0 eq) were slowly added to a solution of 9.5 mg LiAlH₄ (0.25 mmol, 1.0 eq) and 88.1 mg 12-crown-4 (0.50 mmol, 2.0 eq) in 10 mL THF. The solution turns slowly yellow and a slight evolution of hydrogen is observed. After a few hours the reaction turned light orange. Occurring insoluble solids were removed *via* centrifugation. The product was isolated as red crystals after cooling the solution to -30°C, which turned out to be suitable for single crystal X-Ray diffraction. Yield: red crystals. ¹¹⁹Sn NMR (111.92 MHz, C₆D₆) δ -316.81 (¹J_{Sn,117Sn} = 5020 Hz, ¹J_{Sn,117Sn} = 3610 Hz, ²J_{Sn,117/119Sn} = 770/807 Hz, ²J_{Sn,117Sn} = 240 Hz, ³J_{Sn,117Sn} = 17 Hz; Sn⁻-Ph₂Sn-Ph₂Sn-Sn⁻), -286.97 (¹J_{Sn,117Sn} = 5020 Hz, ²J_{Sn,117/119Sn} = 770/807; Sn⁻-Ph₂Sn-Ph₂Sn-Sn⁻) ppm.

Synthesis of [bicyclo[2.2.2]Sn₈Ph₁₃][Li(12cr4)₂] (46)

275 mg Ph₂SnH₂ (1.00 mmol, 8.0 eq) were slowly added to a solution of 4.8 mg LiAlH₄ (0.13 mmol, 1.0 eq) and 48 mg 12-crown-4 (0.27 mmol, 2.1 eq) in 10 mL THF. The solution turns slowly yellow and a slight evolution of hydrogen is observed. After a few hours the reaction turned orange. Occurring insoluble solids were removed *via* centrifugation. The product was isolated as orange crystals after cooling the solution to -30°C, which are suitable for X-Ray crystallography.

Yield: yellow crystals. ¹¹⁹Sn NMR (111.92 MHz, CD₃CN) δ -183.18 (¹J_{Sn,Sn} = 708 Hz, ²J_{Sn,Sn} = 548 Hz; Sn⁻-Ph₂Sn-Ph₂Sn-SnPh), -238.75 (²J_{Sn,117Sn} = 2274 Hz, ¹J_{Sn,117/119Sn} = 1020/1170 Hz, ¹J_{Sn,117/119Sn} = 916/957 Hz, ²J_{Sn,Sn} = 131 Hz; Sn⁻-Ph₂Sn-Ph₂Sn-SnPh), -471.10 (¹J_{Sn,Sn} = 1170 Hz, ²J_{Sn,Sn} = 548 Hz, ³J_{Sn,Sn} = 170 Hz; Sn⁻-Ph₂Sn-Ph₂Sn-SnPh), -758.24 (¹J_{Sn,117/119Sn} = 6126/6422 Hz, ³J_{Sn,Sn} = 170 Hz; Sn⁻-Ph₂Sn-Ph₂Sn-SnPh) ppm.

Synthesis of [Ph₃AlH][Li(12cr4)(DME)] (47)

275 mg Ph₂SnH₂ (1.00 mmol, 0.75 eq) were slowly added to a solution of 50.6 mg LiAlH₄ (1.33 mmol, 1.0 eq) and 470 mg 12-crown-4 (2.67 mmol, 2.0 eq) in 10 mL DME. Evolution of hydrogen and the slow formation of elemental tin were observed. After some days the elemental tin was removed *via* filtration from the colourless solution. The product crystallised from the solution as colourless crystals, which turned out to be suitable for X-Ray crystallography.

Synthesis of [PhAlH₃][Li(12cr4)₂] (48)

275 mg Ph₂SnH₂ (1.00 mmol, 2.0 eq) were slowly added to a solution of 19.0 mg LiAlH₄ (0.50 mmol, 1.0 eq) and 176 mg 12-crown-4 (1.00 mmol, 2.0 eq) in 10 mL DME. Evolution of hydrogen and the slow formation of elemental tin were observed. After some days the elemental tin was removed *via* filtration. The product was isolated as colourless crystals from the colourless reaction, which were suitable for X-Ray crystallography.

7.2.7.2 Reactions of Ph₂SnH₂ with Benzyl Sodium and Benzyl Potassium

Synthesis of [bicyclo[2.2.1]Sn₇Ph₁₀][M(crown)₂]₂ (M = Na (**44a**), K (**44b**))

To a solution of 275 mg Ph₂SnH₂ (1.0 mmol, 1.0 eq) and 110 mg 15-crown-5 (0.50 mmol, 0.5 eq) in 10 mL DME 57 mg Benzyl Sodium (0.50 mmol, 0.5 eq) were added slowly at -30°C. The solution turns slowly yellow and a slight evolution of hydrogen is observed. Occurring insoluble solids were removed *via* centrifugation. The product was isolated as orange crystals, which turned out be suitable for X-Ray crystallography. A similar procedure for the corresponding Potassium compound (65 mg, 182 mg dibenzo-18-crown-6) was applied.

Yield: orange crystals. ¹¹⁹Sn NMR data correspond to the data found **44**.

7.2.8 Synthesis of Clusters and molecules with non-classical bonding situation

7.2.8.1 Reactions of Tripp₂SnH₂ with E(II) amides (E = Ge, Sn)

Synthesis of Sn₄H₂Tripp₆ (**53**)

A solution of 440 mg Sn(N(SiMe₃)₂)₂ (1.0 mmol, 1.0 eq) in 7 mL THF was added dropwise to 528 mg Tripp₂SnH₂ (1.0 mmol, 1.0 eq) dissolved in 7 mL THF. The solution turned briefly red and then orange. After 12 h the reaction appeared dark brown. The product crystallised after 25 days from the dark brown solution as colourless crystals, which turned out to be suitable for single crystal X-Ray diffraction.

Yield: 58 mg (7%), off-white crystals. m.p.: 210-228°C (decomposition). Anal. Calcd. for C₉₀H₁₄₀Sn₄: C, 63.70; H, 8.32. Found: C, 62.66; H, 8.15. ¹H NMR (300.22 MHz, C₆D₆) δ 8.42 (s, ¹J_{H,119Sn} = 1177 Hz, ¹J_{H,117Sn} = 1127 Hz, ²J_{H,Sn} = 69 Hz, 2 H; 2xSnH), 7.42 (s, 1 H; H^{Ar}), 7.20 (s, 5 H; 5xH^{Ar}, covered by solvent peak), 6.89 (s, 1 H; H^{Ar}), 6.82 (s, 5 H; 5xH^{Ar}), 4.38-4.30 (m, 4 H; 4x*p*-CH(CH₃)₂), 4.07-3.98 (m, 2 H; 2x*p*-CH(CH₃)₂), 3.41-3.36 (m, 4 H; 4x*o*-CH(CH₃)₂), 2.71-2.64 (m, 8 H; 8x*o*-CH(CH₃)₂), 1.74 (d, ³J_{H,H} = 6.6 Hz, 12 H; 2x*p*-CH(CH₃)₂), 1.65 (d, ³J_{H,H} = 6.6 Hz, 12 H; 2x*p*-CH(CH₃)₂), 1.58 (d, ³J_{H,H} = 6.8 Hz, 12 H; 2x*p*-CH(CH₃)₂), 1.14-1.09 (m, 36 H; 6x*o*-CH(CH₃)₂), 0.79 (d, ³J_{H,H} = 6.8 Hz, 12 H; 2x*o*-CH(CH₃)₂), 0.64-0.60 (m, 24 H; 4x*o*-CH(CH₃)₂) ppm. ¹³C (75.5 MHz, C₆D₆) δ 156.26 (*o*-C^{Ar}), 155.16 (*o*-C^{Ar}), 154.78 (*o*-C^{Ar}), 154.26 (*p*-C^{Ar}), 149.71 (*p*-C^{Ar}), 149.25 (*p*-C^{Ar}), 143.80 (*ipso*-C^{Ar}), 142.73 (*ipso*-C^{Ar}), 129.24 (*ipso*-C^{Ar}), 123.05 (*m*-C^{Ar}), 122.60 (*m*-C^{Ar}), 121.35 (*m*-C^{Ar}), 42.64 (*p*-CH(CH₃)₂), 39.41 (*p*-CH(CH₃)₂), 38.86 (*p*-CH(CH₃)₂), 37.45 (*o*-CH(CH₃)₂), 34.52 (*o*-CH(CH₃)₂), 34.43 (*o*-CH(CH₃)₂), 29.82 (*o*-CH(CH₃)₂), 25.59 (*o*-CH(CH₃)₂), 25.44 (*o*-CH(CH₃)₂), 25.33 (*o*-CH(CH₃)₂), 24.67 (*o*-CH(CH₃)₂), 24.27 (*o*-CH(CH₃)₂), 24.18 (*o*-CH(CH₃)₂), 24.10 (*o*-CH(CH₃)₂), 24.08 (*o*-CH(CH₃)₂) ppm. ¹¹⁹Sn NMR (111.92 MHz, C₆D₆) δ -166.71 (¹J_{Sn,H} = 1177 Hz, ³J_{Sn,H} = 158 Hz; SnH), -192.89 (²J_{H,Sn} = 69 Hz; Tripp₂Sn) ppm. ATR-FTIR 1834 (w; ν_s SnH) cm⁻¹.

Synthesis of Sn₁₀Tripp₈ (55)

A solution of 263 mg Sn(NEt₂)₂ (1.0 mmol, 1.0 eq) in 7 mL THF was added dropwise to 527 mg Tripp₂SnH₂ (1.0 mmol, 1.0 eq) dissolved in 7 mL THF. The solution turned briefly red, then yellow and then slowly dark brown. After 9 days a colourless solid crystallises, which turned out to be Sn₄H₂Tripp₆. Alongside the colourless crystals also the product as dark purple crystals were observed. Over time the colourless crystals seemed to dissolve again and more of the purple crystals were formed. After an overall reaction time of 1 month the product was isolated in a reasonable yield.

Yield: 28 mg (4%), dark, purple solid. ¹H NMR (300.22 MHz, C₆D₆) δ 7.19 (s, 8 H; H^{Ar}, covered by solvent peak), 7.00 (s, 8 H; H^{Ar}), 4.36-4.30 (m, 2 H; 2xCH(CH₃)₂), 4.10-3.98 (m, 2 H; 2xCH(CH₃)₂), 4.45-3.33 (m, 4 H; 4xCH(CH₃)₂), 2.86-2.77 (m, 8 H; 8xCH(CH₃)₂), 2.74-2.60 (m, 8 H; 8xCH(CH₃)₂), 1.74 (d, 6 H, ³J_{H,H} = 6.8 Hz; 1xCH(CH₃)₂), 1.65 (d, 6 H, ³J_{H,H} = 6.5 Hz; 1xCH(CH₃)₂), 1.58 (d, 6 H, ³J_{H,H} = 6.9 Hz; 1xCH(CH₃)₂), 1.52 (d, 6 H, ³J_{H,H} = 5.9 Hz; 1xCH(CH₃)₂), 1.40 (d, 6 H, ³J_{H,H} = 7.5 Hz; 1xCH(CH₃)₂), 1.24 (d, 48 H, ³J_{H,H} = 6.8 Hz; 8xo-CH(CH₃)₂), 1.14-1.12 (m, 48 H; 8xCH(CH₃)₂), 0.78 (d, 6 H, ³J_{H,H} = 6.5 Hz; 1xCH(CH₃)₂), 0.63-0.60 (m, 12 H; 2xCH(CH₃)₂) ppm.

Reaction of Tripp₂SnH₂ with Ge(N(SiMe₃)₂)₂

A solution of 197 mg Ge(N(SiMe₃)₂)₂ (0.50 mmol, 1.0 eq) in 7 mL THF was added dropwise to 264 mg Tripp₂SnH₂ (0.50 mmol, 1.0 eq) dissolved in 7 mL THF. The reaction turns quickly red, but its colour fades slowly to orange. After 5 days ¹H coupled ¹¹⁹Sn NMR analysis (C₆D₆ was added to the NMR sample for locking) shows next to signals for dimeric (Tripp₂SnH)₂ (57) (-319.14, -320.49, -332.94, -334.51 ppm) also a shift at -65.25 ppm.

7.2.8.2 Reactions of Dipp₂SnH₂ with E(II) amides (E = Ge, Sn)**Synthesis of Sn₄H₂Dipp₆ (54)**

A solution of 440 mg Sn(N(SiMe₃)₂)₂ (1.0 mmol, 1.0 eq) in 7 mL THF was added dropwise to 443 mg Dipp₂SnH₂ (1.0 mmol, 1.0 eq) in 7 mL THF. The solution turned orange and hazy. After 12 h the reaction appears dark brown. The product crystallised after 5 days from the dark brown solution as colourless solid.

Yield: 420 mg (58%), off-white crystals. m.p. 228-237°C (decomposition). Anal. Calcd. for C₇₂H₁₀₄Sn₄: C, 59.87; H, 7.26. Found: C, 59.08; H, 7.21. ¹H NMR (300.22 MHz, C₆D₆) δ 8.46 (s, ¹J_{H,119Sn} = 1198 Hz, ¹J_{H,115Sn} = 1152 Hz, ²J_{H,Sn} = 69 Hz, 2 H; 2xSnH), 7.72 (s, 1 H, H^{Ar}), 7.22-7.10 (m, 11 H; 11xH^{Ar}, covered by solvent peak), 6.89-6.79 (m, 6 H; 6xH^{Ar}), 4.31-4.23 (m, 4 H; 4xCH(CH₃)₂), 3.95-3.91 (m, 2 H; 2xCH(CH₃)₂), 3.37-3.28 (m, 4 H; 4xCH(CH₃)₂), 2.63-2.55 (m, 2 H; 2xCH(CH₃)₂), 1.63 (d, ³J_{H,H} = 6.6 Hz, 12 H; 2xCH(CH₃)₂), 1.54 (d, ³J_{H,H} = 6.7 Hz, 12 H; 2xCH(CH₃)₂), 1.50 (d, ³J_{H,H} = 6.7 Hz, 12 H; 2xCH(CH₃)₂), 0.74 (d, ³J_{H,H} = 6.7 Hz, 12 H; 2xCH(CH₃)₂), 0.57 (d, ³J_{H,H} = 6.6 Hz, 12 H; 2xCH(CH₃)₂), 0.53 (d, ³J_{H,H} =

6.5 Hz, 12 H; $2x\text{CH}(\text{CH}_3)_2$) ppm. ^{13}C (75.5 MHz, THF- d_8) δ 156.70 (*o*- C^{Ar}), 155.63 (*o*- C^{Ar}), 155.42 (*o*- C^{Ar}), 130.03 (*ipso*- C^{Ar}), 129.69 (*ipso*- C^{Ar}), 129.15 (*ipso*- C^{Ar}), 125.64 (*p*- C^{Ar}), 125.52 (*p*- C^{Ar}), 125.18 (*p*- C^{Ar}), 124.58 (*m*- C^{Ar}), 123.93 (*m*- C^{Ar}), 123.82 (*m*- C^{Ar}), 40.04 ($\text{CH}(\text{CH}_3)_2$), 39.59 ($\text{CH}(\text{CH}_3)_2$), 38.05 ($\text{CH}(\text{CH}_3)_2$), 38.01 ($\text{CH}(\text{CH}_3)_2$), 32.61 ($\text{CH}(\text{CH}_3)_2$), 30.20 ($\text{CH}(\text{CH}_3)_2$), 26.75 ($\text{CH}(\text{CH}_3)_2$), 26.09 ($\text{CH}(\text{CH}_3)_2$, covered by solvent peaks), 25.82 ($\text{CH}(\text{CH}_3)_2$, covered by solvent peaks), 24.64 ($\text{CH}(\text{CH}_3)_2$) ppm. ^{119}Sn NMR (111.92 MHz, THF/ C_6D_6) δ -163.55 ($^1J_{\text{Sn,H}} = 1189$ Hz; $^2J_{\text{Sn,H}} = 138$ Hz; SnH), -195.41 ($^2J_{\text{H,Sn}} = 69$ Hz; Dipp_2Sn) ppm. ATR-FTIR 1838 (w; $\nu_{\text{S SnH}}$) cm^{-1} .

Reaction of $\text{Dipp}_2\text{SnH}_2$ with $\text{Sn}(\text{NEt}_2)_2$

A solution of 263 mg $\text{Sn}(\text{NEt}_2)_2$ (1.0 mmol, 1.0 eq) in 7 mL THF was added dropwise 443 mg $\text{Dipp}_2\text{SnH}_2$ (1.0 mmol, 1.0 eq) in 7 mL THF. The solution turned briefly red, then yellow and then slowly dark brown. After 9 days a colourless solid crystallises, which turned out to be $\text{Sn}_4\text{H}_2\text{Dipp}_6$ (**54**). Alongside the colourless crystals also the product as dark purple crystals were observed. Over time the colourless crystals seemed to dissolve again and more of dark purple crystals suitable for single crystal X-Ray diffraction were formed. X-Ray crystallography revealed the formation $\text{Sn}_{10}\text{Dipp}_8$ (**56**), a structural analogue to **55**. Since still colourless crystals of **54** are still present, no pure $\text{Sn}_{10}\text{Dipp}_8$ could be isolated.

Synthesis of $(\text{Dipp}_2\text{SnH})_2$ (**58**)

A solution of 393 mg $\text{Ge}(\text{N}(\text{SiMe}_3)_2)_2$ (1.00 mmol, 1.0 eq) in 7 mL THF was added dropwise to 443 mg $\text{Dipp}_2\text{SnH}_2$ (1.00 mmol, 1.0 eq) dissolved in 7 mL THF. The reaction turns quickly red, but its colour fades slowly to yellow. After 3 days ^1H coupled ^{119}Sn NMR analysis shows only resonances of the product $(\text{Dipp}_2\text{SnH})_2$. Crystals suitable for X-Ray crystallography precipitated after one week. When using only 0.5 eq of $\text{Ge}(\text{N}(\text{SiMe}_3)_2)_2$, additionally to dimeric $(\text{Dipp}_2\text{SnH})_2$ also resonances of **54** are observable in ^{119}Sn NMR.

Yield: yellowish, nearly colourless crystals. ^{119}Sn NMR (111.92 MHz, THF/ C_6D_6) δ -325.97 ($^1J_{\text{Sn,1H}} = 1556$ Hz, $^2J_{\text{Sn,1H}} = 157$ Hz) ppm.

7.2.8.3 Reactions of Dep_2SnH_2 with E(II) amides (E = Ge, Sn)

Reaction of Dep_2SnH_2 with $\text{Sn}(\text{N}(\text{SiMe}_3)_2)_2$

A solution of 359 mg $\text{Sn}(\text{N}(\text{SiMe}_3)_2)_2$ (0.82 mmol, 1.0 eq) in 7 mL THF was added dropwise to 316 mg Dep_2SnH_2 (0.82 mmol, 1.0 eq) in 7 mL THF. The solution turned yellow, then slowly red and later brownish red. After 12 h the reaction appears dark brown. After 2 days the reaction solution is investigated by ^{119}Sn NMR (C_6D_6 was added to the NMR sample for locking). Resonances at 354.31 and -1757.93 as well as thin layer chromatography (*n*-heptane/toluene=5/3) showing a violet spot at

$R_f = 0.8$ may indicate formation of pentastanna[1.1.1]propellane. Other resonances were found at (-128.47, -145.58, -157.07, -175.79, -203.61, -243.22 and -297.47 ppm. Most of these peaks disappeared after 6 days. No assignment could be done for still present peaks at -157.07 and -203.61 ppm and the new formed resonance at -74.10 ppm.

Reaction of Dep_2SnH_2 with $\text{Sn}(\text{NEt}_2)_2$

A solution of 440 mg $\text{Sn}(\text{N}(\text{SiMe}_3)_2)_2$ (1.00 mmol, 1.0 eq) in 7 mL was added dropwise to 387 mg Dep_2SnH_2 (1.00 mmol, 1.0 eq) in 7 mL THF. The solution turns brown after a few minutes. After 2 days ^{119}Sn NMR (C_6D_6 was added to the NMR sample for locking) shows resonances at 356 and -1751 ppm, indicating the formation of a pentastanna[1.1.1]propellane, and at -21.3, suggesting the presence of decastanna[5]prismane (DepSn)₁₀. Also a violet spot in thin layer chromatography (*n*-heptane/toluene = 10/1) is indicative for the pentastanna[1.1.1]propellane. After narrowing the solution brownish crystals of **49** precipitated and were suitable for X-Ray crystallography. The remaining narrowed reaction solution was applied on a silica gel chromatography column (*n*-heptane/toluene = 10/1 to 5/1). Elution under ambient pressure provided fractions from which, in order of elution purple **50** and yellowish **51** were obtained.

Reaction of $\text{Tripp}_2\text{SnH}_2$ with $\text{Ge}(\text{N}(\text{SiMe}_3)_2)_2$

A solution of 197 mg $\text{Ge}(\text{N}(\text{SiMe}_3)_2)_2$ (0.50 mmol, 1.0 eq) in 7 mL THF was added dropwise to 194 mg Dep_2SnH_2 (0.50 mmol, 1.0 eq) dissolved in 7 mL THF. The reaction turns quickly red, but its colour fades slowly to orange. After 5 days ^1H coupled ^{119}Sn NMR analysis (C_6D_6 was added to the NMR sample for locking) shows next to signals for dimeric $(\text{Dep}_2\text{SnH})_2$ (**52**) (-271.68, -274.14, -286.96, -289.43 ppm) also a shift at -418.91 ppm, which could not be assigned.

8 References

- [1] M. S. Hill, in *Met. Bond.* (Ed.: G. Parking), Springer-Verlag, Berlin Heidelberg, **2010**, pp. 189–216.
- [2] N. Wiberg, P. P. Power, in *Mol. Clust. Main Gr. Elem.* (Eds.: M. Driess, H. Nöth), Wiley-VCH Verlag GmbH & Co. KGaA, Weinheim, FRG, **2005**, pp. 188–208.
- [3] A. Schnepf, in *Struct. Bond.*, **2016**, pp. 193–223.
- [4] C. U. Pittman, C. E. Carraher, M. Zeldin, J. E. Sheats, B. M. Culbertson, Eds. , *Metal-Containing Polymeric Materials*, Springer US, Boston, MA, **1996**.
- [5] J. L. Brédas, R. Silbey, Eds. , *Conjugated Polymers*, Springer Netherlands, Dordrecht, **2012**.
- [6] G. Schmid, M. Bäuml, M. Geerkens, I. Heim, C. Osemann, T. Sawitowski, *Chem. Soc. Rev.* **1999**, *28*, 179–185.
- [7] Y. Lu, W. Chen, *Chem. Soc. Rev.* **2012**, *41*, 3594–3623.
- [8] P. Braunstein, X. Morise, *Chem. Rev.* **2000**, *100*, 3542–3552.
- [9] L. R. Sita, I. Kinoshita, *J. Am. Chem. Soc.* **1991**, *113*, 1856–1857.
- [10] L. R. Sita, I. Kinoshita, *J. Am. Chem. Soc.* **1992**, *114*, 7024–7029.
- [11] C. P. Sindlinger, L. Wesemann, *Chem. Sci.* **2014**, *5*, 2739–2746.
- [12] C. Schrenk, A. Schnepf, *Rev. Inorg. Chem.* **2014**, *34*, 93–118.
- [13] S. C. Sevov, J. M. Goicoechea, *Organometallics* **2006**, *25*, 5678–5692.
- [14] F. Holleman, E. Wiberg, DeGruyter, Berlin, **1995**, pp. 143, 275.
- [15] A. G. Davies, P. J. Smith, in *Compr. Organomet. Chem.* (Ed.: G. Wilkinson), Elsevier Science Ltd., Amsterdam, **1982**, pp. 519–627.
- [16] A. G. Davies, in *Compr. Organomet. Chem. III Compd. Groups 13-15* (Eds.: D.M.P. Mingos, R.H. Crabtree), Elsevier Ltd., Oxford, **2007**, pp. 809–883.

- [17] H. Kriegsmann, K. Ulbricht, *Zeitschrift für Anorg. und Allg. Chemie* **1964**, *328*, 90–104.
- [18] A. E. Finholt, A. C. Bond, K. E. Wilzbach, H. I. Schlesinger, *J. Am. Chem. Soc.* **1947**, *69*, 2692–2696.
- [19] A. G. Davies, in *Organotin Chem.*, Wiley-VCH Verlag GmbH & Co, Weinheim, **2004**, pp. 244–265.
- [20] M. Ohara, R. Okawara, *J. Organomet. Chem.* **1965**, *3*, 484.
- [21] H. G. Kuivila, A. K. Sawyer, A. A. G., *J. Org. Chem.* **1961**, *26*, 1426–1429.
- [22] M. Connil, B. Jousseume, N. Noiret, M. Pereyre, *Organometallics* **1994**, *13*, 24–25.
- [23] V. I. Dodero, L. C. Koll, S. D. Mandolesi, J. C. Podestá, *J. Organomet. Chem.* **2002**, *650*, 173–180.
- [24] E. Vedejs, S. M. Duncan, a. R. Haight, *J. Org. Chem.* **1993**, *58*, 3046–3050.
- [25] N. D. Smith, J. Mancuso, M. Lautens, *Chem. Rev.* **2000**, *100*, 3257–3282.
- [26] P. Riviere, A. Castel, M. Riviere-Baudet, in *Chem. Org. Ger. Tin Lead Compd.* (Ed.: Z. Rappoport), John Wiley & Sons, Ltd., **2002**, pp. 653–748.
- [27] J. C. Podesta, A. B. Chopa, N. N. Giagante, A. E. Zúniga, *J. Organo* **1995**, *494*, 5–10.
- [28] K. Mochida, N. Matsushige, M. Hamashima, *Bull. Chem. Soc. Jpn.* **1985**, *58*, 1443–1447.
- [29] P. M. Uberman, S. E. Martín, R. A. Rossi, *J. Org. Chem.* **2005**, *70*, 9063–9066.
- [30] H. J. Emeleus, S. F. A. Kettle, *J. Chem. Soc.* **1958**, 2444–2448.
- [31] M. Trummer, W. Caseri, *Organometallics* **2010**, *29*, 3862–3867.
- [32] M. Saito, R. Haga, M. Yoshioka, *Chem. Commun.* **2002**, 1002–1003.
- [33] L. Pu, M. O. Senge, M. M. Olmstead, P. P. Power, *J. Am. Chem. Soc.* **1998**, *120*, 12682–12683.
- [34] N. Scotti, U. Zachwieja, H. Jacobs, *Zeitschrift für Anorg. Allg. Chemie* **1997**, *623*, 1503–1505.

-
- [35] F. Flacke, H. Jacobs, *Eur. J. Solid State Inorg. Chem.* **1997**, *34*, 495–501.
- [36] K. Wiesler, C. Suchentrunk, N. Korber, *Helv. Chim. Acta* **2006**, *89*, 1158–1168.
- [37] K. Wiesler, N. Korber, *Z. Krist.* **2005**, *220*, 188–191.
- [38] H. Gilman, W. H. Atwell, G. L. Schweke, *Chem. Ind.* **1964**, 1063.
- [39] H. Gilman, W. H. Atwell, G. L. Schwebke, *J. Organomet. Chem.* **1964**, *2*, 369–371.
- [40] S. Adams, M. Dräger, *Angew. Chemie* **1987**, *99*, 1280–1282.
- [41] S. Adams, M. Dräger, *Main Gr. Met. Chem.* **1988**, *151*, 151–180.
- [42] R. D. Miller, J. Michl, *Chem. Rev.* **1989**, *89*, 1359–1410.
- [43] R. West, P. Trefonas, *J. Polym. Sci. Polym. Chem. Ed.* **1985**, *23*, 2099–2107.
- [44] R. D. Miller, R. Sooriyakumaran, *J. Polym. Sci. Part A Polym. Chem.* **1987**, *25*, 111–125.
- [45] V. Lu, T. D. Tilley, *Macromolecules* **1996**, *29*, 5763–5764.
- [46] J. M. Buriak, *Chem. Rev.* **2002**, *102*, 1271.
- [47] K. T. Wong, B. Shong, W. Sun, S. F. Bent, *J. Phys. Chem. C* **2013**, *117*, 26628–26635.
- [48] J.-J. Maudrich, C. P. Sindlinger, F. S. W. Aicher, K. Eichele, H. Schubert, L. Wesemann, *Chem. - A Eur. J.* **2016**, DOI 10.1002/chem.201605317.
- [49] B. Wrackmeyer, T. Chivers, D. J. Eisler, F. Ribot, V. Chandrasekhar, P. Singh, K. Gopal, H. Hpfl, S. C. Sevov, J. B. Lambert, et al., in *Tin Chem.* (Eds.: M. Gielen, A. Davies, K. Pannell, E. Tiekink), John Wiley & Sons, Ltd, Chichester, UK, **2008**, pp. 17–283.
- [50] D. Nied, F. Breher, *Chem. Soc. Rev.* **2011**, *40*, 3455–3466.
- [51] J. Wiederkehr, C. Wölper, S. Schulz, *Chem. Commun.* **2016**, *52*, 12282–12285.
- [52] D. J. Chapman, S. C. Sevov, *Inorg. Chem.* **2008**, *47*, 6009–6013.
- [53] M. Brynda, R. Herber, P. B. Hitchcock, M. F. Lappert, I. Nowik, P. P. Power, A. V. Protchenko, A.

- Růžička, J. Steiner, *Angew. Chemie - Int. Ed.* **2006**, *45*, 4333–4337.
- [54] M. Wagner, M. Lutter, B. Zobel, W. Hiller, M. H. Prosenc, K. Jurkschat, *Chem. Commun.* **2015**, *51*, 153–156.
- [55] G. Prabusankar, A. Kempter, C. Gemel, M.-K. Schröter, R. A. Fischer, *Angew. Chemie - Int. Ed.* **2008**, *47*, 7234–7237.
- [56] N. Wiberg, H. Lerner, H. Nöth, W. Ponikwar, *Angew. Chemie - Int. Ed.* **1999**, *38*, 1103–1105.
- [57] E. Rivard, J. Steiner, J. C. Fettingner, J. R. Giuliani, M. P. Augustine, P. P. Power, *Chem. Commun.* **2007**, *32*, 4919–4921.
- [58] A. F. Richards, B. E. Eichler, M. Brynda, M. M. Olmstead, P. P. Power, *Angew. Chemie - Int. Ed.* **2005**, *44*, 2546–2549.
- [59] L. R. Sita, R. D. Bickerstaff, *J. Am. Chem. Soc.* **1989**, *111*, 6454–6456.
- [60] L. R. Sita, I. Kinoshita, *Organometallics* **1990**, *9*, 2865–2867.
- [61] N. Wiberg, H. W. Lerner, S. Wagner, H. Nöth, T. Seifert, *Zeitschrift für Naturforsch. B* **1999**, *54*, 877–880.
- [62] H. Schmidbaur, A. Bauer, *Phosphorus. Sulfur. Silicon Relat. Elem.* **1995**, *102*, 217–219.
- [63] K. Wade, *Adv. Inorg. Chem. Radiochem.* **1976**, *18*, 1–66.
- [64] A. Purath, R. Köppe, H. Schnöckel, *Angew. Chemie - Int. Ed.* **1999**, *38*, 2926–2928.
- [65] D. Nied, E. Matern, H. Berberich, M. Neumaier, F. Breher, *Organometallics* **2010**, *29*, 6028–6037.
- [66] C. Drost, M. Hildebrand, P. Lönnecke, *Main Gr. Met. Chem.* **2002**, *25*, 93–98.
- [67] D. Nied, W. Klopper, F. Breher, *Angew. Chem. Int. Ed. Engl.* **2009**, *48*, 1411–6.
- [68] D. Nied, R. Köppe, W. Klopper, H. Schnöckel, F. Breher, *J. Am. Chem. Soc.* **2010**, *132*, 10264–10265.
- [69] P. Schleyer, R. Janoschek, *Angew. Chemie* **1987**, *99*, 1312–1313.

-
- [70] S. Nagase, T. Kudo, *Organometallics* **1987**, *6*, 2456–2458.
- [71] W. W. Schoeller, T. Dabisch, T. Busch, *Inorg. Chem.* **1987**, *26*, 4383–4389.
- [72] L. R. Sita, I. Kinoshita, *J. Am. Chem. Soc.* **1991**, *113*, 5070–5072.
- [73] D. Nied, P. Ona-Burgos, W. Klopper, F. Breher, *Organometallics* **2011**, *30*, 1419–1428.
- [74] P. P. Power, *Nature* **2010**, *463*, 171–177.
- [75] G. H. Spikes, J. C. Fettinger, P. P. Power, *J. Am. Chem. Soc.* **2005**, *127*, 12232–12233.
- [76] G. C. Welch, R. R. S. Juan, J. D. Masuda, D. W. Stephan, *Science* **2006**, *314*, 1124–1126.
- [77] Y. Peng, B. D. Ellis, X. Wang, P. P. Power, *J. Am. Chem. Soc.* **2008**, *130*, 12268–12269.
- [78] Z. D. Brown, P. Vasko, J. C. Fettinger, H. M. Tuononen, P. P. Power, *J. Am. Chem. Soc.* **2012**, *134*, 4045–4048.
- [79] L. E. Longobardi, C. A. Russell, M. Green, N. S. Townsend, K. Wang, A. J. Holmes, S. B. Duckett, J. E. McGrady, D. W. Stephan, *J. Am. Chem. Soc.* **2014**, *136*, 13453–13457.
- [80] T. J. Hadlington, M. Hermann, G. Frenking, C. Jones, *J. Am. Chem. Soc.* **2014**, *136*, 3028–3031.
- [81] P. Vasko, S. Wang, H. M. Tuononen, P. P. Power, *Angew. Chemie - Int. Ed.* **2015**, *54*, 3802–3805.
- [82] C. Zeppek, J. Pichler, A. Torvisco, M. Flock, F. Uhlig, *J. Organomet. Chem.* **2013**, *740*, 41–49.
- [83] P. Brown, M. F. Mahon, K. C. Molloy, *J. Organomet. Chem.* **1992**, *435*, 265–273.
- [84] S. Harrypersad, D. Foucher, *Chem. Commun.* **2015**, *51*, 7120–7123.
- [85] N. R. Neale, T. D. Tilley, *J. Am. Chem. Soc.* **2002**, *124*, 3802–3803.
- [86] C. P. Sindlinger, S. Weiß, H. Schubert, L. Wesemann, *Angew. Chemie - Int. Ed.* **2015**, *54*, 4087–4091.
- [87] B. P. T. Greene, R. F. Bryan, *J. Chem. Soc.* **1971**, 2549–2554.

-
- [88] T. Kräuter, B. Neumüller, *Zeitschrift für Naturforsch. B* **1998**, *53*, 503–505.
- [89] H. K. Sharma, F. Cervantes-lee, J. S. Mahmoud, K. H. Pannell, *Organometallics* **1999**, *18*, 399–403.
- [90] M. Weidenbruch, K. Schäfers, S. Pohl, W. Saak, K. Peters, H. G. von Schnering, *J. Organomet. Chem.* **1988**, *346*, 171–180.
- [91] C. Zeppek, Amine Base Induced Polymerization of Aryltin Hydrides: Mechanistic Insights & Nanomaterial Characterization, TU Graz, **2015**.
- [92] K. Schittelkopf, R. C. Fischer, S. Meyer, P. Wilfling, F. Uhlig, *Appl. Organomet. Chem.* **2010**, *24*, 897–901.
- [93] J. Lahournère, J. Valade, *J. Organomet. Chem.* **1970**, *22*, C3–C4.
- [94] K. Tiefling, B. Steller, A. Wilson, D. J. Liptrot, R. C. Fischer, M. S. Hill, *Unpubl. results n.d.*
- [95] R. J. Wehmschulte, J. J. Ellison, K. Ruhlandt-Senge, P. P. Power, *Inorg. Chem.* **1994**, *33*, 6300–6306.
- [96] K. Goto, J. Kobayashi, R. Okazaki, *Organometallics* **1999**, *18*, 1357–1359.
- [97] C. Elschenbroich, *Organometallicchemie*, Vieweg+Teubner, Wiesbaden, **2008**.
- [98] Y. Hu, L. O. Gustafson, H. Zhu, E. Y.-X. Chen, *J. Polym. Sci. Part A Polym. Chem.* **2011**, *49*, 2008–2017.
- [99] I. B. Gorrell, P. B. Hitchcock, J. D. Smith, *J. Chem. Soc. Chem. Commun.* **1993**, 189–190.
- [100] K. Decker, Darstellung Und Charakterisierung Cyclicher Stannylverbindungen Mit Elementen Der 4.Hauptgruppe, TU Graz, **2007**.
- [101] U. Englich, U. Hermann, I. Prass, T. Schollmeier, K. Ruhlandt-Senge, F. Uhlig, *J. Organometallic Chem.* **2002**, *646*, 271–276.
- [102] S. Masamune, L. R. Sita, D. J. Williams, *J. Am. Chem. Soc.* **1983**, *105*, 630–631.
- [103] B. E. Eichler, P. P. Power, *Angew. Chemie Int. Ed.* **2001**, *8*, 796–797.

-
- [104] J. W. Williams, *Org. Synth.* **1943**, 23, 63.
- [105] R. H. Blessing, *Acta Crystallogr. Sect. A* **1995**, A51, 33–38.
- [106] G. M. Sheldrick, *SADABS Version 2.10 Siemens Area Detector Correction.*, Universitaet Goettingen, Goettingen, Germany, **2003**.
- [107] G. M. Sheldrick, *SHELXTL Version 6.1. Bruker AXS, Inc.*, Madison, WI, **2002**.
- [108] G. M. Sheldrick, *GM SHELXS97 and SHELXL97*, Universitaet Goettingen, Goettingen, Germany, **2002**.
- [109] A. L. Spek, *J. Appl. Crystallogr.* **2003**, 36, 7–13.
- [110] A. L. Spek, *Acta Crystallogr. Sect. D Biol. Crystallogr.* **2009**, 65, 148–155.
- [111] G. M. Whitesides, M. Eisenhut, W. M. Bunting, *J. Am. Chem. Soc.* **1974**, 96, 5398–5407.
- [112] H. Gilman, L. A. J. Gist, *J. Org. Chem.* **1957**, 22, 368–371.
- [113] H. Berwe, A. Haas, *Chem. Ber.* **1987**, 120, 1175–1182.
- [114] D. H. Harris, M. F. Lappert, *J. Chem. Soc. Chem. Commun.* **1974**, 895–896.
- [115] C. Marschner, *Eur. J. Inorg. Chem.* **1998**, 221–226.
- [116] H. Bock, J. Meuret, K. Ruppert, *J. Organomet. Chem.* **1993**, 445, 19–28.

9 Appendix

9.1 Abbreviations

Chemicals

12cr4	crown ether, 12-crown-4
15cr5	crown ether, 15-crown-5
18cr6	crown ether, 18-crown-6
b18cr6	dibenzo-18-crown-6
Ar	Aryl group
ArBr	Arylbromide
Bu	butyl
Cp	cyclopentadienyl
DCM	Dichloromethane
Dep	2,6-Diethylphenyl
DepBr	2-bromo-1,3-diethylbenzene
DIBAL-H	Diisobutylaluminium hydride
Diglyme	bis(2-methoxyethyl)ether
Dipp	2,6-diisopropylphenyl
DippBr	2-bromo-1,3-diisopropylbenzene
DME	Dimethoxyethane
DMSO	Dimethyl sulfoxide
Et	Ethyl
Et ₂ O	Diethyl ether
HMDS	Hexamethyldisilazane
iPr	Isopropyl
<i>i</i> Pr ₂ NLi	Lithium diisopropylamide
KC ₈	potassium graphite
Me	methyl
Mel	Methyl iodide
MeLi	methyllithium
Mes	2,4,6-trimethylphenyl
Mes*	2,4,6- <i>t</i> -Bu ₃ C ₆ H ₂
MesBr	2-bromo-1,3,5-trimethylbenzene

Nph	Neophyl
Pfp	Pentafluorophenyl
Ph	phenyl
Sn ^b	bridgehead atom
tBuOMe	Methyl tert-butylether
THF	Tetrahydrofurane
TMS	trimethylsilyl
Tripp	2,4,6-triisopropylphenyl
TrippBr	2-bromo-1,3,5-triisopropylbenzene

Analytical terms

ATR	attenuated total reflection
bs	Broad singlet
d	Doublet
DI	Direct Insertion
EI	Electron ionization
eV	Electronvolt
FTIR	Fourier transform infrared spectroscopy
Hz	Hertz
IR	infrared spectroscopy
J	Coupling constant
m	Multiplet
m/z	Mass-to-charge ratio
M ⁺	Molecular peak
MHz	Megahertz
MS	Mass spectrometry
NMR	Nuclear magnetic resonance
ppm	Parts per million
R _f	Retention factor
t	Triplet
UV	Ultraviolet
Vis	visual
δ	Delta

Others

%	Percent
°	degree
°C	Degree centigrade
Å	Angström
avg.	average
conc	Concentrated
eq	Equivalents
g	Gram
h	Hours
K	Kelvin
L	Liter
M	Molar
mg	Milligram
min	Minutes
mL	Milliliter
mmol	Millimol
nm	Nanometer
rt	Room temperature

9.2 Crystal Structure Analysis Data

Table 9.1 Crystal data and structure refinement for **24**.

Empirical formula	C ₂₄ H ₃₄ Cl ₂ Sn	
Formula weight	512.10	
Temperature	100(2) K	
Wavelength	0.71073 Å	
Crystal system	Triclinic	
Space group	P-1	
Unit cell dimensions	a = 17.0642(6) Å	α = 68.820(2)°
	b = 17.7819(7) Å	β = 78.214(2)°
	c = 17.9897(7) Å	γ = 89.951(2)°
Volume	4966.7(3) Å ³	
Z	8	
Density (calculated)	1.370 Mg/m ³	
Absorption coefficient	1.250 mm ⁻¹	
F(000)	2096	
Crystal size	0.360 x 0.210 x 0.170 mm ³	
Theta range f. data collection	1.223 to 25.499°	
Index ranges	-20 ≤ h ≤ 19, -20 ≤ k ≤ 21, -19 ≤ l ≤ 21	
Reflections collected	66468	
Independent reflections	18360 [R(int) = 0.1273]	
Completeness to theta max	99.3 %	
Absorption correction	Multi-Scan / SADABS	
Refinement method	Full-matrix least-squares on F ²	
Data / restraints / parameters	18360 / 0 / 1005	
Goodness-of-fit on F2	1.028	
Final R indices [I > 2σ(I)]	R1 = 0.0650, wR2 = 0.1178	
R indices (all data)	R1 = 0.1104, wR2 = 0.1421	
Largest diff. peak and hole	1.723 and -2.146 eÅ ⁻³	

Table 9.2 Crystal data and structure refinement for **25**.

Empirical formula	C ₂₀ H ₂₆ Cl ₂ Sn	
Formula weight	456.00	
Temperature	100(2) K	
Wavelength	0.71073 Å	
Crystal system	Monoclinic	
Space group	C2/c	
Unit cell dimensions	a = 28.465(7) Å	α = 90°
	b = 9.1865(19) Å	β = 117.87(2)°
	c = 17.460(7) Å	γ = 90°
Volume	4036(2) Å ³	
Z	8	
Density (calculated)	1.501 Mg/m ³	
Absorption coefficient	1.529 mm ⁻¹	
F(000)	1840	
Crystal size	0.36 x 0.33 x 0.19 mm ³	
Theta range f. data collection	1.62 to 27.98°	
Index ranges	-37 ≤ h ≤ 37, -12 ≤ k ≤ 12, -22 ≤ l ≤ 22	
Reflections collected	48654	
Independent reflections	4844 [R(int) = 0.0634]	
Completeness to theta max	99.5 %	
Absorption correction	Multi-Scan / SADABS	
Refinement method	Full-matrix least-squares on F ²	
Data / restraints / parameters	4844 / 24 / 232	
Goodness-of-fit on F2	1.024	
Final R indices [I > 2σ(I)]	R1 = 0.0267, wR2 = 0.0468	
R indices (all data)	R1 = 0.0411, wR2 = 0.0529	
Largest diff. peak and hole	0.995 and -0.509 eÅ ⁻³	

Table 9.3 Crystal data and structure refinement for **28**.

Empirical formula	C ₃₀ H ₄₈ Sn	
Formula weight	527.37	
Temperature	100(2) K	
Wavelength	0.71073 Å	
Crystal system	Monoclinic	
Space group	P2 ₁ /n	
Unit cell dimensions	a = 6.0409(3) Å	α = 90°
	b = 19.0922(11) Å	β = 96.079(3)°
	c = 24.6833(14) Å	γ = 90°
Volume	2830.8(3) Å ³	
Z	4	
Density (calculated)	1.237 Mg/m ³	
Absorption coefficient	0.916 mm ⁻¹	
F(000)	1112	
Crystal size	0.18 x 0.14 x 0.11 mm ³	
Theta range f. data collection	2.289 to 30.093°	
Index ranges	-7 ≤ h ≤ 8, -26 ≤ k ≤ 26, -34 ≤ l ≤ 34	
Reflections collected	170177	
Independent reflections	8300 [R(int) = 0.0447]	
Completeness to theta max	99.8 %	
Absorption correction	Multi-Scan / SADABS	
Refinement method	Full-matrix least-squares on F ²	
Data / restraints / parameters	8300 / 0 / 298	
Goodness-of-fit on F2	1.101	
Final R indices [I > 2σ(I)]	R1 = 0.0227, wR2 = 0.0444	
R indices (all data)	R1 = 0.0288, wR2 = 0.0465	
Largest diff. peak and hole	0.466 and -0.479 eÅ ⁻³	

Table 9.4 Crystal data and structure refinement for 29.

Empirical formula	C ₂₄ H ₃₆ Sn	
Formula weight	443.22	
Temperature	100(2) K	
Wavelength	0.71073 Å	
Crystal system	Orthorhombic	
Space group	Pca2 ₁	
Unit cell dimensions	a = 17.4894(6) Å	α = 90°
	b = 14.0836(5) Å	β = 90°
	c = 37.0349(11) Å	γ = 90°
Volume	9122.2(5) Å ³	
Z	16	
Density (calculated)	1.291 Mg/m ³	
Absorption coefficient	1.124 mm ⁻¹	
F(000)	3680	
Crystal size	0.27 x 0.16 x 0.10 mm ³	
Theta range f. data collection	1.100 to 30.038°	
Index ranges	-24 ≤ h ≤ 24, -19 ≤ k ≤ 19, -50 ≤ l ≤ 52	
Reflections collected	275534	
Independent reflections	25572 [R(int) = 0.0334]	
Completeness to theta max	100.0 %	
Absorption correction	Multi-Scan / SADABS	
Refinement method	Full-matrix least-squares on F ²	
Data / restraints / parameters	25572 / 29 / 957	
Goodness-of-fit on F2	0.996	
Final R indices [I > 2σ(I)]	R1 = 0.0181, wR2 = 0.0459	
R indices (all data)	R1 = 0.0191, wR2 = 0.0469	
Largest diff. peak and hole	0.733 and -0.434 eÅ ⁻³	

Table 9.5 Crystal data and structure refinement for **30**.

Empirical formula	C ₂₀ H ₂₈ Sn	
Formula weight	387.11	
Temperature	100(2) K	
Wavelength	0.71073 Å	
Crystal system	Triclinic	
Space group	P-1	
Unit cell dimensions	a = 9.0978(5) Å	α = 68.636(2)°
	b = 9.9367(5) Å	β = 87.350(2)°
	c = 11.1101(5) Å	γ = 78.987(2)°
Volume	917.84(8) Å ³	
Z	2	
Density (calculated)	1.401 Mg/m ³	
Absorption coefficient	1.385 mm ⁻¹	
F(000)	396	
Crystal size	0.210 x 0.180 x 0.150 mm ³	
Theta range f. data collection	2.883 to 29.998°	
Index ranges	-12 ≤ h ≤ 12, -13 ≤ k ≤ 13, -15 ≤ l ≤ 15	
Reflections collected	72916	
Independent reflections	5349 [R(int) = 0.0622]	
Completeness to theta max	99.9 %	
Absorption correction	Multi-Scan / SADABS	
Refinement method	Full-matrix least-squares on F ²	
Data / restraints / parameters	5349 / 0 / 200	
Goodness-of-fit on F2	1.012	
Final R indices [I > 2σ(I)]	R1 = 0.0224, wR2 = 0.0611	
R indices (all data)	R1 = 0.0263, wR2 = 0.0642	
Largest diff. peak and hole	1.221 and -0.622 eÅ ⁻³	

Table 9.6 Crystal data and structure refinement for **31a**.

Empirical formula	C ₇₆ H ₉₈ K ₂ O ₁₄ Sn ₄	
Formula weight	1788.62	
Temperature	100(2) K	
Wavelength	0.71073 Å	
Crystal system	Triclinic	
Space group	$\bar{P}1$	
Unit cell dimensions	a = 11.7758(8) Å	$\alpha = 98.994(3)^\circ$
	b = 13.0949(9) Å	$\beta = 111.635(2)^\circ$
	c = 14.7231(10) Å	$\gamma = 105.774(3)^\circ$
Volume	1945.6(2) Å ³	
Z	1	
Density (calculated)	8.868 Mg/m ³	
Absorption coefficient	2.468 mm ⁻¹	
F(000)	5178	
Crystal size	0.89 x 0.17 x 0.14 mm ³	
Theta range f. data collection	2.10 to 30.00°	
Index ranges	-16 ≤ h ≤ 16, -18 ≤ k ≤ 18, -20 ≤ l ≤ 20	
Reflections collected	74333	
Independent reflections	11325 [R(int) = 0.0432]	
Completeness to theta max	99.9 %	
Absorption correction	Multi-Scan / SADABS	
Refinement method	Full-matrix least-squares on F ²	
Data / restraints / parameters	11325 / 0 / 443	
Goodness-of-fit on F2	1.034	
Final R indices [I > 2σ(I)]	R1 = 0.0410, wR2 = 0.1171	
R indices(all data)	R1 = 0.0470, wR2 = 0.1242	
Largest diff. peak and hole	5.298 and -1.643 eÅ ⁻³	

Table 9.7 Crystal data and structure refinement for **32**.

Empirical formula	C ₁₂₆ H ₁₃₀ O ₁₆ Na ₂ Sn ₈	
Formula weight	1091.88	
Temperature	100(2) K	
Wavelength	0.71073 Å	
Crystal system	Monoclinic	
Space group	P2(1)/n	
Unit cell dimensions	a = 10.4164(4) Å	A = 90°
	b = 35.1800(12) Å	β = 102.919(2)°
	c = 17.2642(5) Å	γ = 90°
Volume	6166.3(4) Å ³	
Z	4	
Density (calculated)	1.630 Mg/m ³	
Absorption coefficient	2.445 mm ⁻¹	
F(000)	2960	
Crystal size	0.21 x 0.08 x 0.07 mm ³	
Theta range f. data collection	1.67 to 27.00°	
Index ranges	-13 ≤ h ≤ 13, -44 ≤ k ≤ 44, -22 ≤ l ≤ 22	
Reflections collected	94591	
Independent reflections	13437 [R(int) = 0.0457]	
Completeness to theta max	99.9 %	
Absorption correction	Multi-Scan / SADABS	
Refinement method	Full-matrix least-squares on F ²	
Data / restraints / parameters	13437 / 0 / 689	
Goodness-of-fit on F2	1.486	
Final R indices [I > 2σ(I)]	R1 = 0.0541, wR2 = 0.1843	
R indices (all data)	R1 = 0.0647, wR2 = 0.1913	
Largest diff. peak and hole	0.956 and -3.052 eÅ ⁻³	

Table 9.8 Crystal data and structure refinement for **33a**.

Empirical formula	C ₈₄ H ₈₈ K ₂ O ₆ Sn ₆	
Formula weight	1983.88	
Temperature	100(2) K	
Wavelength	0.71073 Å	
Crystal system	Triclinic	
Space group	$P\bar{1}$	
Unit cell dimensions	a = 10.2922(3) Å	$\alpha = 102.7380(10)^\circ$.
	b = 13.4599(4) Å	$\beta = 98.0040(10)^\circ$.
	c = 15.9194(5) Å	$\gamma = 106.8610(10)^\circ$.
Volume	2009.23(10) Å ³	
Z	1	
Density (calculated)	1.640 Mg/m ³	
Absorption coefficient	1.990 mm ⁻¹	
F(000)	978	
Crystal size	0.29 x 0.15 x 0.14 mm ³	
Theta range f. data collection	1.64 to 32.55°	
Index ranges	-15 ≤ h ≤ 15, , -20 ≤ k ≤ 16, -23 ≤ l ≤ 24	
Reflections collected	104239	
Independent reflections	24764 [R(int) = 0.0312]	
Completeness to theta max	99.6 %	
Absorption correction	Multi-Scan / SADABS	
Refinement method	Full-matrix least-squares on F ²	
Data / restraints / parameters	24764 / 3 / 888	
Goodness-of-fit on F2	1.027	
Final R indices [I > 2σ(I)]	R1 = 0.0194, wR2 = 0.0464	
R indices (all data)	R1 = 0.0209, wR2 = 0.0473	
Largest diff. peak and hole	1.018 and -0.920 eÅ ⁻³	

Table 9.9 Crystal data and structure refinement for **34a**.

Empirical formula	C ₉₆ H ₁₁₀ K ₂ O ₁₂ Sn ₆	
Formula weight	2246.18	
Temperature	100(2) K	
Wavelength	0.71073 Å	
Crystal system	Triclinic	
Space group	$P\bar{1}$	
Unit cell dimensions	a = 13.897(14) Å	a = 94.81(3)°
	b = 13.910(13) Å	b = 90.76(4)°
	c = 14.14(3) Å	g = 119.566(19)°
Volume	2365(5) Å ³	
Z	1	
Density (calculated)	1.577 Mg/m ³	
Absorption coefficient	1.705 mm ⁻¹	
F(000)	1120	
Crystal size	0.23 x 0.16 x 0.13 mm ³	
Theta range f. data collection	1.69 to 28.01°	
Index ranges	-18 ≤ h ≤ 18, -18 ≤ k ≤ 18, -18 ≤ l ≤ 16	
Reflections collected	104596	
Independent reflections	11048 [R(int) = 0.0532]	
Completeness to theta max	99.8 %	
Absorption correction	Multi-Scan / SADABS	
Refinement method	Full-matrix least-squares on F ²	
Data / restraints / parameters	11048 / 0 / 524	
Goodness-of-fit on F2	1.041	
Final R indices [I > 2σ(I)]	R1 = 0.0578, wR2 = 0.1422	
R indices (all data)	R1 = 0.0942, wR2 = 0.1734	
Largest diff. peak and hole	4.535 and -1.985 eÅ ⁻³	

Table 9.10 Crystal data and structure refinement for **35a**.

Empirical formula	C ₇₈ H ₈₁ KO ₆ Sn ₄	
Formula weight	1628.29	
Temperature	100(2) K	
Wavelength	0.71073 Å	
Crystal system	Monoclinic	
Space group	P2(1)/n	
Unit cell dimensions	a = 13.5837(3) Å	α = 90°
	b = 23.6887(6) Å	β = 95.3390(10)°
	c = 22.4027(5) Å	γ = 90°
Volume	7177.5(3) Å ³	
Z	4	
Density (calculated)	1.507 Mg/m ³	
Absorption coefficient	1.484 mm ⁻¹	
F(000)	3264	
Crystal size	0.25 x 0.24 x 0.08 mm ³	
Theta range f. data collection	1.69 to 27.00°	
Index ranges	-16 ≤ h ≤ 17, -30 ≤ k ≤ 30, -28 ≤ l ≤ 28	
Reflections collected	153664	
Independent reflections	15669 [R(int) = 0.0483]	
Completeness to theta max	100.0 %	
Absorption correction	Multi-Scan / SADABS	
Refinement method	Full-matrix least-squares on F ²	
Data / restraints / parameters	15669 / 0 / 802	
Goodness-of-fit on F2	1.093	
Final R indices [I > 2σ(I)]	R1 = 0.0220, wR2 = 0.0464	
R indices (all data)	R1 = 0.0354, wR2 = 0.0532	
Largest diff. peak and hole	0.667 and -0.734 eÅ ⁻³	

Table 9.11 Crystal data and structure refinement for **44**.

Empirical formula	$C_{102}H_{114}Li_2O_{18.5}Sn_7$	
Formula weight	2480.64	
Temperature	100(2) K	
Wavelength	0.71073 Å	
Crystal system	Triclinic	
Space group	$P\bar{1}$	
Unit cell dimensions	$a = 14.3301(9)$ Å	$\alpha = 82.634(2)$
	$b = 15.1075(10)$ Å	$\beta = 76.623(3)$
	$c = 26.1181(19)$ Å	$\gamma = 70.379(2)$
Volume	$5173.7(6)$ Å ³	
Z	4	
Density (calculated)	1.592 Mg/m ³	
Absorption coefficient	1.725 mm ⁻¹	
F(000)	2460	
Crystal size	0.35 x 0.21 x 0.14 mm ³	
Theta range f. data collection	1.87 to 31.24°	
Index ranges	-20 ≤ h ≤ 20, -21 ≤ k ≤ 22, -38 ≤ l ≤ 34	
Reflections collected	151767	
Independent reflections	33153 [R(int) = 0.0282]	
Completeness to theta max	99.3 %	
Absorption correction	Multi-Scan / SADABS	
Refinement method	Full-matrix least-squares on F ²	
Data / restraints / parameters	33153 / 0 / 1459	
Goodness-of-fit on F2	1.023	
Final R indices [I > 2σ(I)]	R1 = 0.0362, wR2 = 0.0900	
R indices (all data)	R1 = 0.0605, wR2 = 0.1105	
Largest diff. peak and hole	1.494 and -1.434 eÅ ⁻³	

Table 9.12 Crystal data and structure refinement for **44a**.

Empirical formula	C ₈₈ H ₁₁₀ Na ₂ O ₁₄ Sn ₇	
Formula weight	2268.56	
Temperature	100(2) K	
Wavelength	0.71073 Å	
Crystal system	Monoclinic	
Space group	P2 ₁ /c	
Unit cell dimensions	a = 12.6040(6) Å	a = 90°
	b = 27.4888(14) Å	b = 103.056(2)°
	c = 26.9560(12) Å	g = 90°
Volume	9098.0(8) Å ³	
Z	4	
Density (calculated)	1.656 Mg/m ³	
Absorption coefficient	1.958 mm ⁻¹	
F(000)	4488	
Crystal size	0.240 x 0.210 x 0.160 mm ³	
Theta range f. data collection	1.072 to 26.998°	
Index ranges	-16 ≤ h ≤ 16, -35 ≤ k ≤ 35, -32 ≤ l ≤ 34	
Reflections collected	431440	
Independent reflections	19848 [R(int) = 0.0590]	
Completeness to theta max	99.9 %	
Absorption correction	Multi-Scan / SADABS	
Refinement method	Full-matrix least-squares on F ²	
Data / restraints / parameters	19848 / 0 / 1222	
Goodness-of-fit on F2	1.094	
Final R indices [I > 2σ(I)]	R1 = 0.0195, wR2 = 0.0419	
R indices (all data)	R1 = 0.0240, wR2 = 0.0441	
Largest diff. peak and hole	0.592 and -0.474 eÅ ⁻³	

Table 9.13 Crystal data and structure refinement for **44b**.

Empirical formula	$C_{108}H_{118}K_2O_{16}Sn_7$	
Formula weight	2581.05	
Temperature	100(2) K	
Wavelength	0.71073 Å	
Crystal system	Trigonal	
Space group	$P3_121$	
Unit cell dimensions	$a = 14.0802(3)$ Å	$\alpha = 90^\circ$
	$b = 14.0802(3)$ Å	$\beta = 90^\circ$
	$c = 45.6034(14)$ Å	$\gamma = 120^\circ$
Volume	$7829.7(4)$ Å ³	
Z	3	
Density (calculated)	1.642 Mg/m ³	
Absorption coefficient	1.790 mm ⁻¹	
F(000)	3846	
Crystal size	0.21 x 0.17 x 0.14 mm ³	
Theta range f. data collection	2.680 to 26.996°	
Index ranges	-17 ≤ h ≤ 17, -17 ≤ k ≤ 17, -58 ≤ l ≤ 58	
Reflections collected	183101	
Independent reflections	11370 [R(int) = 0.0482]	
Completeness to theta max	99.8 %	
Absorption correction	Multi-Scan / SADABS	
Refinement method	Full-matrix least-squares on F ²	
Data / restraints / parameters	11370 / 24 / 602	
Goodness-of-fit on F2	1.368	
Final R indices [I > 2σ(I)]	R1 = 0.0382, wR2 = 0.0882	
R indices (all data)	R1 = 0.0383, wR2 = 0.0882	
Largest diff. peak and hole	1.093 and -1.096 eÅ ⁻³	

Table 9.14 Crystal data and structure refinement for 45.

Empirical formula	$C_{112}H_{140}Li_2O_{18}Sn_8$	
Formula weight	2713.01	
Temperature	100(2) K	
Wavelength	0.71073 Å	
Crystal system	Monoclinic	
Space group	P2(1)/c	
Unit cell dimensions	a = 29.253(2) Å	$\alpha = 90^\circ$
	b = 14.3128(9) Å	$\beta = 90.276(3)^\circ$
	c = 26.5807(17) Å	$\gamma = 90^\circ$
Volume	11128.9(13) Å ³	
Z	4	
Density (calculated)	1.619 Mg/m ³	
Absorption coefficient	1.807 mm ⁻¹	
F(000)	5400	
Crystal size	0.27 x 0.25 x 0.16 mm ³	
Theta range f. data collection	1.53 to 27.36°	
Index ranges	-37 ≤ h ≤ 37, -18 ≤ k ≤ 18, -34 ≤ l ≤ 34	
Reflections collected	421438	
Independent reflections	24812 [R(int) = 0.0639]	
Completeness to theta max	98.4 %	
Absorption correction	Multi-Scan / SADABS	
Refinement method	Full-matrix least-squares on F ²	
Data / restraints / parameters	24812 / 0 / 1387	
Goodness-of-fit on F2	1.226	
Final R indices [I > 2σ(I)]	R1 = 0.0580, wR2 = 0.1129	
R indices (all data)	R1 = 0.0907, wR2 = 0.1392	
Largest diff. peak and hole	1.810 and -2.141 eÅ ⁻³	

Table 9.15 Crystal data and structure refinement for **46**.

Empirical formula	C ₉₀ H ₈₉ LiO ₆ Sn ₈	
Formula weight	2223.07	
Temperature	100(2) K	
Wavelength	0.71073 Å	
Crystal system	Triclinic	
Space group	P-1	
Unit cell dimensions	a = 14.2707(6) Å	α = 70.797(2)°
	b = 14.2569(6) Å	β = 67.696(2)°
	c = 31.4766(13) Å	γ = 60.735(2)°
Volume	5086.5(4) Å ³	
Z	2	
Density (calculated)	1.451 Mg/m ³	
Absorption coefficient	1.973 mm ⁻¹	
F(000)	2160	
Crystal size	0.12 x 0.04 x 0.03 mm ³	
Theta range f. data collection	1.655 to 26.000°	
Index ranges	-16 ≤ h ≤ 17, -16 ≤ k ≤ 17, 0 ≤ l ≤ 38	
Reflections collected	19955	
Independent reflections	19955	
Completeness to theta max	99.5 %	
Absorption correction	Multi-Scan / SADABS	
Refinement method	Full-matrix least-squares on F ²	
Data / restraints / parameters	19955 / 770 / 1058	
Goodness-of-fit on F2	1.073	
Final R indices [I > 2σ(I)]	R1 = 0.1261, wR2 = 0.3035	
R indices (all data)	R1 = 0.1680, wR2 = 0.3485	
Largest diff. peak and hole	8.460 and -2.987 eÅ ⁻³	

Table 9.16 Crystal data and structure refinement for 47.

Empirical formula	C ₃₀ H ₄₂ AlLiO ₆	
Formula weight	532.56	
Temperature	100(2) K	
Wavelength	0.71073 Å	
Crystal system	Monoclinic	
Space group	P2(1)/c	
Unit cell dimensions	a = 11.8667(4) Å	α = 90°
	b = 20.5281(8) Å	β = 106.3590(10)°
	c = 12.5639(5) Å	γ = 90°
Volume	2936.67(19) Å ³	
Z	4	
Density (calculated)	1.205 Mg/m ³	
Absorption coefficient	0.109 mm ⁻¹	
F(000)	1144	
Crystal size	0.20 x 0.17 x 0.14 mm ³	
Theta range f. data collection	2.05 to 27.22°	
Index ranges	-15 ≤ h ≤ 11, -26 ≤ k ≤ 25, -13 ≤ l ≤ 16	
Reflections collected	15895	
Independent reflections	6495 [R(int) = 0.0626]	
Completeness to theta max	99.1 %	
Absorption correction	Multi-Scan / SADABS	
Refinement method	Full-matrix least-squares on F ²	
Data / restraints / parameters	6495 / 0 / 349	
Goodness-of-fit on F2	1.057	
Final R indices [I > 2σ(I)]	R1 = 0.0717, wR2 = 0.1899	
R indices (all data)	R1 = 0.0991, wR2 = 0.2087	
Largest diff. peak and hole	1.234 and -0.732 eÅ ⁻³	

Table 9.17 Crystal data and structure refinement for **48**.

Empirical formula	C ₂₂ H ₄₀ AlLiO ₈	
Formula weight	466.46	
Temperature	100(2) K	
Wavelength	0.71073 Å	
Crystal system	Orthorhombic	
Space group	Pbca	
Unit cell dimensions	a = 14.856(11) Å	α = 90°
	b = 14.196(10) Å	β = 90°
	c = 23.825(16) Å	γ = 90°
Volume	5024(6) Å ³	
Z	8	
Density (calculated)	1.233 Mg/m ³	
Absorption coefficient	0.122 mm ⁻¹	
F(000)	2016	
Crystal size	0.21 x 0.19 x 0.16 mm ³	
Theta range f. data collection	1.71 to 28.01°	
Index ranges	-19 ≤ h ≤ 19, -18 ≤ k ≤ 18, -31 ≤ l ≤ 31	
Reflections collected	149765	
Independent reflections	6072 [R(int) = 0.0593]	
Completeness to theta max	100.0 %	
Absorption correction	Multi-Scan / SADABS	
Refinement method	Full-matrix least-squares on F ²	
Data / restraints / parameters	6072 / 0 / 301	
Goodness-of-fit on F2	1.133	
Final R indices [I > 2σ(I)]	R1 = 0.0710, wR2 = 0.1953	
R indices (all data)	R1 = 0.0953, wR2 = 0.2172	
Largest diff. peak and hole	1.454 and -0.604 eÅ ⁻³	

Table 9.18 Crystal data and structure refinement for 49.

Empirical formula	C ₂₄ H ₃₆ NSn ₂	
Formula weight	575.92	
Temperature	100(2) K	
Wavelength	0.71073 Å	
Crystal system	Monoclinic	
Space group	C2/c	
Unit cell dimensions	a = 22.0956(15) Å	a = 90°
	b = 11.4014(6) Å	b = 119.049(5)°
	c = 21.2395(14) Å	g = 90°
Volume	4677.6(5) Å ³	
Z	8	
Density (calculated)	1.636 Mg/m ³	
Absorption coefficient	2.144 mm ⁻¹	
F(000)	2296	
Crystal size	0.36 x 0.28 x 0.19 mm ³	
Theta range f. data collection	2.074 to 28.181°	
Index ranges	-29 ≤ h ≤ 29, -15 ≤ k ≤ 15, -28 ≤ l ≤ 28	
Reflections collected	97617	
Independent reflections	5674 [R(int) = 0.0641]	
Completeness to theta max	99.8 %	
Absorption correction	Multi-Scan / SADABS	
Refinement method	Full-matrix least-squares on F ²	
Data / restraints / parameters	5674 / 0 / 250	
Goodness-of-fit on F2	1.261	
Final R indices [I > 2σ(I)]	R1 = 0.0327, wR2 = 0.0970	
R indices (all data)	R1 = 0.0491, wR2 = 0.1093	
Largest diff. peak and hole	1.187 and -1.720 eÅ ⁻³	

Table 9.19 Crystal data and structure refinement for 50.

Empirical formula	$C_{60}H_{78}Sn_5$	
Formula weight	1392.67	
Temperature	100(2) K	
Wavelength	0.71073 Å	
Crystal system	Monoclinic	
Space group	$P2_1/c$	
Unit cell dimensions	$a = 21.4165(9)$ Å	$\alpha = 90^\circ$
	$b = 9.6493(5)$ Å	$\beta = 93.257(2)^\circ$
	$c = 27.9442(12)$ Å	$\gamma = 90^\circ$
Volume	$5765.5(5)$ Å ³	
Z	4	
Density (calculated)	1.604 Mg/m ³	
Absorption coefficient	2.171 mm ⁻¹	
F(000)	2752	
Crystal size	0.21 x 0.16 x 0.15 mm ³	
Theta range f. data collection	0.952 to 25.999°	
Index ranges	-26 ≤ h ≤ 26, -11 ≤ k ≤ 11, -34 ≤ l ≤ 31	
Reflections collected	66525	
Independent reflections	11322 [R(int) = 0.0785]	
Completeness to theta max	100.0 %	
Absorption correction	Multi-Scan / SADABS	
Refinement method	Full-matrix least-squares on F ²	
Data / restraints / parameters	11322 / 0 / 609	
Goodness-of-fit on F2	1.088	
Final R indices [I > 2σ(I)]	R1 = 0.0422, wR2 = 0.0928	
R indices (all data)	R1 = 0.1001, wR2 = 0.1279	
Largest diff. peak and hole	1.006 and -1.531 eÅ ⁻³	

Table 9.20 Crystal data and structure refinement for 51.

Empirical formula	$C_{60}H_{78}Sn_3$	
Formula weight	1155.29	
Temperature	100(2) K	
Wavelength	0.71073 Å	
Crystal system	Monoclinic	
Space group	P2/c	
Unit cell dimensions	a = 20.6793(13) Å	a = 90°
	b = 12.8053(9) Å	b = 96.458(3)°
	c = 21.0302(14) Å	g = 90°
Volume	5533.6(6) Å ³	
Z	4	
Density (calculated)	1.387 Mg/m ³	
Absorption coefficient	1.378 mm ⁻¹	
F(000)	2352	
Crystal size	0.240 x 0.160 x 0.130 mm ³	
Theta range f. data collection	1.865 to 27.247°	
Index ranges	-26 ≤ h ≤ 26, 0 ≤ k ≤ 16, 0 ≤ l ≤ 26	
Reflections collected	12172	
Independent reflections	12172 [R(int) = ?]	
Completeness to theta max	99.3 %	
Absorption correction	Multi-Scan / SADABS	
Refinement method	Full-matrix least-squares on F2	
Data / restraints / parameters	12172 / 0 / 581	
Goodness-of-fit on F2	1.012	
Final R indices [I > 2σ(I)]	R1 = 0.0885, wR2 = 0.2386	
R indices (all data)	R1 = 0.1263, wR2 = 0.2776	
Largest diff. peak and hole	3.747 and -3.612 eÅ ⁻³	

Table 9.21 Crystal data and structure refinement for **53**.

Empirical formula	C ₉₀ H ₁₄₀ Sn ₄	
Formula weight	1696.77	
Temperature	296(2) K	
Wavelength	0.71073 Å	
Crystal system	Triclinic	
Space group	P-1	
Unit cell dimensions	a = 13.4821(18) Å	α = 104.744(5)°
	b = 14.0325(19) Å	β = 115.121(5)°
	c = 14.416(2) Å	γ = 98.249(5)°
Volume	2287.5(6) Å ³	
Z	1	
Density (calculated)	1.232 Mg/m ³	
Absorption coefficient	1.117 mm ⁻¹	
F(000)	880	
Crystal size	0.31 x 0.24 x 0.12 mm ³	
Theta range f. data collection	1.736 to 27.989°	
Index ranges	-17 ≤ h ≤ 17, -17 ≤ k ≤ 18, -19 ≤ l ≤ 18	
Reflections collected	71473	
Independent reflections	10966 [R(int) = 0.0454]	
Completeness to theta max	99.4 %	
Absorption correction	Multi-Scan / SADABS	
Refinement method	Full-matrix least-squares on F ²	
Data / restraints / parameters	10966 / 26 / 475	
Goodness-of-fit on F2	1.143	
Final R indices [I > 2σ(I)]	R1 = 0.0333, wR2 = 0.0738	
R indices (all data)	R1 = 0.0566, wR2 = 0.0957	
Largest diff. peak and hole	1.753 and -0.968 eÅ ⁻³	

Table 9.22 Crystal data and structure refinement for 54.

Empirical formula	C ₇₂ H ₁₀₄ Sn ₄	
Formula weight	1444.31	
Temperature	100(2) K	
Wavelength	0.71073 Å	
Crystal system	Triclinic	
Space group	P-1	
Unit cell dimensions	a = 13.1752(7) Å	a = 73.525(3)°
	b = 13.9590(7) Å	b = 84.889(3)°
	c = 21.1669(13) Å	g = 63.283(3)°
Volume	3331.1(3) Å ³	
Z	2	
Density (calculated)	1.440 Mg/m ³	
Absorption coefficient	1.521 mm ⁻¹	
F(000)	1472	
Crystal size	0.17 x 0.14 x 0.10 mm ³	
Theta range f. data collection	1.004 to 25.499°	
Index ranges	-15 ≤ h ≤ 15, -16 ≤ k ≤ 14, -25 ≤ l ≤ 25	
Reflections collected	35565	
Independent reflections	12190 [R(int) = 0.1607]	
Completeness to theta max	98.5 %	
Absorption correction	Multi-Scan / SADABS	
Refinement method	Full-matrix least-squares on F ²	
Data / restraints / parameters	12190 / 432 / 715	
Goodness-of-fit on F2	1.053	
Final R indices [I > 2σ(I)]	R1 = 0.0895, wR2 = 0.1340	
R indices (all data)	R1 = 0.2044, wR2 = 0.1730	
Largest diff. peak and hole	2.660 and -1.904 eÅ ⁻³	

Table 9.23 Crystal data and structure refinement for 55.

Empirical formula	C ₁₃₆ H ₂₀₀ O ₄ Sn ₁₀	
Formula weight	3085.85	
Temperature	100(2) K	
Wavelength	0.71073 Å	
Crystal system	Triclinic	
Space group	P-1	
Unit cell dimensions	a = 14.2463(11) Å	α = 102.840(4)°
	b = 15.1847(12) Å	β = 98.913(4)°
	c = 16.5794(13) Å	γ = 99.124(4)°
Volume	3384.6(5) Å ³	
Z	1	
Density (calculated)	1.514 Mg/m ³	
Absorption coefficient	1.859 mm ⁻¹	
F(000)	1548	
Crystal size	0.23 x 0.17 x 0.13 mm ³	
Theta range f. data collection	1.285 to 26.000°	
Index ranges	-17<=h<=17, -18<=k<=18, -20<=l<=20	
Reflections collected	182609	
Independent reflections	13290 [R(int) = 0.0496]	
Completeness to theta max	99.7 %	
Absorption correction	Multi-Scan / SADABS	
Refinement method	Full-matrix least-squares on F ²	
Data / restraints / parameters	13290 / 9 / 756	
Goodness-of-fit on F2	0.875	
Final R indices [I>2σ(I)]	R1 = 0.0302, wR2 = 0.0899	
R indices (all data)	R1 = 0.0406, wR2 = 0.1197	
Largest diff. peak and hole	2.082 and -1.172 eÅ ⁻³	

Table 9.24 Crystal data and structure refinement for 56.

Empirical formula	C ₁₁₂ H ₁₆₈ O ₄ Sn ₁₀	
Formula weight	2765.35	
Temperature	100(2) K	
Wavelength	0.71073 Å	
Crystal system	Triclinic	
Space group	P-1	
Unit cell dimensions	a = 11.7790(7) Å	α = 61.708(2)°
	b = 16.7894(9) Å	β = 77.830(3)°
	c = 17.1129(9) Å	γ = 69.479(3)°
Volume	2786.8(3) Å ³	
Z	1	
Density (calculated)	1.648 Mg/m ³	
Absorption coefficient	2.247 mm ⁻¹	
F(000)	1372	
Crystal size	0.260 x 0.210 x 0.130 mm ³	
Theta range f. data collection	1.484 to 28.000°	
Index ranges	-15 ≤ h ≤ 15, -22 ≤ k ≤ 22, -22 ≤ l ≤ 22	
Reflections collected	165238	
Independent reflections	13445 [R(int) = 0.1021]	
Completeness to theta max	99.9 %	
Absorption correction	Multi-Scan / SADABS	
Refinement method	Full-matrix least-squares on F ²	
Data / restraints / parameters	13445 / 26 / 603	
Goodness-of-fit on F2	1.092	
Final R indices [I > 2σ(I)]	R1 = 0.0319, wR2 = 0.0719	
R indices (all data)	R1 = 0.0442, wR2 = 0.0845	
Largest diff. peak and hole	1.046 and -1.839 eÅ ⁻³	

Table 9.25 Crystal data and structure refinement for 58.

Empirical formula	C ₂₄ H ₃₅ Sn	
Formula weight	442.21	
Temperature	100(2) K	
Wavelength	0.71073 Å	
Crystal system	Monoclinic	
Space group	C2/c	
Unit cell dimensions	a = 23.7685(16) Å	α = 90°
	b = 11.4764(10) Å	β = 109.214(4)°
	c = 17.3426(16) Å	γ = 90°
Volume	4467.1(6) Å ³	
Z	8	
Density (calculated)	1.315 Mg/m ³	
Absorption coefficient	1.148 mm ⁻¹	
F(000)	1832	
Crystal size	0.270 x 0.220 x 0.140 mm ³	
Theta range f. data collection	1.993 to 26.498°	
Index ranges	-29 ≤ h ≤ 27, -14 ≤ k ≤ 14, -21 ≤ l ≤ 21	
Reflections collected	49489	
Independent reflections	4628 [R(int) = 0.0874]	
Completeness to theta max	99.9 %	
Absorption correction	Multi-Scan / SADABS	
Refinement method	Full-matrix least-squares on F ²	
Data / restraints / parameters	4628 / 1 / 237	
Goodness-of-fit on F2	1.049	
Final R indices [I > 2σ(I)]	R1 = 0.0370, wR2 = 0.0871	
R indices (all data)	R1 = 0.0509, wR2 = 0.0967	
Largest diff. peak and hole	1.479 and -1.090 eÅ ⁻³	